UNCONVENTIONAL PERMEABLE MICROSTRUCTURES

AN ENGINEERED POROUS MATERIAL

Designing the microstructure of a dynamic insulation component using additive manufacturing and evaluating its effect on airflow rate and pattern

Seyedeh Kiana Mousavi

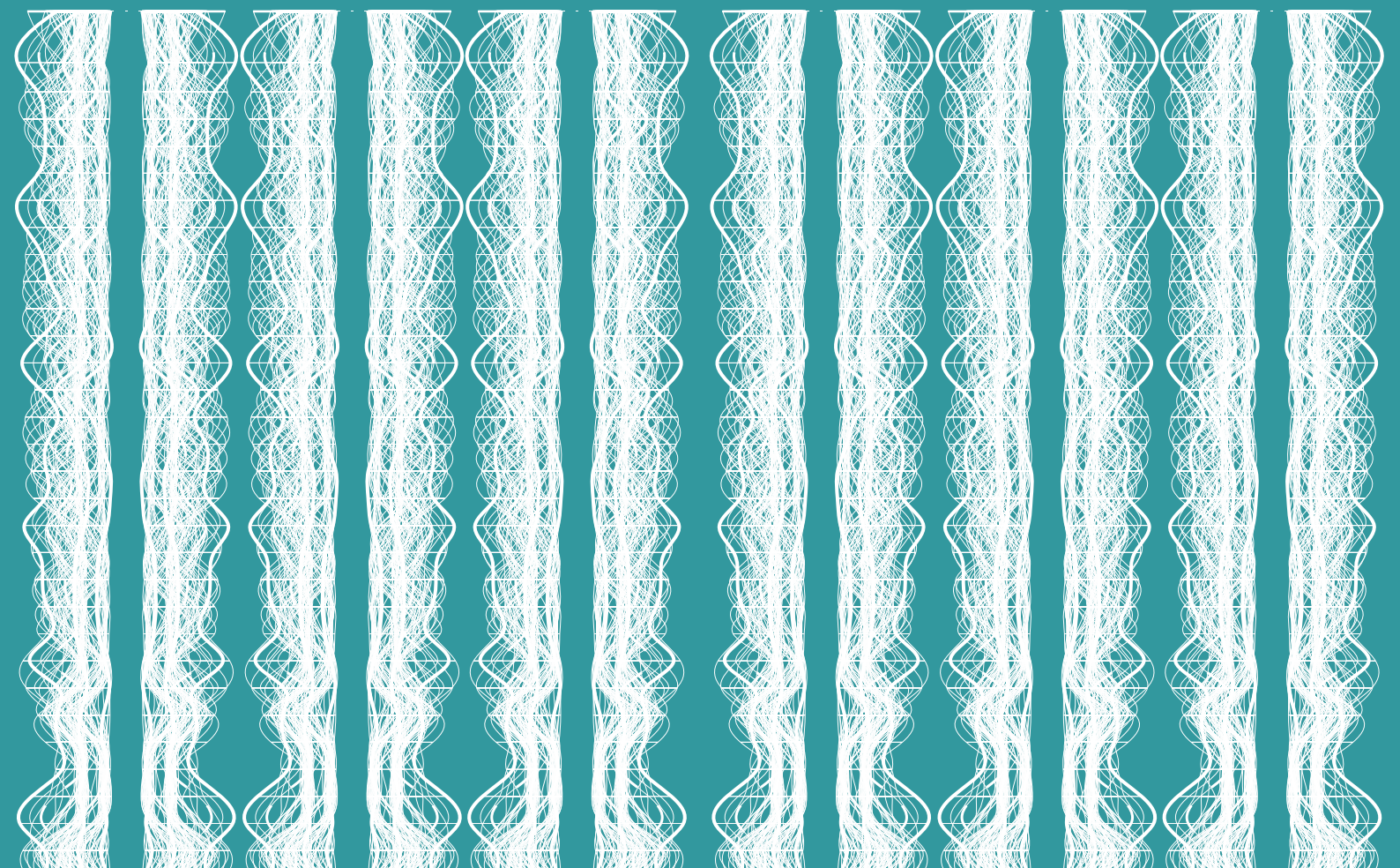

Sustainable Design Graduation Studio

Author
Kiana Mousavi | 4878736

Mentors
Dr. ir. Michela Turrin - Design Informatics
Dr. ir Willem van der Spoel - Building Physics
Department of Architectural Engineering + Technology

Delegate of the board of examiners
Dr. Harry Boumeester

Delft University of Technology
Faculty of Architecture and the Built Environment
MSc Building Technology

Acknowledgments

As this thesis closes my chapter at TU Delft, I have realized that these two years have been more than just an educational experience for me. I was challenged at high levels and motivated at the same time, and my mentality towards many aspects of life was changed. For this, I will be forever grateful.

This research could not have been accomplished without the support of many people.

I would like to express my sincere appreciation and gratitude to my mentors, Dr. Michela Turrin and Dr. Willem van der Spoel, for their invaluable guidance. I cannot describe how grateful I am for their tremendous support throughout this journey. Dr. Turrin's mentality and scientific approach was definitely a source of inspiration to me and encouraged me to move forward, expand my horizon and investigate every single aspect of the research. Dr. van der Spoel's insight and vision always motivated me to have a mindful approach towards the aspects of the research. His critical mindset was so admirable to me that every consultation session was more than a lesson for me.

Special thanks to Mohammad Mobarak, Doctoral researcher at Friedrich-Alexander- University of Erlangen-Nürnberg, for his invaluable help and support for performing the CFD simulations in Ansys Fluent, during the outbreak of Coronavirus and when all the experts on campus were out of reach. I cannot thank you enough for your share of knowledge.

To my amazing family in Delft; Steph, Q, Grammatiki and Iro. Thank you for always being present and your limitless support and kindness.

And last but not least, I would like to thank my parents, Abbas and Niknaz, and my sister, Kati. There are no words to thank you for your unconditional love and support. I would not have been here without you and I am blessed to have you as my family.

Abstract

Designing energy-efficient facades can have a significant impact on reducing the building's energy consumption while providing comfort for the occupants. While highly-insulated buildings have good thermal insulation and high airtightness, they deal with the risk of overheating issues. Dynamic insulation, a technology consisting of porous materials, is a responsive building element that has been introduced to the built environment to tackle these problems.

Due to the current lack of information and available resources on dynamic insulation, and its possible contribution to the built environment, the presented research focuses on the effect of complex geometries as the air channels in dynamic insulation, and as part of the overall building wall. This thesis aims to discover whether and how a designed microstructure (now possible by Additive Manufacturing) in dynamic insulation can offer a solution for controlling the airflow passing through the wall and therefore, improving the performance of the dynamic insulation.

The methodology of the thesis started with the literature review and studying different articles and books. Then in a design-through-research approach, various parameters were identified that could affect the airflow rate and pattern. These parameters were categorized in two groups with relation to geometry and texture. The dominant factors were then selected to be further analyzed. Next, different geometries were generated using the 3D sampling method, based on different textures with different properties. The engineered geometries are texture-based metamaterials with cavities. To investigate the behavior of airflow in these geometries, CFD simulations were performed in Ansys Fluent. The results were evaluated based on their correspondence to the research objectives and conclusions were drawn to answer the research questions.

Keywords: Texture-based metamaterials with cavities, complex geometries, dynamic insulation, porous materials, airflow behavior, responsive building elements.

INTRODUCTION

The building sector is responsible for 40% of the global primary energy consumption and around 30% of CO2 emissions (Costa, Keane, Torrens & Corry, 2013). Many factors including climate change, increased demand for building functions, and population growth have led to a significant increase in building energy use in the past decade (Cao, Dai & Liu, 2016). At an annual rate of around 1.5%, the energy use in Europe is rising due to the growth of the building industry, economic development, and the spread of building services, especially HVAC systems, which is mainly due to the increasing demand for better thermal comfort (Costa et al, 2013). Currently, HVAC systems in Europe comprise around 50% of the buildings' energy consumption and 10-20% of global energy consumption (de Gracia, 2019). Therefore, the major potential of this sector in saving energy cannot be ignored. The building industry is to reach the goals of the EU 20-20-20 and the low carbon economy roadmap 2050 (Wehringer, Scherberich, Groezinger, Boermans, John & Seehusen, 2014). To achieve these goals, different rules and regulations had to be established to guide the building sector towards the concepts of Net-Zero Energy Buildings (NZEB) (European Union, 2010). In the process of buildings becoming net-zero energy, first, it is crucial to accomplish substantial savings at the consumption level by implementing energy efficiency actions to reduce the energy demand (Voss, Sartori, & Lollini, 2012). In this context, the efficient design of the building envelope has a significant impact on reducing building energy consumption while providing occupants' comfort (de Gracia, 2019).

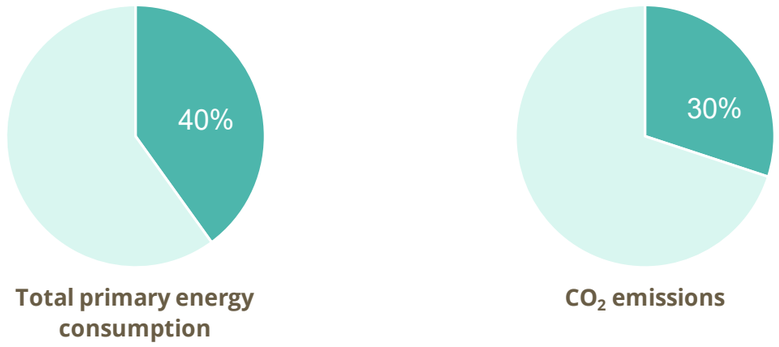

Figure 1: Share of building industry in energy consumption and CO_2 emissions. Source: Costa, Keane, Torrens & Corry, 2013.

Following the EU national building regulations and to reduce the energy consumption of the buildings, one of the main targets has been to increase the airtightness of the envelope and thermal insulation levels (LaFrance, 2013). However, highly insulated buildings deal with the risk of major overheating issues because the interior temperature gets affected more easily by the increase of solar and internal gains (Toledo, Cropper & Wright, 2016). Also, making a fully-airtight building affects occupants' comfort and indoor air quality. To overcome this issue, air infiltration can reduce the risk of vapor condensation, accumulation of indoor pollutants, and risk of sick building syndrome (Ascione, Bianco, De Stasio, Mauro & Vanoli, 2015).

The concept of breathing envelopes uses porous materials to tackle the issue of fully-airtight buildings by allowing the air to penetrate through the wall and enter the room while providing air particle filtration and noise attenuation (Zhao, Zhang, Wang & Geng, 2011). In this approach, the goal is to achieve adaptive thermal insulation that not only responds to the environmental conditions but also allows for the possibility of controlling the thermal conductivity in a preferred range. As a result, it would be possible to regulate the heat flow through the envelope based on the temperature difference between the outdoor and indoor (Jin, Favoino & Overend, 2015). Following the same principle, dynamic insulation is a system implemented in the envelope of the building to reduce the ventilation demand and heat losses through the building envelope while reaching a better indoor air quality (IAQ) (Taylor & Imbabi, 1998).

Although terminologies such as "breathing wall" or "dynamic insulation" are interchangeable in the currently existing literature, it has to be mentioned that there is a difference between these two. "Breathing wall/envelope" specifically indicates the flow of moisture and pollutants through the wall, mostly due to concentration gradients, while "Dynamic insulation" indicates that the thermal transmittance of the envelope changes due to the flow of air. For better consistency, the term "dynamic insulation" is used in this thesis which refers to the system itself, and "breathing envelope" covers the broader concept of the flow of air, moisture, and pollutants (Ascione, Bianco, De Stasio, Mauro & Vanoli, 2015).

The performance of dynamic insulation is dependent on several factors. Some of them concern the building installations, such as the method of room heating in winter. Some are related to environmental conditions, such as the temperature difference between inside and outside. Some of them regard the wall system per se, such as its material selection and its permeability. Some regard the resulting physical phenomena occurring within the wall, such as how the heat from the room reaches the interior surface of the wall, the airflow velocity in the wall's cavities, etc. Among these factors, the airflow velocity is one of the important ones and this factor requires further research. In fact, in the current literature, specific requirements are not mentioned for the airflow velocity to reach the optimum performance of the dynamic insulation system.

Among many other advances in technology, the advantages of additive manufacturing (3D printing) have made it one of the most promising ones. In comparison with the traditional manufacturing technique which is a subtractive process, additive manufacturing creates objects in an additive manner and layer by layer, resulting in less cost and time spent on the fabrication process (Tractus3D, n.d.). However, the potentials of additive manufacturing are still not investigated in some areas of the building industry. 3D printing can be used at a micro-scale, to design materials that their microstructure influences their performance.

RESEARCH FRAMEWORK

2.1 Problem statement

Alongi, Angelotti, and Mazzarella (2019) found out that while the increase of air velocity increased the heat recovery rate through the ventilation flow, it also increased the conduction heat losses at the interior surface of the porous wall. "*An increasing air velocity from outside through the wall reduces the capability of the component to dampen and shift the external temperature wave*" (Alongi, Angelotti & Mazzarella, 2019). Therefore, it is known that air velocity has a large impact on the performance of dynamic insulation.

Despite being ideal to have control over the thermal conductivity and heat flows within a desirable range, yet in the current design of dynamic insulation, the airflow and heat transfer cannot be regulated. Geometry can have a significant impact on airflow and heat transfer. Therefore, it is possible to expect the geometry of the insulation's channels (pores) affects the velocity of the incoming outside air (different geometries having different effects on airflow and heat transfer). Yet in current literature, the geometry of the air channels inside the porous material is mostly limited to simple geometries. Studies on complex geometric configurations are needed. Finally, it is worth noting that also studies on different materials are lacking so far. While possibly different materials could eventually lead to a better/worse performance of the dynamic insulation.

While additive manufacturing offers the production of complex geometries and the use of various materials, the potential of this technology is not investigated in the design of dynamic insulation components at the micro-scale. Using 3D printing, complex microstructure geometries can be generated.

2.2 Research objective

The main problem tackled in this thesis regards the current lack of knowledge on the effect of complex geometries in the dynamic insulation channels, as part of the overall building wall. To approach this problem, the thesis focuses on discovering whether and how a designed microstructure (now possible by Additive Manufacturing) in dynamic insulation can offer a solution for controlling the airflow passing through the wall and therefore, improving the performance of the dynamic insulation.

2.3 Research question

According to the aforementioned problems, the main objective of this thesis is to explore different geometries using additive manufacturing potentials and investigate their effect on the airflow rate and behavior in the pores and the performance of the dynamic insulation component. Therefore, the following main research question is formulated:

How can complex microscale geometries contribute to regulating the air flow rate and pattern inside dynamic insulation, using the potentials of additive manufacturing?

The sub research questions are defined as the following:

1. What are the complex geometries? How can they be generated and how can their properties be evaluated?
2. Why implementing complex geometries in the design of dynamic insulation could offer a potential contribution to the performance of the system?
3. What is the effect of texture on the airflow rate and pattern?
4. What is the effect of surface roughness on the airflow rate and pattern?
5. What are the effects of the geometry's changing cavity volume and morphology of the air channels on the airflow rate and pattern?
6. What is the potential contribution of additive manufacturing to this process and research?

2.4 Research methodology

This research has been structured into the following phases:

Figure 2: Phases of research methodology. Source: Author.

2.4.1 Literature study

To obtain a better understanding of the topic and gather the necessary background information, the literature research has been done by studying various research papers, books, journals, conference papers and presentations, and websites – on the following subjects:

- Net-zero energy buildings, fully-airtight buildings, and their problems
- Responsive building concepts and elements
- Dynamic insulation
- Material exploration (functionally graded materials, metamaterials, latent heat storage materials, thermal insulators, texture-based metamaterials)
- Additive manufacturing (processes, materials, performance-based design)
- Airflow behavior and the possible parameters affecting it
- Fluid-structure interaction (principles, mechanisms, manufacturing techniques)
- Computational Fluid Dynamics analysis (CFD)

2.4.2 Establishing design requirements

Based on the results of the literature study, different variables are defined as the preliminary design requirements including the initial texture as the input for 3D sampling, volume of the cavities, air channel geometry, level of surface roughness, different permeability levels and thermal insulation.

2.4.3 Design through research

To achieve the research objectives, various determinants and aspects must be investigated in a design-through-research process including:

- Research on different textures and the 3D sampling method
- Geometry-related factors affecting airflow rate and pattern
- Environmental factors affecting airflow rate and pattern
- Texture-related factors affecting airflow rate and pattern
- Geometry generation

The dominant features of different textures are identified and established as categorizing parameters for textures. Then using the "3D sampling" process, different geometries are generated based on textures with different properties, with the expectation that they would result in different airflow behavior inside the geometries.

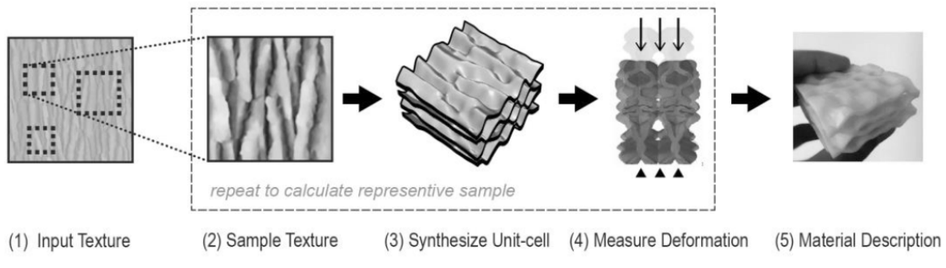

Figure 3: Conceptual workflow of 3D sampling process. Source: Reverse natures: Design synthesis of Texture-Based Metamaterials (TBMs) (p. 512).

The obtained geometries are validated in the evaluation step. Thus, some designs might not be suitable based on the evaluation criteria.

2.4.4 Evaluation

To assess the airflow properties in the created geometries, CFD simulations are used as the analysis tool. Geometries are evaluated using computational fluid dynamics analysis in Ansys Fluent to investigate the effect of different factors on airflow rate and pattern. Fluent is a CFD solver that is part of the Ansys Workbench platform. During the evaluation process, various parameters such as pressure drop, outlet velocity, streamlines' distribution, etc. are monitored and the results are evaluated according to their correspondence to the research objective.

2.4.5 Conclusion

Based on the obtained outcome from the CFD simulations, relevant comparisons are made and conclusions are drawn and categorized to answer the main research question and sub-questions. Yet, because the results are derived from a limited number of geometries, it might not be possible to draw definite conclusions with regards to specific aspects of the research.

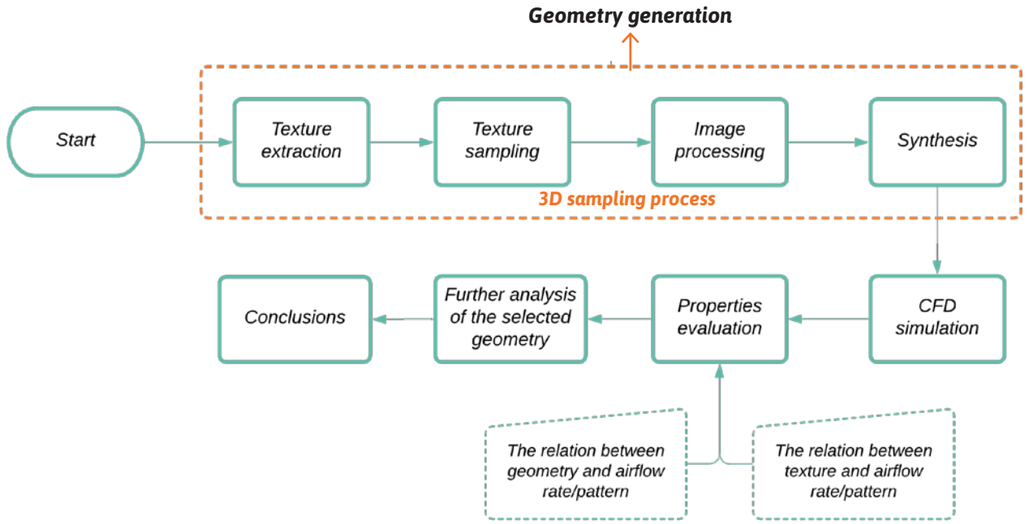

Figure 4: Digital workflow. Source: Author.

2.5 Relevance

2.5.1 Scientific relevance

The current lack of information and resources about dynamic insulation in the built environment is quite evident. While the microstructure of the material can have a rather high impact on its function and performance, the influence of air channels with complex geometries on the airflow rate and pattern is not yet investigated in the design of dynamic insulation. Implementing complex microstructures introduces various aspects to the design of the system and allows for optimization and improving the performance of the system by changing the geometry of the microstructure, the selection of materials, etc. During the fabrication process of dynamic insulation (using additive manufacturing), the geometry can be locally fine-tuned by using different materials based on the design requirements. In further developments of the research, it is expected that a design toolkit could be created which is based on specific established guidelines.

2.5.2 Societal relevance

Despite being introduced in the 1970s, the topic of dynamic insulation is still relatively new and there are vague aspects that need to be explored and investigated. As a result, this system is not commonly known in the building industry and the traditional insulation systems are still used in the design and construction process.

Due to the variable U value, dynamic insulation allows for thinner insulation layers, resulting in more lightweight construction. However, this benefit is not explored in the current constructions.

As 3D printing allows for combining multiple design variables, optimum complex geometry can be designed and manufactured according to the climate and context. However, there is a trade-off between the more lightweight, efficient construction and the production cost, which I think would be less problematic in the future once this system is more recognized in the building industry.

LITERATURE REVIEW

3.1 Thermal insulation materials: from traditional to state-of-the-art

Thermal insulation materials are used to thermally insulate the interior space from the outdoor environment. The optimum aim is to save energy while achieving high levels of indoor thermal comfort. In practice, the materials with higher R-Values (thermal resistance) are chosen due to higher thermal insulation levels (Homem, 2016).

Currently, thermal insulation materials with static thermal resistance include conventional and high performance (state-of-the-art) insulation materials. The high-performance type has remarkably higher thermal resistance compared to the traditional one. Some examples of traditional insulation materials are cork, cellulose, expanded or extruded polystyrene (EPS, XPS), mineral wool, and polyurethane (PUR) which have rather high thermal conductivity levels from 20 to 50 W/m²K (Table 1). A material's thermal conductivity can be affected by different factors including temperature, mass density, moisture content, and possible perforation of the material (Jelle, 2011).

To achieve lower thermal conductivity compared to those of traditional materials, high-performance insulation materials have been developed which do not need any increase in the thickness of the insulation layer. For instance, aerogels and vacuum insulation panels (VIP) can achieve as low thermal conductivity levels as 3 W/m²K. Having a thermal conductivity level of lower than 4 W/m²K, developing examples of this category are gas insulation materials (GIM), nano insulation materials (NIM), and vacuum insulation materials(VIM) (Homem, 2016).

	Material	Thermal Conductivity
Conventional	Cellulose Cork	40-50 mW/(m.K)
	Mineral Wool Expanded Polystyrene (EPS) Extruded Polystyrene (XPS)	30-40 mW/(m.K)
	Polyurethane (PUR)	20-30 mW/(m.K)
State-of-the-art (High Performance)	Aerogels	13-14 mW/(m.K)
	Vacuum Insulation Panels (VIP)	3-4 mW/(m.K)
	Vacuum Insulation Materials (VIM) Gas Insulation Materials (GIM) Nano Insulation Materials (GIM)	< 4 mW/(m.K)

Table 1: Comparison between traditional and state-of-the-art insulation materials. Source: Dynamic insulation as a strategy for net-zero energy buildings (p. 3).

However, the optimal design is the one that achieves the highest thermal resistance (lowest thermal conductivity) while allowing for managing it in a desirable range. In other words, the mentioned ideal design allows controlling the heat flow through the building envelope based on the temperature difference between the indoor and outdoor environments (Jin et al., 2015).

3.2 An innovative approach to energy efficiency improvement

Maximizing the building energy efficiency has been one of the main targets of the building industry for the past few decades. In Europe, regulations have been established to guide the building sector towards the reduction of energy use. In this regard, the main focus has been on increasing the level of thermal insulation and airtightness of the building envelope (LaFrance, 2013). However, as mentioned earlier, highly insulated buildings deal with several issues such as the risk of major overheating problems, accumulation of indoor pollutants and low indoor air quality.

To achieve buildings with higher energy efficiency, steps have been taken to improve the efficiency of particular building elements (such as the building envelope and its components) and building services equipment (HVAC and lighting). Despite showing good results, this approach might be limited. Responsive Building Elements, an overlap of the fields Building Technology and Building Services, is a promising approach in the process of energy-efficient improvements (Van der Aa, Heiselberg & Perino, 2011).

3.3 Responsive building concepts

In regards to environmental considerations and approaches, buildings' designs can be classified into two categories. The first approach separates the outdoor and indoor environment by using a highly insulated building envelope and automatic mechanical systems to achieve energy savings and indoor comfort ("Exclusive" approach). In the second approach, the building is similar to a living envelope that surrounds the occupants, allowing them to be in contact with the outdoor environment while protecting them when necessary. In this "Selective" approach, occupants have control over the mechanical systems and the building envelope to achieve indoor comfort, and the main target for the building is to adapt to the constant changes of the occupants' needs and the outdoor environment (Van der Aa et al., 2011).

In a responsive building, the challenge is to keep the balance between the requirements for comfort, health, and energy consumption, which sometimes can be conflicting. While the building tries to provide a close connection between the outdoor and indoor environment, it also needs to separate these two at certain times for energy-saving purposes. Therefore, depending on the preferred interior conditions, the building envelope becomes a transitional zone that can collect, reject, store, alter, transmit or redirect the energy (Van der Aa et al., 2011).

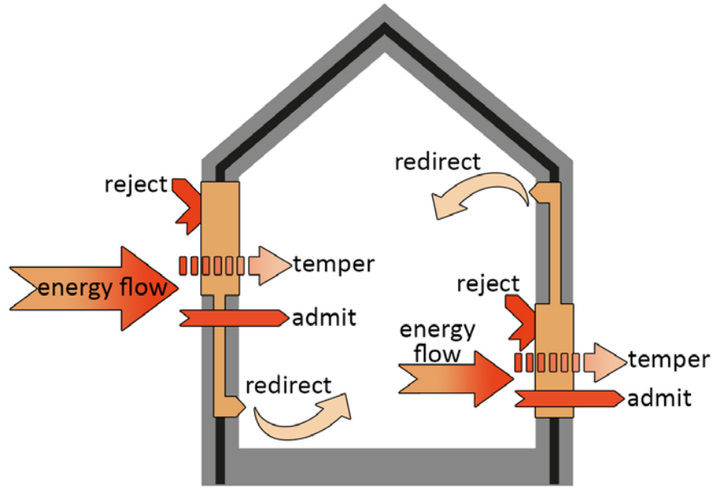

Figure 5: Illustrations of the responsive actions of the building envelope. Source: IEA-ECBCS Annex 44: Designing with Responsive Building Elements (p. 14).

Van der Aa et al. (2011) define the responsive building concepts as "*design solutions that maintain an appropriate balance between optimum interior conditions and environmental performance by reacting in a controlled and holistic manner to changes in external or internal conditions and occupant intervention*".

As a result of an integrated design, these concepts enhance the energy efficiency of the building by combining architectural ideas and human-related factors. "*The main difference between responsive building concepts and other energy-efficient building concepts is the application of responsive building elements and their integration with building services systems and energy systems in combination with advanced control*" (Van der Aa et al., 2011).

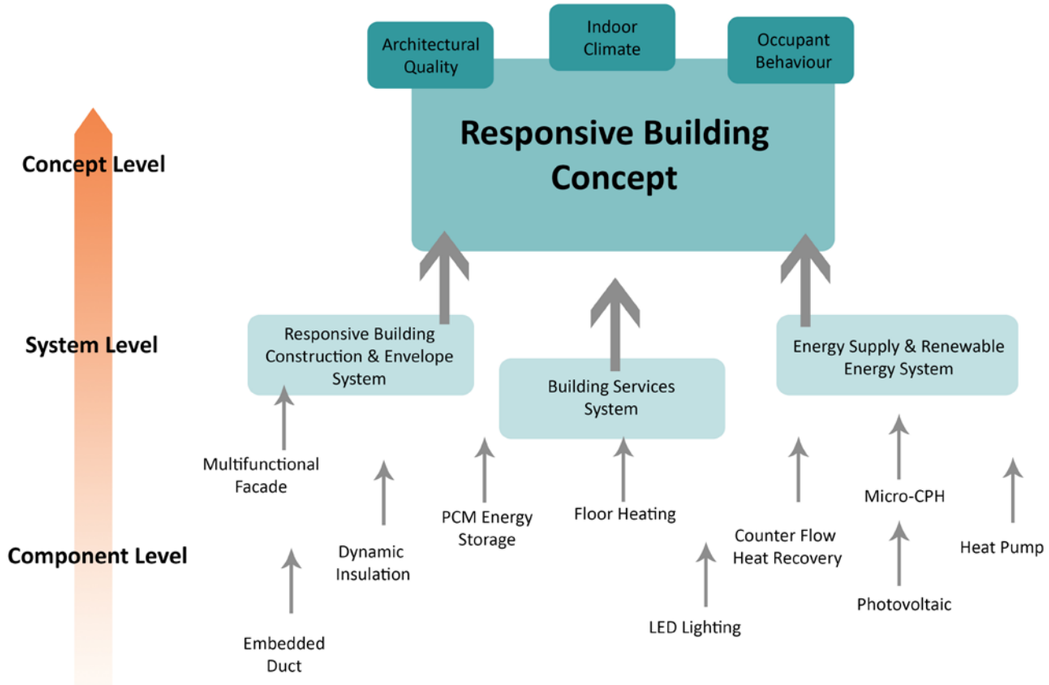

Figure 6: Illustration of the Responsive Building Concept. Source: IEA-ECBCS Annex 44: Designing with Responsive Building Elements (p. 10).

Despite having a great potential for saving energy in the building, the use of responsive building concepts and elements in the design process is still not widespread due to the lack of information, usability guidelines, reference projects and expertise (Van der Aa et al., 2011).

Categorization of responsive building concepts

The responsive building concepts presented in Table 2 are categorized based on the following categories and parameters:

Category	Parameter
Climate	Cold, moderate, warm, hot-dry, hot humid, ...
Context	Urban, suburban, rural
Building use	Office, school, residential, ...
Building type	High-rise, low-rise, row-houses, single houses, multifamily buildings, ...
Design approach	Selective, exclusive
Demand reduction strategies	Thermal insulation, air tightness, buffering, reduction of heat and contaminant loads, building form, zoning, demand control, efficient air distribution, solar shading,...
Responsive building elements	Multi-functional facades, earth coupling, thermal mass activation, dynamic insulation, ...
Low Exergy Building Services systems	Low temperature heating, high temperature cooling, low pressure mechanical ventilation, ...
Renewable energy technologies	Passive and active solar heating, wind, natural cooling, geothermal heat/cool, biomass, daylight, natural ventilation,..
Efficient energy conversion	CHP, HE gas boiler, heat pump, ...
Control strategy	Adaptive/rigid, user control/automatic

Table 2: Categories and parameters for classification of Responsive Building Concepts. Source: IEA-ECBCS Annex 44: Designing with Responsive Building Elements (p. 16).

3.4 Responsive building elements

As mentioned in section 3.3, Responsive Building Elements (RBE) as a category of Responsive Building Concepts are "*design solutions that assist to maintain an appropriate balance between optimum interior conditions and environmental performance by reacting in a controlled and holistic manner to changes in external or internal conditions and occupant intervention*" (Van der Aa et al., 2011).

3.4.1 Characteristics of responsive building elements

According to the type of responsive action, the main features of responsive building elements are categorized as the following (Van der Aa et al., 2011):

- Dynamic behavior
- Adaptability
- Ability to perform various functions
- Intelligent control (allows for achieving the ideal balance between the indoor conditions and energy efficiency)

3.4.2 Categorization of responsive building elements

The type of responsive intervention in responsive building elements can be put into two categories:

- Surface intervention
- Internal intervention

Whether on the surface or inside the RBE, the varying conditions can change the physical behavior of the element. Internal intervention can alter the energy flows inside the element (Van der Aa et al., 2011). Based on the change in physical behavior, responsive building elements can be classified into 4 categories:

Heat-flux related RBEs

Having a variable U-Value, these elements can decrease the cooling demand in summer by reducing the insulation level. Similarly, by increasing the insulation level, the heating demand in winter is decreased. The heat flow in these elements is proportional to the insulation level and a certain separating area, such as the glass area. Dynamic insulation and double skin facades are examples of this category (Van der Aa et al., 2011).

Thermal-storage related RBEs

These elements can store thermal energy during times when cooling is required and release this energy during the heating demand period, thus reducing the energy demand. Phase change materials (PCM), earth coupling systems, and thermal mass activation are examples of this category (Van der Aa et al., 2011).

Transparency related RBEs

Depending on the heat or daylight radiation wavelength, these elements can have changeable transparency. Fenestration and glazed facades are examples of this category (Van der Aa et al., 2011).

Permeability (ventilation) related RBEs

These elements have a variable ventilation performance by having an adaptive permeability. The heat flow in these elements is proportional to the airflow rate. Embedded ducts and ventilated facades are examples of this category (Van der Aa et al., 2011).

Table 3 illustrates responsive building elements based on their structural function and location in the building (the full names of the abbreviated elements below can be found in the appendix).

According to Van der Aa et al. (2011), among the RBEs, the following categories are more widespread and have more potential to be used in the building industry:

- Advanced Integrated Façades (AIF)
- Thermal Mass Activation (TMA)
- Earth Coupling (EC)
- Phase Change Materials (PCM)
- Dynamic Insulation (DI)

RBE		Responsive Action						Possible type of RBE
		Intervention		Physical behaviour				
Buiding system	Element	Surface	Internal	Heat flux	Thermal storage	Transparancy	Permeability	
Envelope	Wall							AIF(TVF, OVF, PVT, PVO, SC, TM, SA, CA), DI, PCM
	Roof							AIR(TVR, OVR, PVTR, PVOR, SCR,TIMR), TMA(SA, CA) DI, PCM
	Ceiling							TMA(SA, CA), PCM
	Fenestration							AIF (Swindow)
Super structure	Colum/beam	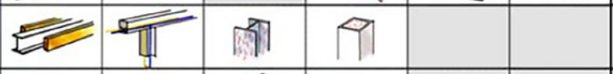						TMA(SA, CA), PCM
	Load bearing wall	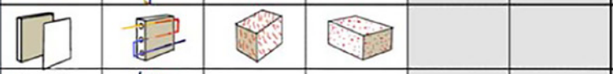						TMA(SA, CA), PCM
	Load bearing floor							TMA(SA, CA), PCM
Sub structure	Piles		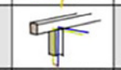					TMA(CA), EC
	Foundation beams		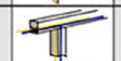					TMA(CA), EC
Underground structure	Earth to air heat exchangers		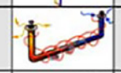					EC
Renders and finishes	Partition wall							TMA(SA), EC
	Floor							PMC
	Ceiling							PMC

Table 3: Potential building applications of responsive building elements. Source: IEA-ECBCS Annex 44: Designing with Responsive Building Elements (p. 30).

3.5 Dynamic insulation

As part of the building envelope, dynamic insulation is an air-permeable component that consists of porous materials and allows airflow to pass through the porous layers into the room (Van der Aa et al., 2011). This technology can be integrated into the design of walls and roofs (Alongi et al., 2019). Before entering the room, the penetrative outdoor air will be pre-heated in winter and pre-cooled in summer using the energy that if not used, would be lost through the building envelope. As a result, the heat losses through the envelope in winter are reduced while achieving better indoor air quality (IAQ) (Van der Aa et al., 2011).

According to Arquis & Langlais (1986), based on the direction of the airflow and heat flux, two primary

operating modes can be defined for dynamic insulation:

1- Pro-flux, when the airflow and heat flux move in the same direction
2- Contra-flux, when the airflow and heat flux are in opposite directions.

Using dynamic insulation has several key advantages:

- Better IAQ (indoor air quality) is achieved by crossing sufficient airflow through the envelope instead of using conventional HVAC systems (Imbabi, 2006).
- Air filtration of airborne particulate matter (PM) (Van der Aa et al., 2011).
- The envelope containing the dynamic insulation performs as a heat exchanger, as the airflow gets pre-heated or pre-cooled depending on the operating modes, resulting in better energy performance (Taylor & Imbabi, 1998).
- When performing in contra-flux mode, the dynamic insulation prevents the transmission of water vapor to the indoor environment; thus having a lower risk of interstitial condensation and mold growth (Van der Aa et al., 2011).
- A reduction in costs and installation of ventilation ducts is achieved as the breathing envelope supplies and distributes the air itself (Van der Aa et al., 2011).
- Since a thin dynamic insulated wall can have a small amount of heat loss, a thinner construction can replace the thick conventional wall. This can still meet the building requirements and also has a more lightweight and less expensive construction (Van der Aa et al., 2011).
- Keeping the inside temperature needs less energy, resulting in less operating expenses for heating and cooling (Van der Aa et al., 2011).

However, the considerations and challenges mentioned below have to be taken into account for the dynamic insulation to perform properly:

- Optimum performance of the dynamic insulation requires the airflow to penetrate only through the breathing part of the wall. Any air leakage or uncontrolled infiltration should be avoided (Alongi et al., 2019). If there are cracks on the building envelopes, such as a small joint clearance in the windows or doors, the air will go across the breathing part because of larger flow resistance (Baker, 2003; Dimoudi, Androutsopoulos & Lykoudis, 2004).
- The velocity and direction of the outside air change constantly. Therefore, it is difficult to guarantee a specific path for the air to permeate through (Zhao, Zhang, Wang & Geng, 2011).
- According to Alongi et al. (2019), "*the ventilation system has to be carefully designed, to allow inversion of the airflow and to provide an effective link with the porous wall*".

Generic types of dynamic insulation

1- Permeodynamic insulation

In this type, airflow passes perpendicular to the wall and through the dynamic insulation (Figure 7). Permeable materials are used in this type (Imbabi, 2012).

According to Van der Aa, Heiselberg and Perino (2011), a permeodynamic insulated construction usually contains three main layers:

- The external layer, through which the fresh supply air can be directed into the building.
- The breathing layer, containing porous materials like cellulose fiber insulation or mineral wool. It causes a low pressure-drop between the outdoor and indoor environment, thus permeating the supply air into the room.
- An air gap, as a separation between the two mentioned layers.

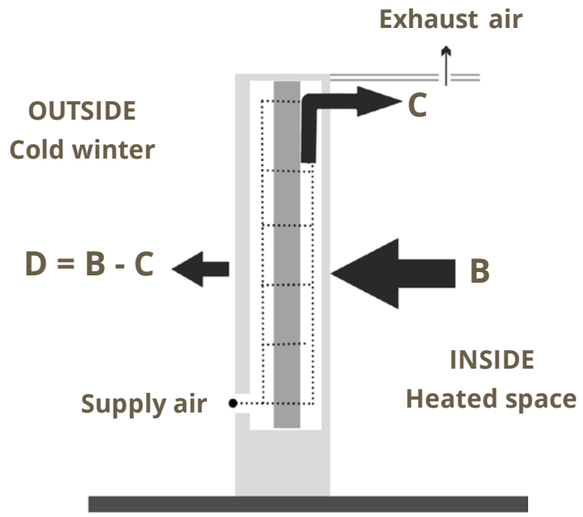

Figure 7: Permeodynamic wall construction. Source: A passive–active dynamic insulation system for all climates (p. 248).

In this type of dynamic insulation, the dynamic R-Value ($R_{d\text{-}ef}$) in a wall or building envelope element is (Imbabi, 2006):

$$R_{d\text{-}ef} = \frac{\exp(v_a \rho_a C_a R_c) - 1}{v_a \rho_a C_a}$$

where:

v_a = air flow rate per unit area of insulation

ρ_a = air density

C_a = specific heat capacity of air

R_c = static thermal resistance (R-value) of the dynamic insulation layer in the absence of airflow

2- Parietodynamic insulation

In Parietodynamic insulation, the air moves into a cavity which is in parallel to the plane of the wall (Figure 8). The direction of the airflow here is perpendicular to the heat flux. Mostly impermeable materials are used in this system and the cavity can be exposed or hidden (Imbabi, 2012). This type of dynamic insulation is also called the "*Cavity wall*" (Van der Aa et al., 2011).

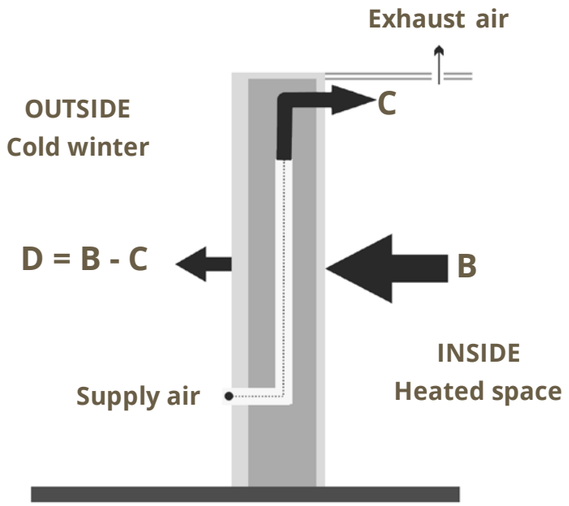

Figure 8: Parietodynamic wall construction. Source: A passive–active dynamic insulation system for all climates (p. 248).

Here, the height-averaged dynamic R-value of a parietodynamically insulated wall is (Imbabi, 2006):

$$\mathbf{R_{d\text{-}ch}} = \frac{(T_i - T_o) * NR_o}{(M - T_o) * (e^{-N+} N - 1)}$$

where

$M = (R_o T_i + R_i T_o) / (R_o + R_i)$

$N = (R_o + R_i) / (v_a \rho_a C_a R_o R_i)$

T_i = indoor temperature

T_o = outdoor temperature

R_i = aggregated thermal resistance (R-value between the airflow channel and the cladding to the ambient interface

R_o = aggregated thermal resistance (R-value between the airflow channel and the cladding to the indoor interface

ρ_a = air density

C_a = specific heat capacity of air

v_u = volume flow rate of air through the channel per unit width of wall

Research was done by Alongi et al. (2019) to measure the behavior and effectiveness of a wall with dynamic insulation. The results showed the following:

> *"The steady-state temperature distribution across the wall sample with dynamic insulation followed an exponential trend. The higher the airflow velocity across the sample, the more the deviation of the temperature profile from a linear trend. In contra-flux winter conditions, the temperature gradient increased from outer to the inner surface, and thus the conductive heat flux density was maximum at the inner surface".*

3.6 Reference projects

McLaren Community Leisure Centre (MCLC), Scotland

The building has squash courts, a bowling hall, a sports hall, and a 20m swimming pool. Each space is provided with fresh air via pressurized ceiling voids through a dynamic insulation layer. After the completion of the building, it was monitored from 1998 to 2000 to evaluate the performance of the system (Gaia Research, n.d.). Some of the assessed factors are mentioned below.

- **Condition & Performance of Dynamic Insulation**
  Using dynamic insulation was effective in heat transfer and preheating the supply air. To evaluate the moisture levels, different samples were taken and it was proved to be low (Gaia Research, n.d.).

- **Air Circulation Patterns**
  Rotary airflows were detected in Swimming Pool and Sports Hall due to down-draughts from cold external walls and windows, and up-draughts from radiators and heated surfaces. These rotary flows caused the air to pass the ceilings much faster than the rate of the incoming supply air, allowing more accelerated heat transmission and temperature consistency than would have been expected (Gaia Research, n.d.).

- **Condensation Risk**
  Rotary air movements supplied the down-draughts passing cold external walls and windows with drier air, resulting in reducing the risk of condensation (Gaia Research, n.d.).

- **Positive Pressures**
  Compared to the outside air and neighboring areas, Swimming Pool and Sports Hall had considerable positive pressures, resulting in the exfiltration of warm humid air from the pool to other spaces and exfiltration cooler, drier air into the street (Gaia Research, n.d.).

Balerno residential building, UK

The Balerno project in the UK is a 4-bedroom detached house and its roof is equipped with dynamic insulation as a part of the air handling and Mechanical Ventilation Heat Recovery (MVHR) system. The dynamically insulated roof contains Energyflo™ cells (Figure 9) which provide the supply air of the MVHR system (Van der Aa et al., 2011).

According to Scotland's 2005 building regulations, the static U-Value of the project was expected to be 0.45 W/m²K. Using a dynamic insulation system in the roof resulted in solar gain during late summer, dynamic heat recovery, and other effects of the system, which changed the expected U-Value to 0.23 W/m²K in late summer and 0.30 in W/m²K early winter. Also, in an 8-hour window, the amount of particulate matter (PM) was reduced from 3673 sub-micron (fine to nano) particles per cm³ to 378 sub-micron particles per cm³ (Van der Aa et al., 2011).

Figure 9: Parietodynamic wall construction. Source: A passive–active dynamic insulation system for all climates (p. 248).

Figure 10: Parietodynamic wall construction. Source: A passive–active dynamic insulation system for all climates (p. 248).

3.7 Material exploration

In the building industry, a material's properties can significantly affect the design and performance of the component/system that the material is applied to. However, during the early stages of the literature review, it was noticed that the potential contribution that a material can have towards the performance of dynamic insulation is not explored yet. This could be mainly because the technology of dynamic insulation is still evolving and the research that has been carried out has been focused on the fundamentals of this system. Since the potential influence of a material's properties could be a driving force in the design process, extensive research was done by the author on different materials that could either be used directly or their concept (how they are composed or can be altered) could be implemented such as functionally graded materials, metamaterials, and texture-based metamaterials. In the following sections, these materials are discussed in more detail to understand their composition, possible applications, and the potentials they can offer.

3.7.1 Functionally graded materials

Shinohara (2013) explains that "*the term 'functionally graded materials' contains two important words: 'functionally' and 'graded'. The word 'functionally' modifies 'graded'. These refer to not only simple functional materials but also to graded materials*". The main difference between a regular composite material and a functionally graded one is that in the composite, a sudden change in properties occurs while in a functionally graded material, the change is gradual (Shinohara, 2013). Figure 11 illustrates this.

Functionally graded materials (FGMs) have gradually-changing porosity, microstructure or chemical composition over the entire volume of the material (Niino, Hirai & Watanabe, 1987, as cited in Mahamood & Akinlabi, 2017). The varying properties of FGMs result in having particular functions and performance (Miyamoto, Niino & Koizumi, 1997, as cited in Mahamood & Akinlabi, 2017). These features depend on the spatial position in the material's structure. The variation of the properties can be different in chemical, thermal, mechanical, magnetic and electrical aspects (Mahamood & Akinlabi, 2017).

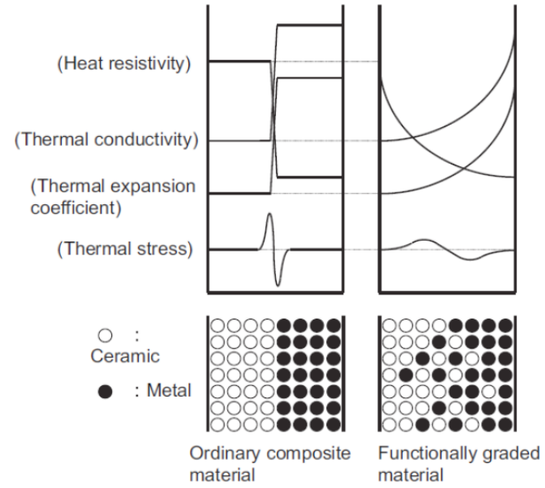

Figure 11: Material structures and properties of ordinary composites and functionally graded materials. Source: Handbook of advanced ceramics: materials, applications, processing, and properties (p. 1180).

There are many types of natural materials with functional gradients. For instance, biological cells respond to external stimuli. This responsive action has generated graded structures against the external force in evolutionary processes. Bamboo and human bone (most livings' bone) are other examples of functionally graded materials in nature (Shinohara, 2013).

Types of Functionally Graded Materials

1) Chemical Composition Gradient Functionally Gradient Materials

Depending on the spatial position in the material, the chemical composition gradually changes in this type of FGM (Mahamood & Akinlabi, 2017). This will result in different phases with different chemical compositions. The production of these different phases depends on the manufacturing conditions and compositional quantity (Khathun, 2018).

2) Porosity Gradient Functionally Gradient Materials

Based on the spatial position in the material, the porosity of the material gradually changes in this type of FGM. The porosity gradation can occur in two forms:

- Porosity density gradation, which is a change in the density of the porosity depending on the spatial location in the volume of the material.
- Pore size gradation, in which the shape or size of the pores or both changes.

The gradient of porosity results in a more lightweight material. Powder deposition is used to produce this type of FGM with a changing mix of different particle shapes and sizes. The change in the pore

size can be achieved by changing the production processing parameters or by using different sintering parameters to create the required porosity gradient (Mahamood & Akinlabi, 2017). Porosity gradation contributes to the thermal insulation of the material, thermal and electrical stress relaxation, tensile strength and Young's modulus (Mahamood & Akinlabi, 2017).

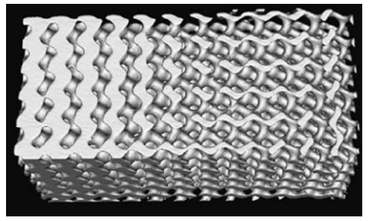

Figure 12: Built PDLLA scaffold with gyroid architecture, showing a gradient in porosity and pore size. Source: Mathematically defined tissue engineering scaffold architectures prepared by stereolithography.

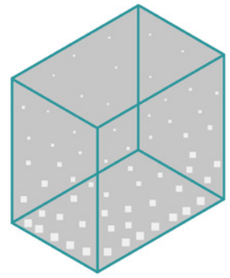

Figure 13: Schematic porosity gradient functionally gradient material. Source: Functionally Graded Materials (p. 11).

3) Microstructure Gradient Functionally Gradient Materials

To achieve specific properties from the material, microstructure gradient FGMs are designed to have a gradually-varied microstructure. This type of FGM is achieved through the process of solidification. For instance, in a quenching process, where the surface of the material experiences a rapid cooling compared to the core of the material that has more time to cool down, the microstructure in the core forms a more equilibrium and organized microstructure.

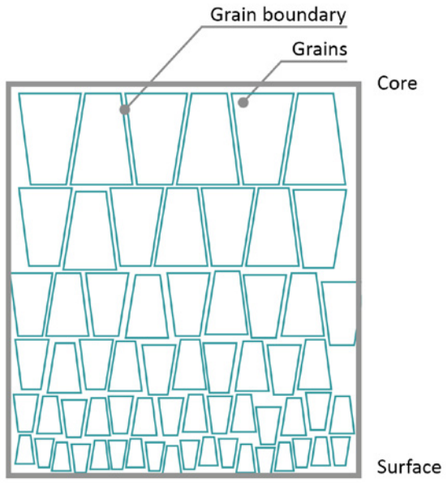

Figure 14: Schematic diagram of a graded microstructure. Source: Functionally Graded Materials (p. 14).

Applications of functionally graded materials

As can be seen in figure 15, FGMs are used in various fields such as automobile, aerospace, defense, energy, biomedical, optoelectronics, etc (Mahamood & Akinlabi, 2017).

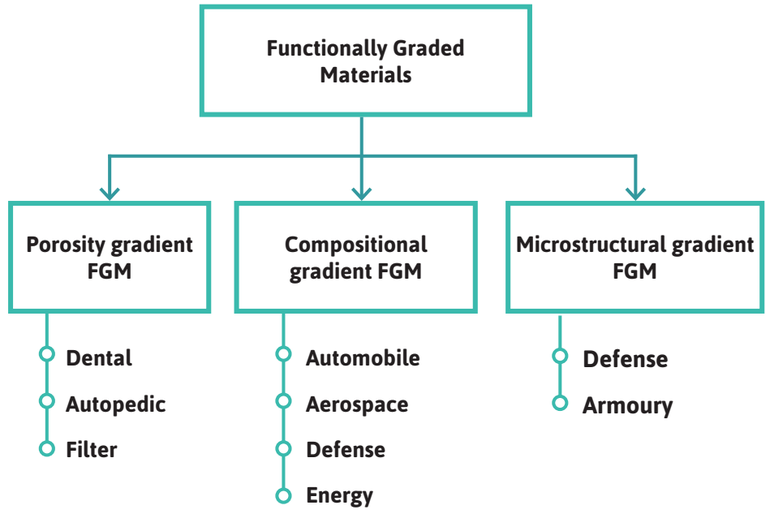

Figure 15: FGMs areas of applications. Source: Functionally Graded Materials (p. 15)

3.7.2 Metamaterials

Cellular materials consist of periodic structures and have optimized strength, stiffness, and overall weight in a specific application (Ashby & Medalist, 1983). In the past, it was not possible to produce these structures as they have complex geometries and very fine details. Today, with recent technological advances, additive manufacturing has made it feasible to produce designed cellular materials (Patel, Mignone, et al., 2017).

Metamaterials, a branch of cellular materials, are engineered composite materials that display significant features that do not exist by nature. The prefix "meta" means beyond, which explains why the term "metamaterial" has been chosen for these materials as these materials exhibit properties that are beyond what is available by nature. Properties of traditional materials are dependent on the innate features of the chemical compositions in the material. However, compared to the bulk materials, the physical properties of metamaterials depend on the internal microstructures of the material. These properties can be modified by altering the internal microstructures (Liu & Zhang, 2011).

The primary concept behind metamaterials is to create new materials by designing microstructural units and assembling them to obtain the target properties and performance. These unit cells (meta-molecules or meta-atoms) are equivalent to the atoms and molecules of traditional materials. Different alterations can be made towards these units, such as changing their size or shape, adjusting the inter-atomic interaction and the lattice constant, etc (Nanowerk, n.d.). For example, by having unit-cell structures with different densities, researchers have created designs consisting of both hard and soft regions (Patel, Mignone, et al., 2017). Metamaterials is an interdisciplinary field of research that involves material science, engineering, physics, chemistry, optics, and nanoscience.

3.7.3 Texture-based metamaterials

Texture-based metamaterials are a type of metamaterials that are generated based on textures as design variables. Texture-based metamaterials can be generated using a design process named

"3D sampling" and offer a wide range of design options to achieve the expected performance. The 3D sampling method will be explained in more detail in section 3.8.

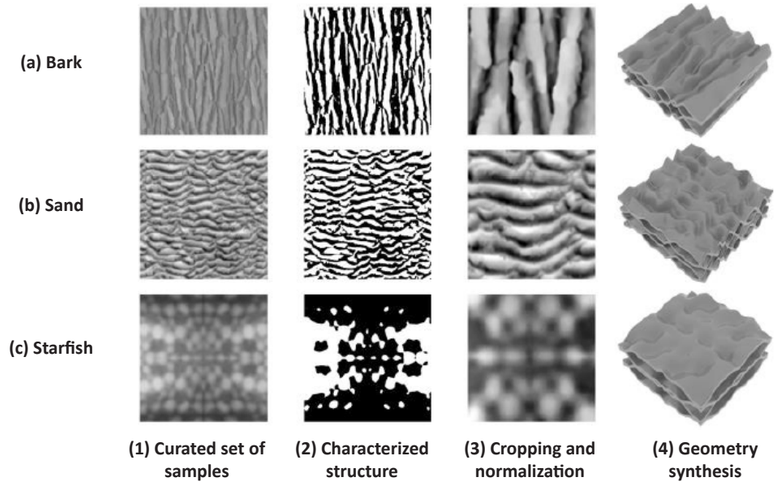

Figure 16: Engineered metamaterials on the right, which are based on the sample textures on the left. From Reverse natures: Design synthesis of Texture-Based Metamaterials (TBMs) (p. 514).

3.8 What is the 3D sampling method?

Today, modeling software is based on calculus and math, which restrains the resulting geometry to be simplified. Due to technological limitations in the past, it was vital to have these simplifications. However, nowadays, developments in computation and manufacturing have facilitated the production of ideas and designs that were once beyond the imagination. The outset of design needs creative thinking at different scales and therefore, innovative techniques are required that can explore complexity and performance at various scales (Patel, Tam, Pushparajan & Mignone, 2017).

3D sampling is a novel robust method that provides the designer with a range of different alternatives to compare their properties. It can be used at the beginning of the design process by identifying the starting points by exploring various designs that can later be further developed in the design process. In this technique, 3D scans generate textures that can be used as sample inputs to synthesize multi-scale characteristics that cannot be produced using conventional modeling software (Patel, Tam, et al., 2017). 3D scanners are devices that gather information about the geometry of physical objects and generate lists of geo-spatial coordinates that are called "point-clouds". Photogrammetry is a similar technology that creates textured 3D meshes from photographs (Patel & Mueller, 2015).

Using 3D sampling, the microstructure of the material can be finely designed, and therefore, new materials with specific features, functions, and even multi-functional properties can be generated. In this process, additive manufacturing can produce geometry with very high accuracy.

According to Patel, Tam, et al. (2017), "*3D sampling procedures combine, transform, and apply primitive design elements called 'textures' *". Figure 17 describes a conceptual workflow of the 3D sampling process.

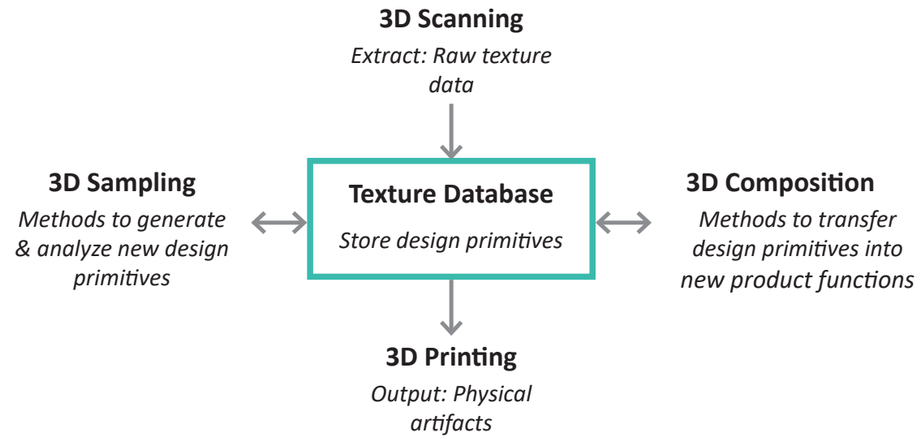

Figure 17: 3D sampling conceptual workflow. Source: 3D Sampling Textures for Creative Design and Manufacturing (p. 466).

3.8.1 General definition of "texture"

A texture is commonly known as a substance's appearance and surface characteristics which are determined by its form, size, density, etc. A texture can be described as soft or hard, rough or smooth, glossy or matte, etc.

The word "texture" is defined by several dictionaries as the following:

"*the quality of something that can be decided by touch; the degree to which something is rough or smooth, or soft or hard*" Cambridge English Dictionary

"*the visual or tactile surface characteristics and appearance of something*" Merriam-Webster Dictionary

"*the way a surface, substance or piece of cloth feels when you touch it, for example how rough, smooth, hard or soft it is*" Oxford English Dictionary

Textures are used in various fields, such as arts, science and technology, and music and they have different definitions in each field. However, they can be mainly divided into two categories, visual and tactile textures. Visual texture is the visual perception that an observer receives and can be related to the local spatial variations of orientation, the intensity in an image or color. Tactile texture is the tangible feel of a surface (Zhou, 2006).

3.8.2 "Texture" in 3D sampling

In the 3D sampling method, texture has a different meaning and functionality. "Textures" are primitive design elements used in 3D sampling. A "texture" represents a "*gray-scale image of point cloud data whereby pixel brightness correlates to surface height at a given point*" (Patel, Tam, et al.,

2017). Patel, Mignone, Tam and Rosen (2017) describe the texture as a functional surface that is continuous over its domain, meaning that "*there is one z-value per coordinate point [x,y], which eliminates the occurrence of overhang conditions*". Textures are accessible by 3D scanners, image editing software, online sources or smartphones. Then, they can be converted into a reusable format in 3D sampling. Textures can be merged, scaled, filtered or remixed to generate various options (Patel, Tam, et al., 2017).

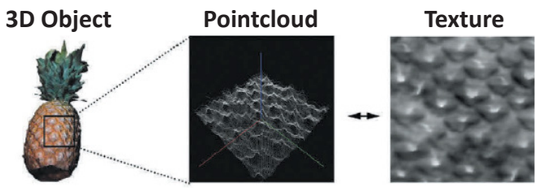

Figure 18: Texture as image-based geometric representation. Source: 3D Sampling Textures for Creative Design and Manufacturing (p. 466).

3.8.3 How are texture-based metamaterials generated?

The process of metamaterials generation is explained in this section. Architectural and engineering software are used in this workflow.

1- Texture extraction: 3D scan

The first step in the process of 3D sampling is "texture extraction" from 3D scan models. As mentioned earlier, textures are continuous functional surfaces, which allow utilizing 2D matrix-based image processing methods in the texture synthesis processes (Patel, Tam & Mueller, 2017).

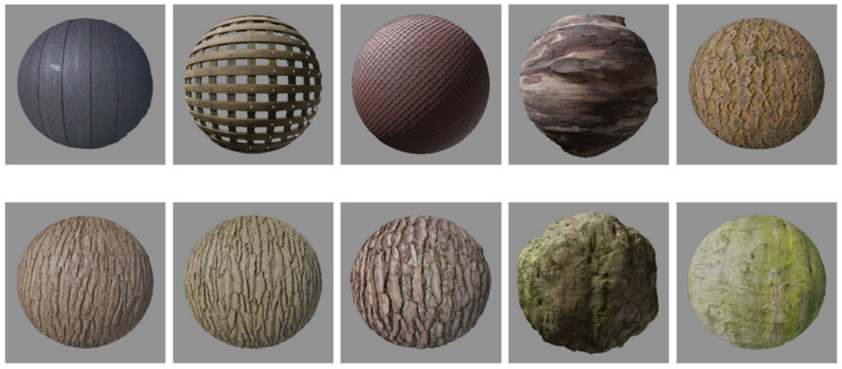

Figure 19: Examples of 3D scanned textures. Source: www.textures.com

2- Sampling: Texture Database

Textures are chosen to seed the unit-generation. As textures illustrate geometries, the 2D matrix-based image processing techniques can be implemented for synthesizing (Patel, Mignone, et al., 2017).

3- Initialization: Image Processing

Using a "histogram equalization" process, textures are normalized for better consistency and easier comparison of the texture samples. In this process, the contrast of the grayscale texture is increased by distributing intensities of the texture sample on the full grayscale spectrum. Scaling and cropping the texture can also be used to adjust the sample size of a texture (Patel, Mignone, et al., 2017).

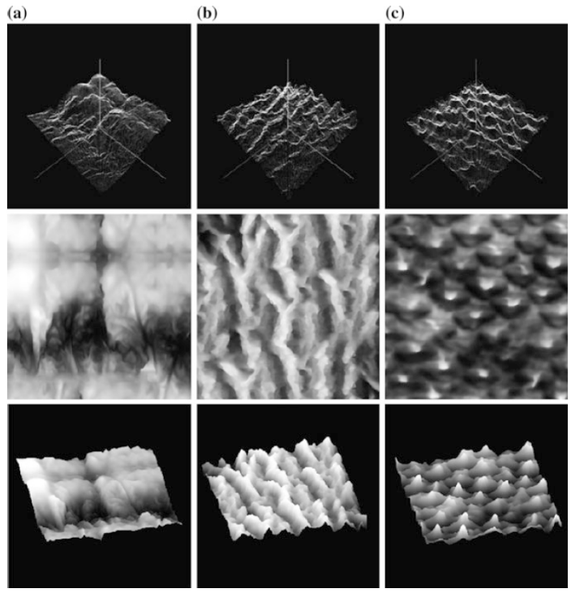

Figure 20: Extraction and initialization of textures: a Lettuce, smooth, continuous; b Bark, sharp, continuous; c Pineapple, rough, discrete Representations; point-clouds (top), 3D depth images (middle), meshes (bottom). Source: 3DJ: An analytical and generative design system for synthesizing high-performance textures from 3D scans (p. 481).

4- Synthesis: Grasshopper and Rhinoceros

In this step, a unit-cell geometry is synthesized. Patel, Mignone, et al. (2017) created a custom modeling tool using Grasshopper and then took the following steps:

1. The texture is imported in Grasshopper.
2. Using Grasshopper, the texture is transformed into a NURBS surface.
3. The surface is 'extruded' to create a polysurface.
4. By 'mirroring' and 'arraying' the polysurface, a stacked assembly is created.
5. Then, 'Boolean Union' is used to merge the polysurfaces to produce a 'water-tight' geometry.

It has to be noted that the above steps are specifically for the mentioned research. However, the framework can be adopted and adjusted to other projects as well.

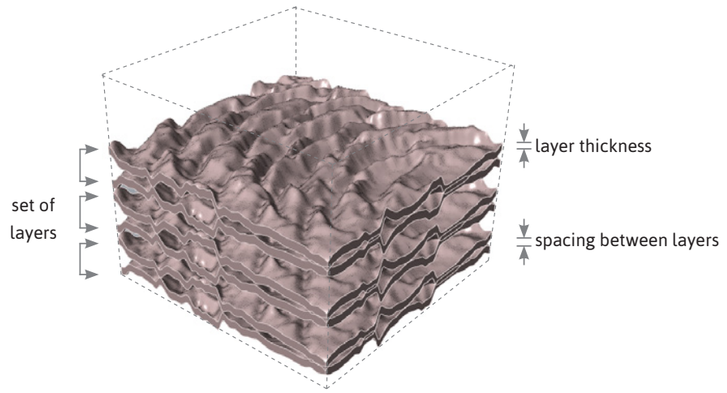

Figure 21: Some of unit-cell design parameters in sample geometries. Source: Author

5- Simulate behavior: Ansys Fluent

Depending on the expected properties from the geometry, simulations are utilized to evaluate those required features. For example, evaluating the effect of the distance between every two surfaces of the geometry or surface roughness on airflow rate passing through the geometry.

3.9 Additive Manufacturing

According to ASTM-F2792 (2010), additive manufacturing (AM) is defined as the "*process of joining materials to make objects from three-dimensional (3D) model data, usually layer upon layer, as opposed to subtractive manufacturing methodologies*" (ASTM, 2010). In this technology, 3D parts are manufactured directly from Computer-Aided Design (3D CAD) models by adding materials layer by layer and without needing process planning (Gibson, Rosen & Stucker, 2015). This enables the possibility of fabricating parts with geometrical complexity.

Despite the advances in additive manufacturing technology, challenges still exist. The range of available materials for AM processes is limited, guidelines and regulations for this technology are missing, the "stair-stepping" effect (which applies to all the AM processes) creates a rather low surface quality, and the consistency and repeatability of the fabricated parts do not have a high quality (Guo & Leu, 2013).

3.9.1 Additive manufacturing processes

1. Material Extrusion

An additive manufacturing process in which the material is dispensed through a nozzle, fabricating the product layer by layer (3D Hubs, n.d.).

- Fused Deposition Modeling (FDM)

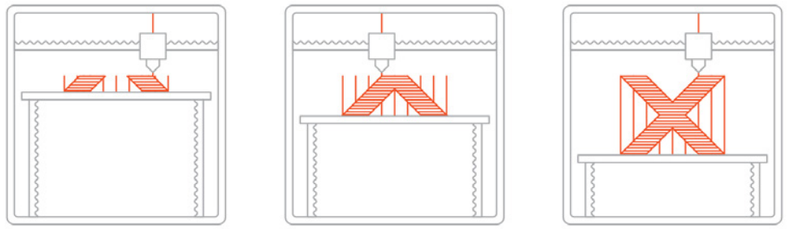

Figure 22: FDM printing process. Source: www.3dhubs.com

2. Vat Photopolymerization

This process uses a vat of liquid photopolymer resin, out of which the product is fabricated layer by layer. The resin is cured (solidified) by being exposed to an ultraviolet (UV) light where required. This process is used to fabricate a solid part one layer at a time (Loughborough University, n.d.; 3D Hubs, n.d.).

- Stereolithography (SLA)
- Direct Light Processing (DLP)
- Continuous Direct Light Processing (CDLP)

3. Powder Bed Fusion (PBF)

In this process, a heat source is used to fuse the material powder one layer at a time, resulting in a solid part. In this process, the powder material is distributed over the previous layers (Loughborough

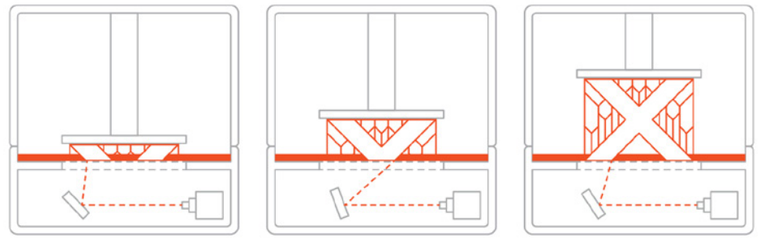

Figure 23: SLA printing process. Source: www.3dcreative.lt

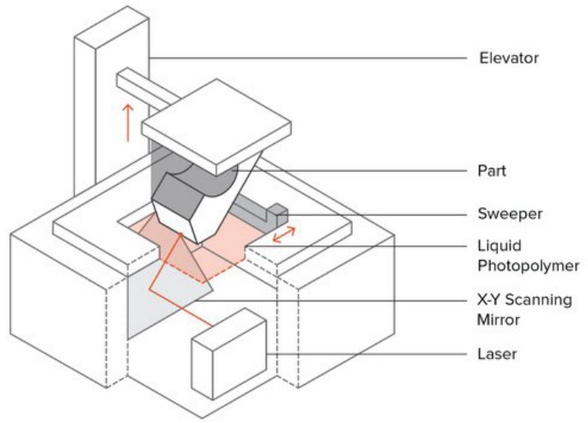

Figure 24: SLA printer. Source: www.indiamart.com

University, n.d.). Different PBF technologies use either laser or electron beams as the heat source, and plastics or metals as the powders used in the process (3D Hubs, n.d.).

- Selective Laser Sintering (SLS)
- Selective Laser Melting (SLM) and Direct Metal Laser Sintering (DMLS)
- Electron Beam Melting (EBM)
- Multi Jet Fusion (MJF)

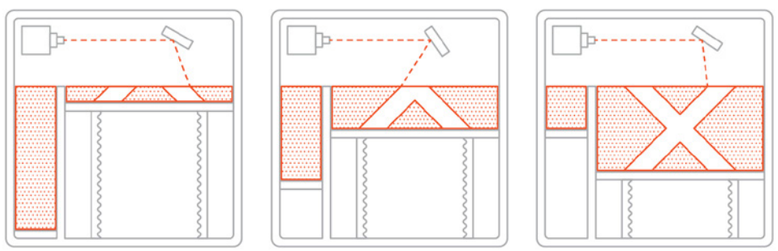

Figure 25: SLS printing process. Source: www.3dcreative.lt

4. Material Jetting

Akin to 2D ink-jetting process, in material jetting the material is dispensed onto the build surface where it solidifies and the product is fabricated layer by layer. Material jetting allows for multi-material fabrication, which is usually utilized to print the supports from a soluble material (3D Hubs, n.d.).

The materials suitable for this process are limited as the material has to be dispensed in droplets. Due

to their viscosity and ability to form drops, polymers and wax are the common materials for this process (Loughborough University, n.d.).

- Material Jetting
- Nano-particle jetting
- Drop-On-Demand (DOD)

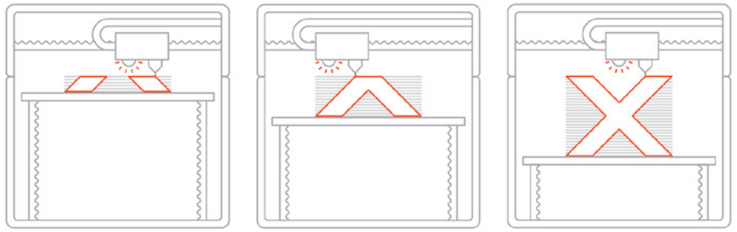

Figure 26: Material jetting printing process. Source: www.3dhubs.com

5. Binder Jetting
An additive manufacturing process in which a binding agent is deposited on a powder-based material to build a part one layer at a time. These layers bind to one another to create a solid object (3D Hubs, n.d.). The binding agent (binder), usually a liquid, functions as an adhesive between powder layers (Loughborough University, n.d.).

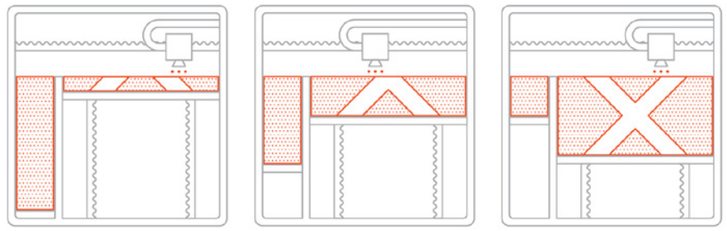

Figure 27: The Binder Jetting process. Source: www.3dhubs.com

6. Direct Energy Deposition (DED)
An additive manufacturing process in which molten material is dispensed onto the build surface where it solidifies. The difference between this process and material extrusion is that the nozzle is not fixed on a particular axis and can move in different directions (Loughborough University, n.d.). This process mostly uses metal powders and is implemented specifically in metal additive manufacturing (referred to as metal deposition) (3D Hubs, n.d.).

- Laser Engineered Net Shape (LENS)
- Electron Beam Additive Manufacture (EBAM)

7. Sheet lamination
An additive manufacturing process in which sheets of paper-based filaments or metal are bonded together to fabricate an object layer by layer. The final product usually does not have a structural function and is often used for aesthetics (Loughborough University, n.d.).

- Ultrasonic additive manufacturing (UAM)
- Laminated object manufacturing (LOM)

3.9.2 Additive manufacturing materials

Additive manufacturing processes use three types of materials: polymers, metals and ceramics. Among these, polymers (including thermoplastics and thermosets) are the most commonly used materials. In general, it is possible to print any material in the layer by layer manner; however, the quality of the final product is highly dependent on the material (Loughborough University, n.d.).

Due to high pressures and temperatures, additive manufacturing processes can alter the material's micro-structure. Thus, after the 3D printing, the material's features might differ from one process to another (Loughborough University, n.d.).

Polymers are low-cost, easy to print and have a low thermal conductivity. Thus, they are widely used as insulators. According to 3D Hubs (n.d.), the commonly used polymers are:

Material	Pros	Cons
PLA	Excellent visual quality Easy to print with	Low impact strength
ABS	Good strength Good temperature resistance	More susceptible to warping
Nylon	High strength Excellent wear and chemical resistance	Low humidity resistance
PETG	Good strength Easy to print with Smooth surface finish	Prone to wear Difficult to glue or paint
Resin	Better resolution Fast manufacturing process Stronger finished products	High cost No option for composite prints Poor availability Difficult post-processing
TPU	Very flexible	Difficult to print accurately
ASA	Strong mechanical properties High chemical resistance UV resistant Easy post-processing	Difficult to print Requires high printing temperatures Fumes
PEI	Excellent strength to weight Excellent fire and chemical resistance	High cost

Table 4: Common polymers in 3D printing. From www.3dhubs.com

3.10 How to regulate the airflow

Air permeability (K_a) is defined as the rate of the airflow which penetrates perpendicularly to a certain area under a specific pressure difference between the two surfaces of a material. Air permeability is a characteristic of porous materials. Most building materials have low permeability. In a construction with different material layers, the higher pressure-drop occurs in the denser material. In other words, lower air permeability leads to higher pressure drop.

If permeability is constant in a material, then pressure is a linear function of position (Wit, 2009), meaning that permeability is not dependent on position and higher pressure drop leads to higher airflow rates. However, considering the fluctuations and dynamic characteristics of the parameters involved in the design of dynamic insulation, permeability should not be constant in this system.

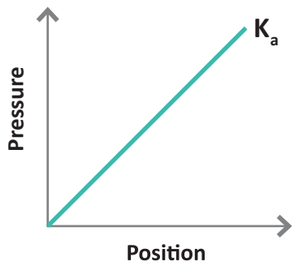

Figure 28: Constant permeability in a material. Source: Author.

According to the laws of conservation, mass is conserved, meaning that it cannot be created or destroyed. Therefore, the rate of the airflow passing through the dynamic insulation should be constant. This indicates that the airflow rate is independent of the position.

To ensure airflow passes through the dynamic insulation in any environmental condition, permeability should not only be dependent on position, but also on another parameter that can be controlled, airflow rate. By doing this, the airflow rate becomes independent of the pressure difference over the facade.

3.10.1 A self-regulating system

Control valves are elements that are commonly used in various engineering fields. Control valves can be set according to different inputs, such as flow rate or pressure.

- Flow regulator: A control valve that maintains a pre-defined airflow rate almost constant and independent from pressure or temperature (Neoperl, n.d.).
- Pressure regulator: A control valve that adjusts the high inlet pressure to pre-defined lower outlet pressure and keeps it constant regardless of the inlet pressure.

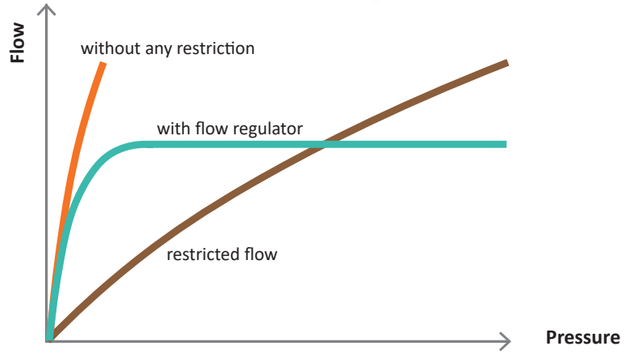

Figure 29: Principle of a flow regulator. Source: www.neoperl.net

In the process of geometry generation, it is ideal that the airflow regulation feature is integrated within the system. As a result, the engineered geometry will adjust itself based on the pressure exerted by the inlet velocity to maintain an almost constant outlet airflow rate.

In this self-regulating system, the porosity of the geometry is defined by the volume of its cavities relative to its total volume. The volume of the solid parts is assumed to be constant and thus, large cavity volume leads to higher permeability in a block of unit cells. The volume of the cavities should depend on the airflow rate. Therefore, the system would have varying permeability based on the environmental conditions, and this in turn makes airflow rate independent of the pressure difference between the inside and outside.

3.10.2 Pressure drop assessment

In the design of ducts, pressure drops are commonly compared to the values derived from the friction loss chart. These smooth ducts are usually circular or rectangular. However, due to surface roughness of the complex geometries designed in this thesis, the resultant pressure drops from the CFD simulations cannot be compared to the values of the friction loss chart as it might lead to inaccurate results. To be able to evaluate the pressure drop in these engineered geometries, these values are compared with the Moody diagram (also known as the Moody chart). The Moody diagram is a non-dimensional graph that connects the Reynolds number, the Darcy friction factor and the relative roughness for fully developed flow in a duct. Two flow regimes can be identified in the Moody diagram: laminar and turbulent.

Reynolds number is a dimensionless value used in fluid flow to predict whether the fluid flow is laminar or turbulent. In the next chapter, this will be discussed in more detail.

Relative roughness is the value that describes the roughness of the duct's inner surface and can be calculated as the following:

$$\textbf{Relative roughness} = \frac{\varepsilon}{D}$$

where ε is the average height of surface irregularities and **D** is the duct's hydraulic diameter. By knowing the relative roughness of the duct's inner surface, its friction factor can be obtained.

The Darcy friction factor is a dimensionless number that is used in the Darcy–Weisbach equation and represents the frictional losses in a duct, pipe or for open-channel flows. The Darcy friction factor is dependent on the Reynolds number of the flow and the relative roughness of the duct's inner surface. In a turbulent flow, the friction factor is highly dependent on the relative roughness. However, in a laminar flow, the friction factor is independent of the relative roughness.

In a laminar flow, the Darcy friction factor can be calculated using the following formula:

$$f_D = \frac{64}{Re}$$

where f_D is the Darcy friction factor and **Re** is the Reynolds number.

In a turbulent flow,

$$\frac{1}{\sqrt{f}} = -2 \log_{10} \left(\frac{\varepsilon}{3.7\, D_h} + \frac{2.51}{Re\sqrt{f}} \right)$$

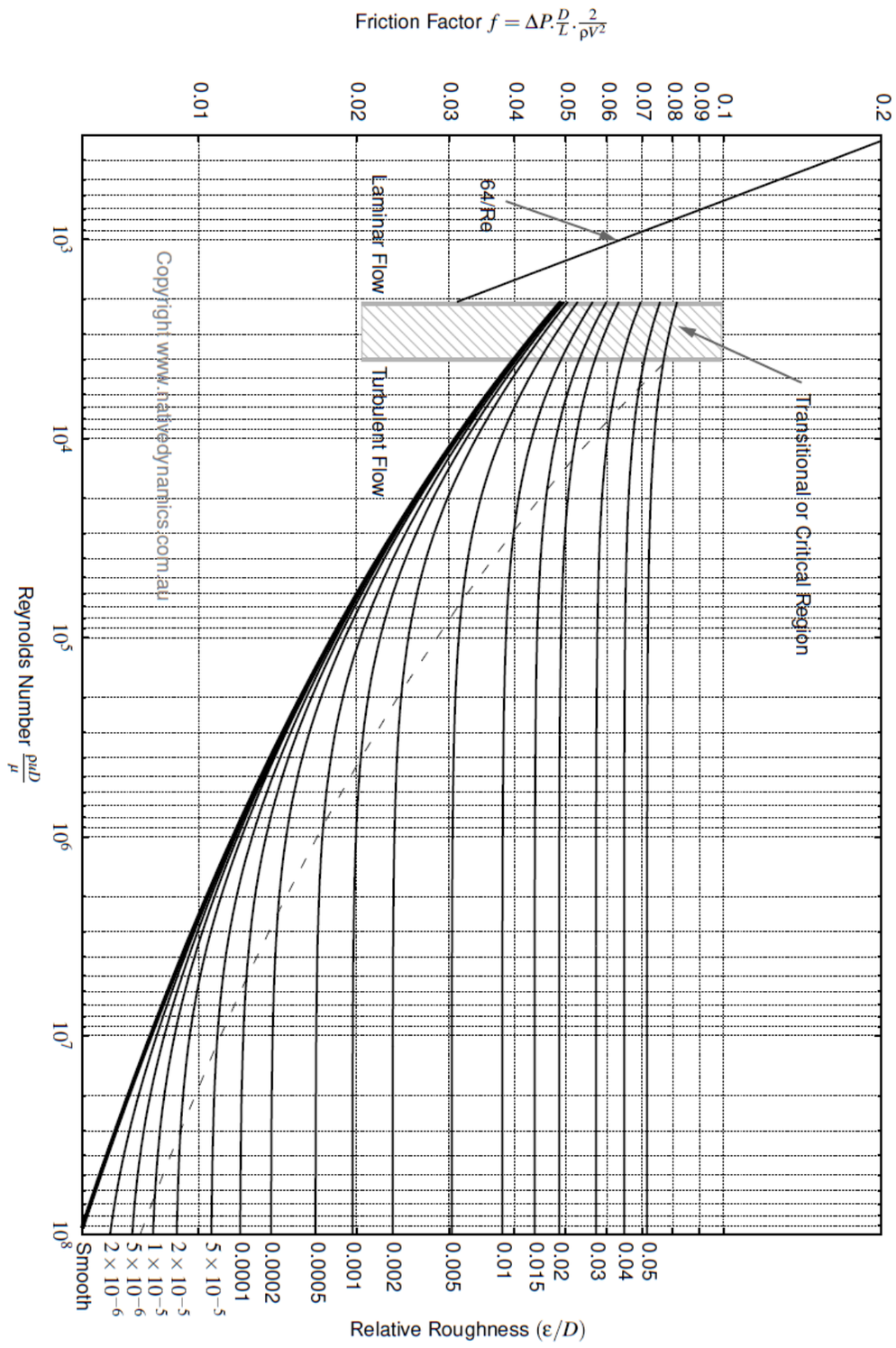

Figure 30: Moody chart . Source: Beck & Collins, University of Sheffield.

Finally, the pressure drop can be determined using the obtained friction factor.

$$\Delta p = f_D \frac{L}{D} \frac{\rho V^2}{2}$$

where **L** is the length of the duct and **D** is the duct's hydraulic diameter

3.11 Fluid-structure interaction (FSI)

Fluid-structure interaction (FSI) is the multiphysics study of the coupling between fluid dynamics and structural mechanics. In this phenomenon, interactions occur between a moving or deformable structure and a fluid flow. These interactions can be fixed or repeated over time (COMSOL, 2017).

When a structure is encountered by a fluid flow, forces are applied to the structure which could result in deformations. The material properties of the structure and the velocity and pressure of the fluid flow are the factors that determine how small or large these deformations would be (COMSOL, 2017).

If the structure's deformations are rather small and it responds slowly to the flow and there are few variations of the structure in the given period, then the impact of the deformations on the fluid flow will be small and the focus of the analysis can be limited to the stresses exerted on the structure. If the structure responds rapidly to the flow, there would be more variations of the structure in the given period. Therefore, even small deformations of the structure will affect the fluid flow. When the deformations are large, they will alter the pressure and velocity fields of the fluid flow. As a result, the analysis becomes a bidirectionally coupled multiphysics study in which the flow and pressure fields influence the deformations of the structure, and the deformations of the structure influence the flow and pressure fields (COMSOL, 2017).

Fabricating a deformable structure can be a challenging task. As a manufacturing technique for the fluid-structure, 4D printing is discussed below.

4D Printing

In 4D printing, 3D static objects can transform their function or form over time. These objects can be triggered by external stimuli such as light, heat, moisture, electrical currents, etc and transform from static structures to smart objects that can change and adapt themselves according to the external stimuli.

Manufacturing a deformable structure requires specific materials that allow for reversible changes in the structure. Research suggests that shape memory polymers are the most promising materials for the target performance of the designed geometries in this thesis. They offer low thermal conductivity, are cost-effective and compared to shape memory alloys, they display a better shape memory effect which allows for large deformations of the structure. Also, by using multiple materials, the composition of the geometry and its aesthetics (being translucent or opaque) can be fine-tuned locally.

However, 3D printed shape memory polymers do not obtain sufficient mechanical stiffness and strength and cannot be used in a heavily load-bearing structure (Li, Challapalli & Li, 2019).

3.12 Computational Fluid Dynamics

Fluid mechanics studies the flow of fluids and how forces affect them. It has two subsections: fluid dynamics and fluid statics. Fluid dynamics focuses on moving fluids and the effect of forces on them. Computational fluid dynamics (CFD) uses algorithms and numerical methods to produce numerical predictions of heat transfer, fluid flow, mass transfer, etc. based on the following conservation laws that govern the fluid flow: conservation of mass, momentum and energy (Hu, 2012; Versteeg & Malalasekera, 2007).

3.12.1 Advantages of CFD simulations

CFD simulations can be used to validate a design and allow for the analysis of flow and heat transfers that might not be feasible to test. This can relatively reduce the cost and time of the analysis. They offer great control over physical phenomena and allow for isolating specific aspects of the study. It is also possible to focus on specific locations in the design and excess simulation time can be avoided.

3.12.2 Available programs/plug-ins

ANSYS Fluent

Fluent is an accurate and reliable CFD solver that is integrated into the ANSYS Workbench environment. Fluent has post-processing capabilities of its own and extensive modeling features to model heat transfer, flow, turbulence, and reactions for industrial applications. The created models using Fluent can vary from small to large scale (ANSYS, n.d.). Despite the accuracy, it is a complicated software for a beginner user of CFD tools to use this solver for initial explorations. Fluent accepts the geometry from Rhino and Grasshopper and it should be meshed before importing into Fluent. The meshing of the geometry significantly affects the accuracy of the results; as having more mesh elements results in a more accurate result. However, a limitation imposed by the academic version of the software is the maximum number of mesh elements which is 512000. This means that meshes with a number of elements above this limit cannot be processed.

Figure 31

ANSYS CFX

CFX is another solver of ANSYS which is a high performance, general-purpose CFD solver that offers reliable, accurate and robust solutions over a wide range of CFD and multiphysics applications (ANSYS, n.d.). Mesh Adaption capabilities are weaker in CFX compared to Fluent. Compared to Fluent, CFX does not have the post-processor of its own.

Figure 32

Butterfly

Butterfly is a Grasshopper/Dynamo plugin and python library. It allows the users to create and run computational fluid dynamics (CFD) simulations using OpenFOAM within the Grasshopper environment. Simulations that are offered by Butterfly include indoor simulations to model thermal comfort and ventilation effectiveness, outdoor simulations to model urban wind patterns, etc (Ladybug Tools, n.d.). While exploring Butterfly, it was observed that this tool was more targeted at outdoor or indoor airflow simulations and using it to simulate airflow inside a cavity-type wall would not produce accurate results.

Figure 33

COMSOL Multiphysics

COMSOL Multiphysics is a finite element analysis and simulation platform. It accepts a wide range of geometries and geometrical complexities at all scales. It also allows for observing the effect of heat transfer and airflow in detail (Farrugia, 2018). As argued by Farrugia (2018), "*computing the airflow field coupled with the heat transfer module is the most accurate form of simulation provided by the software*". It contains all the modeling workflow steps such as defining the geometry, material properties and the physics describing a situation to produce accurate results (COMSOL, n.d.).

Figure 34

PHOENICS VR

PHOENICS Virtual-Reality is an easy tool for quickly setting up a CFD simulation. It has a very simple interface to use especially for first-time users of CFD programs. Geometry can be imported into the program. However, while exploring, it was clear that this program is not intended for airflow simulations inside a complex geometry and it is more suitable for simple geometries in an outdoor or indoor simulation. Also, as a personal observation, it was understood that this program cannot be used for micro-scale models.

Figure 35

Autodesk Flow Design

Autodesk Flow Design is a 3D virtual wind tunnel for simulating airflow over and around the models. A wide range of geometry and formats can be imported into the program. It has different visualization options such as surface pressures, flow lines, and velocity planes. It also offers control over the wind speed, size of the wind tunnel, etc. However, the results cannot be exported as numerical data and only graphical visualization is available. This program has been discontinued since March 2018 (Estrado, 2019).

Figure 36

Figure 31: Ansys Fluent logo. From www.pngimage.net/ansys-logo-png-3/
Figure 32: Ansys CFX logo. From www.marsisinovasyon.com/ansys-cfx/
Figure 33: Butterfly logo. From www.food4rhino.com/app/ladybug-tools
Figure 34: Comsol Multiphysics logo . From www.xiengineering.com/technologies/comsol/
Figure 35: Phoenics VR logo. From www.windsim.com/about/technology-platform-partners.aspx
Figure 36: Autodesk Flow Design logo. From www.appadvice.com/app/autodesk-forceeffect-flow/669869861

3.13 Chapter's conclusions

Target geometry

Environmental conditions such as air velocity change continuously and are considered as dynamic parameters. To ensure air passes through the dynamic insulation in any environmental condition, airflow should become independent of the pressure difference over the facade. To do so, the microstructure has to perform as a self-regulating system that adapts itself according to the pressure exerted by the air velocity and therefore, provides an almost constant flow rate. A fluid (adaptive) microstructure can accommodate variable fluid flow characteristics.

Based on the opportunities offered by functionally graded materials and metamaterials, the goal is to engineer the microstructure of the dynamic insulation to obtain the expected performance. The geometries are metamaterials that are based on textures as primitive design elements and will be generated by designing their unit-cells (meta-molecules). Thus, modifying the unit-cells results in the change of properties such as cavity volume, surface roughness, etc and the gradual change of permeability and shape occurs over time in response to the induced pressure by the outside velocity.

Target performance

As for the performance, it is expected that when the pressure drop over the system is low, the microstructure is smooth with minimum surface roughness and large cavity volume. With the increase of pressure drop, the microstructure has to offer lower permeability to keep an almost constant airflow rate. Compared to the initial position, higher surface roughness leads to smaller cavity volume in the geometry and lower overall permeability. In any part that permeability is mentioned, **it is assumed that the volume of the solid parts in the block of unit-cells is constant and the volume of the cavities is the only variable**.

In the conventional design, dynamic insulation consists of porous materials through which the air can permeate into the room. During the engineering of the microstructure, the **conventional pores** are translated into **cavities** in the geometry. Therefore, displaying variable permeabilities in the geometry occurs by a change in the volume of the cavities.

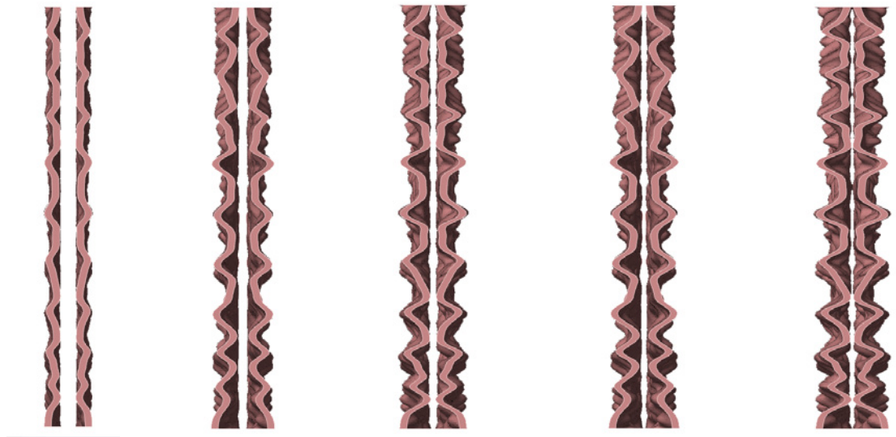

Figure 37: An example unit of an engineered geometry with different surface roughnesses and constant cavity width.
Source: Author.

As an example, a unit-cell with different permeabilities can be seen in figure 37. Here, the cavity width (spacing between the two layers) is constant and the changes in surface roughness affect the volume of the cavity and result in different permeabilities

A design-through-research approach

A group of textures will be selected from the online texture database. These textures will be studied to identify their primary characteristics which allow for later categorization. Then in a design-through-research process, various geometries will be generated based on different initial textures using the 3D sampling method.

Selected software for the evaluation phase

Ansys Fluent is chosen for the CFD analysis due to its robustness and high accuracy. Compared to other available software, Ansys Fluent allows for simulating the airflow within a complex geometry. There is also an online student community (Ansys Student Community) that offers support and guidance for Ansys users, which can be used if there are any questions regarding any aspect of the simulation.

DESIGN THROUGH RESEARCH

4.1 Parameters affecting airflow rate & pattern

Several factors affect the airflow rate and pattern. They can be divided into two main categories, geometry-related factors and environment-related factors. There are more geometry-related factors than the ones mentioned in this section; however, only the ones that are relevant to this thesis are selected. The description of some parameters is exclusive to the designs of this thesis.

4.1.1 Basic principles of relation between geometry and airflow

4.1.1.1 Reynolds number

Reynolds number is a dimensionless value used in fluid flow to predict whether the fluid flow is laminar or turbulent. Laminar flow is a fluid motion that is highly orderly and all the particles of the fluid have the same direction and same speed. In a laminar flow, particles move along a regular streamline. On the other hand, turbulent flow is a fluid motion in which the movement of the particles is irregular or random and the velocity changes at different points.

Reynolds number is described as the ratio of inertial forces to viscous forces (viscosity is the resistance of a fluid, either liquid or gas, to movement). To calculate the Reynolds number, the following formula can be used:

$$Re = \frac{\rho u L}{\mu}$$

where:

Re = Reynolds number
ρ = density of the fluid
u = velocity of the fluid
L = length or diameter of the fluid
μ = viscosity of fluid (at 15 °C, the viscosity of air is 1.81×10^{-5} kg/(m·s) , Pa·s)

If:

Re < 2300 -----> the flow is **laminar**
2300 < Re < 4000 -----> the flow is **transient**
Re > 4000 -----> the flow is **turbulent**

Laminar regime

In a laminar flow, particles of fluid move in regular or smooth paths. The laminar flow is also referred to as the viscous or streamline flow. In this regime, the fluid flows in parallel layers.

Transient regime

In a transient flow, the flow varies with time and from one section of the geometry to another section. In this scenario, the flow is not fully developed (the velocity profile changes in the fluid flow direction).

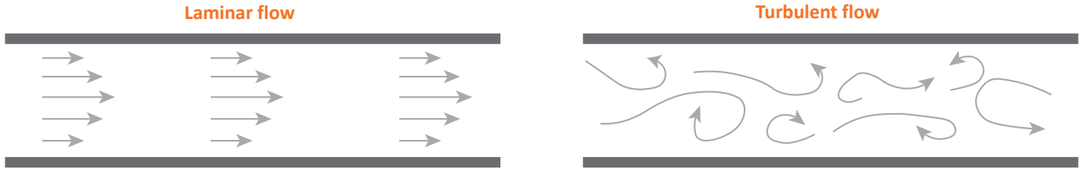

Figure 38 - 39: Illustration of laminar and turbulent flows regimes. Source: Håland, 2017.

Turbulent regime

In a turbulent flow, the fluid's particles do not flow in parallel layers and the movement is irregular. Eddies and recirculation of the particles occur in this regime.

For most scenarios in this thesis, the flow will be in the critical/transition zone between laminar and turbulent.

4.1.1.2 Angle of attack (airflow movement)

The angle at which the airflow meets the geometry is called the angle of attack. This factor is commonly considered in the design of aerofoils in the aerospace industry.

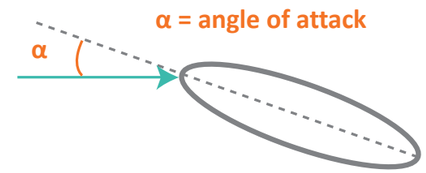

Figure 40: Diagram of angle of attack. Source: www.skybrary.aero

When the geometry changes from the initial position to its another state, the angle at which the airflow hits the geometry changes. This can have several impacts:

- Depending on the angle, it can change the airflow pattern and rate due to the induced drag.
- Depending on the velocity, it can create turbulence.

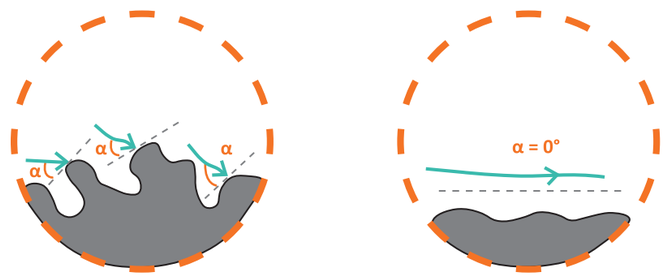

Figure 41: Different angles of airflow hitting the geometry. Source: www.thermal-engineering.org.

4.1.1.3 Surface roughness

The surface roughness of the geometry is one of the parameters that can affect the airflow rate or pattern. Layers with lower surface roughness are smoother and allow higher airflow rates to pass through the geometry. They impose small changes to the airflow pattern. Geometries with high surface roughness experience eddies and backflow in their cavities and have higher pressure drops.

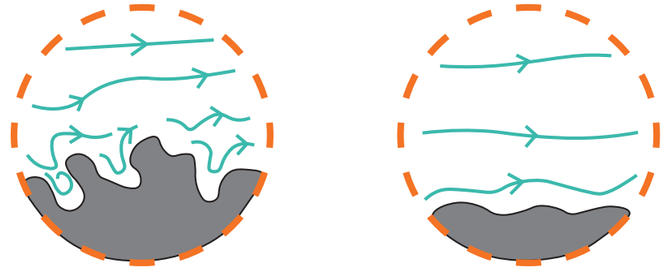

Figure 42: High surface roughness on the left creates eddies and possible backflows, while low surface roughness on the right does not induce a significant change to the flow. Source: Author.

Figures 43 and 44 display two surfaces with different surface roughnesses, the one with low surface roughness at the top and the one with high surface roughness at the bottom. Streamlines in both simulations are irregular. However, the one at the bottom experiences larger turbulence and eddies and backflows in the deeper parts due to very high surface roughness. In section 4.5, two methods are suggested that can define surface roughness.

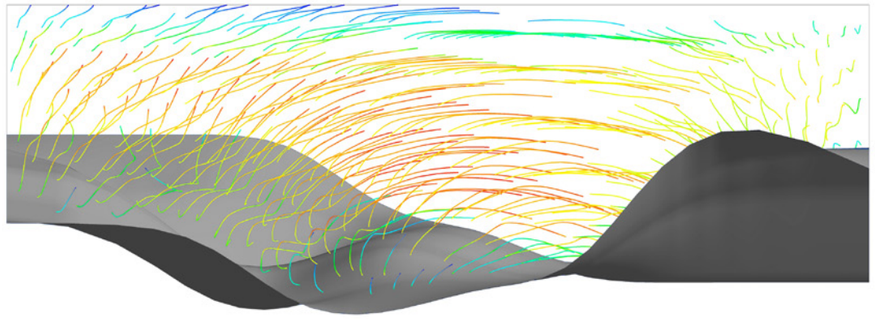

Figure 43: Airflow simulation over a surface with relatively low surface roughness. The surface roughness changes the airflow pattern from almost parallel flow lines to irregular paths. The level of irregularity depends on the surface roughness. Source: Author.

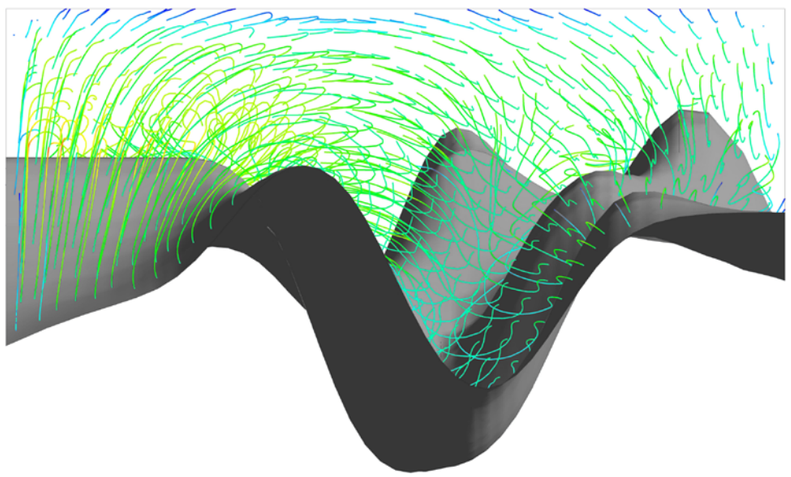

Figure 44: Airflow simulation over a surface with relatively high surface roughness compared to the figure at the top. The flow is turbulent with chaotic flow lines. Eddies and backflow occurs in areas with very high surface roughness. Source: Author.

4.1.1.4 Cavity volume

In a conventional porous material, two parameters are highly determinant: the shape of the solid parts and the spacing between them. In a porous material, porosity (φ) is defined as the ratio of the pore volume to the bulk volume (total volume) of the material (PERM, n.d.). Permeability is a characteristic of a porous medium and is a measure of the ease of fluid transportation in the porous material.

φ = pore volume / bulk volume

where:

bulk volume = solid parts + pore volume

In this thesis, the volume of the solid parts in a block of unit-cells is assumed to be constant and thus, larger cavity volume leads to a higher porosity. Since the cavities here represent the pores of the material in the conventional design, thus, different cavity shapes or sizes result in different permeabilities. Several parameters affect the size or form of the cavity in these geometries:

- The amount of surface roughness of the layers in the unit cell
- The cavity width in the unit cell
- The direction in which a texture is translated to a geometry

Therefore, it is important how the layers in a unit cell are generated. Below are two sample unit cells, with different cavity volumes. As mentioned, it is assumed that the volume of the solid parts in a block of unit-cells is constant and so, porosity can be calculated for a single unit cell.

solid parts = 708.7 cm^3

pore volume = 1445 cm^3

bulk volume = 2153.7

φ = 67%

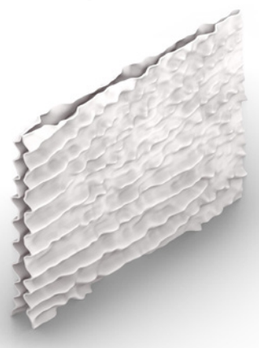

solid parts = 708.7 cm^3

pore volume = 3100 cm^3

bulk volume = 3808.7

φ = 81%

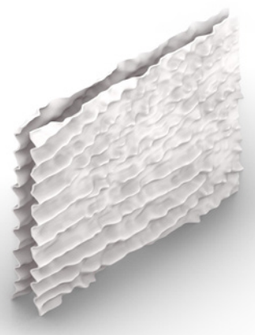

Figure 45: Two sample unit-cells with different cavity volumes. Source: Author.

With the assumption of a constant volume of the solid parts in a block of unit cells, figure 46 shows sample unit cells, with different permeabilities due to different surface roughness levels (on the left) and different cavity widths between the two layers (on the right).

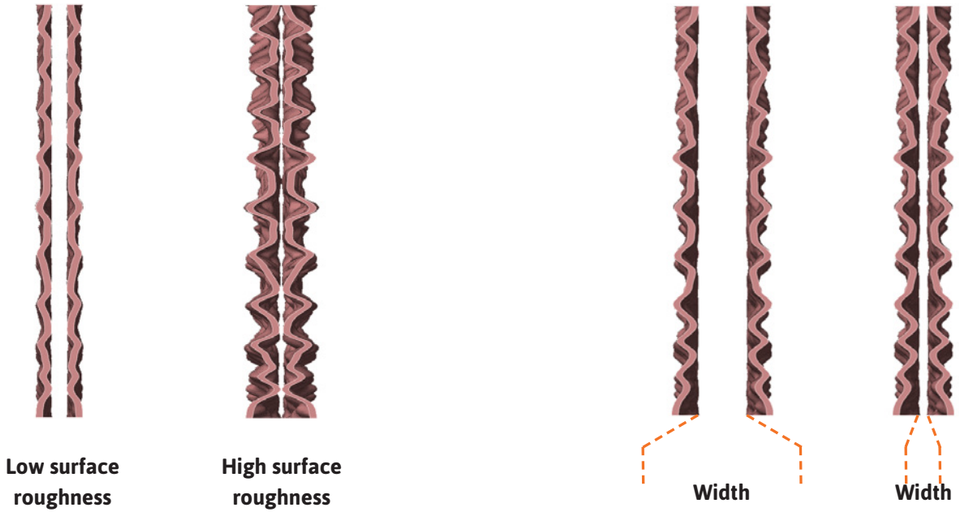

Figure 46: Unit cells with different permeabilities. Source: Author

Direction of the translation of texture to geometry

The pixel brightness of a point in the texture corresponds to the surface height of the given point in the geometry. When the texture is ready to be translated to geometry, two approaches can be taken to generate the geometry:

- White pixels represent mountains, black pixels represent valleys.
- White pixels represent valleys, black pixels represent mountains.

Therefore, depending on the direction of the translation of texture to geometry, the stacked assembly would be different.

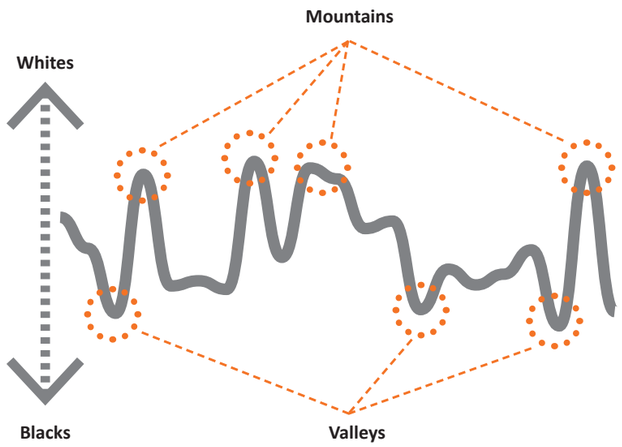

Figure 47: Translation of texture to geometry. Source: Author

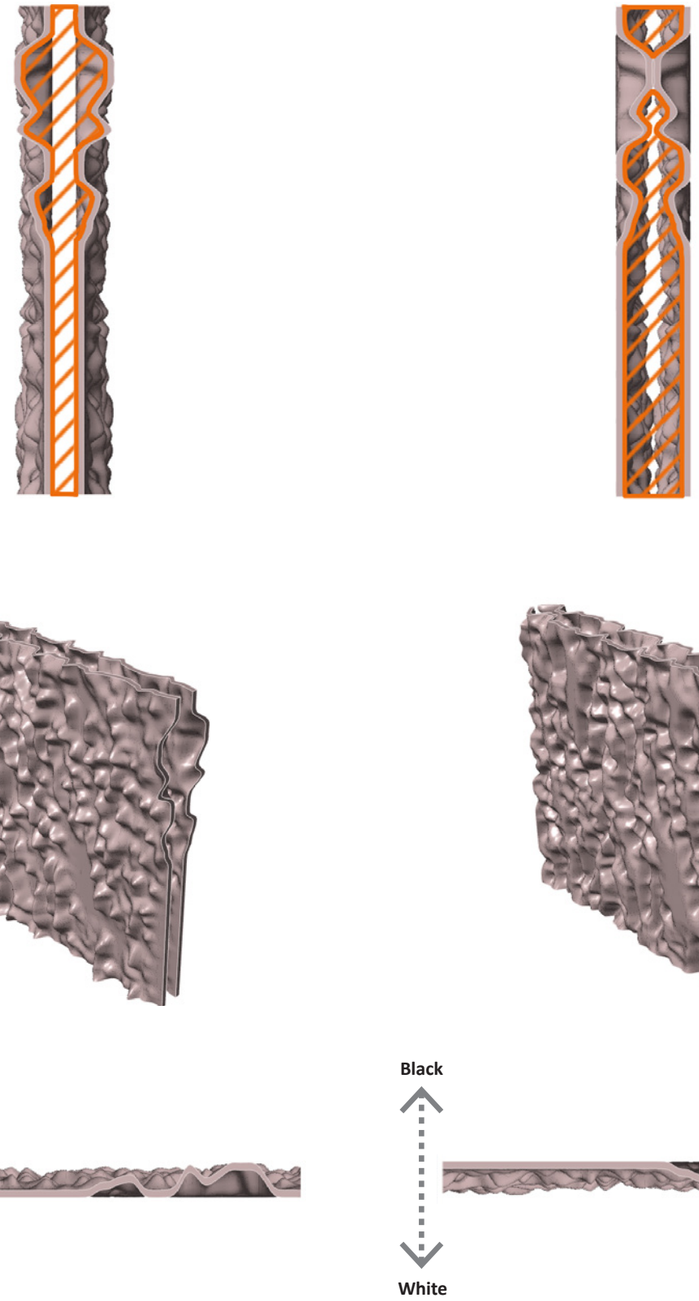

Figure 48: Translation of texture to geometry. Left: White pixels as pikes, right: black pixels as pikes. Source: Author

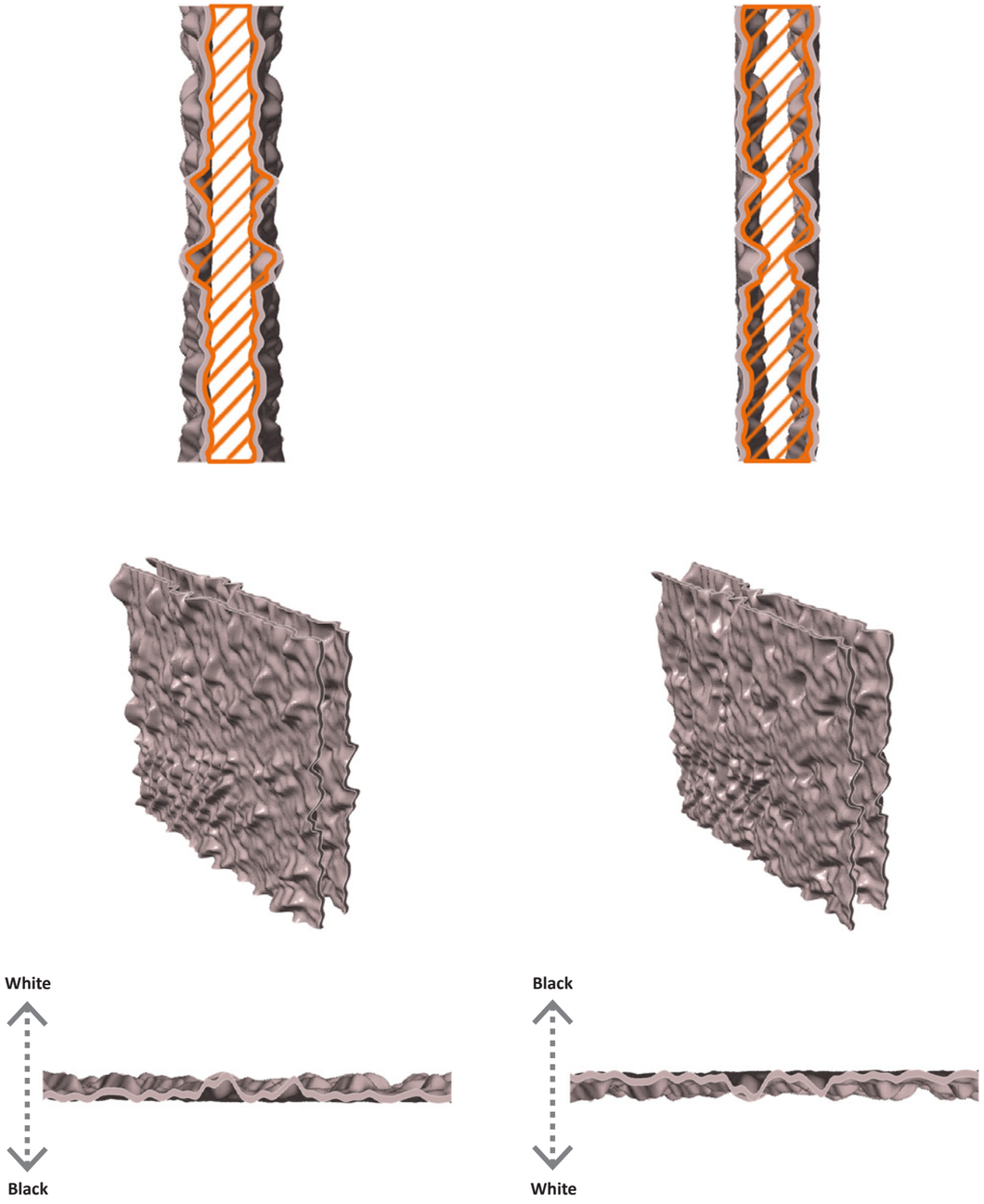

Figure 49: Translation of texture to geometry. Left: White pixels as pikes, right: black pixels as pikes.
Source: Author

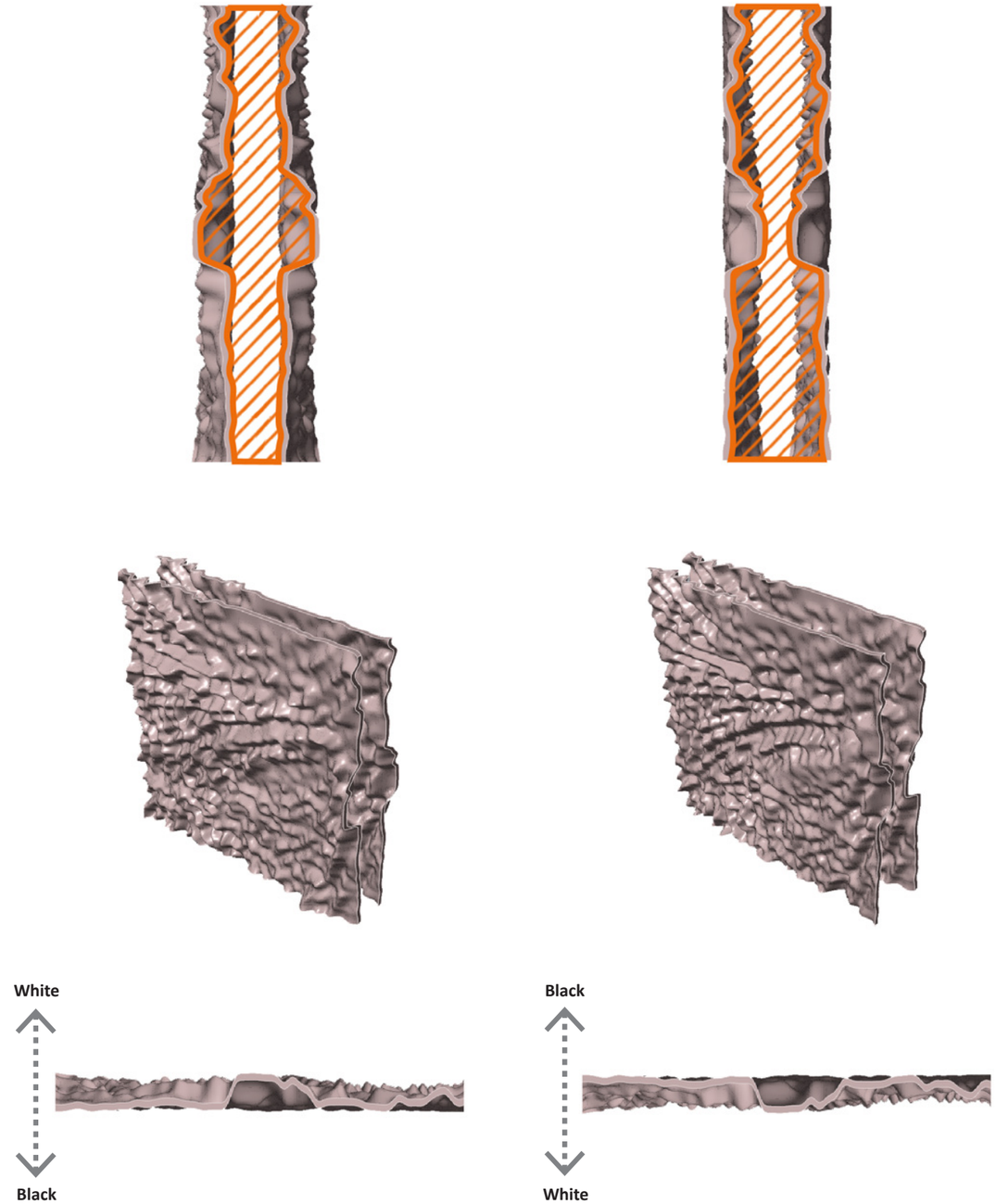

Figure 50: Translation of texture to geometry. Left: White pixels as pikes, right: black pixels as pikes.
Source: Author

4.1.1.5 Cross-section of the passage

Investigating the cross-section of the passage includes exploring two parameters: surface area and surface morphology. Cross-section of the passage at each given point can be different. The surface morphology of the passage determines the surface roughness. The surface roughness increases the surface area, which in turn increases the friction between the air passing through and the surface. Therefore, it affects the airflow speed and pattern. Surface morphology can affect the status of the flow - laminar, transient or turbulent - and alter its pattern.

4.1.1.6 Drag: Form and Friction

Drag is the aerodynamic force on a moving object that resists its movement through a fluid. The drag coefficient is a dimensionless value that is used to determine this force. There are two types of drag: friction drag and pressure (form) drag.

Friction drag is the surface friction between the moving body and the particles of the fluid. Since skin friction is an interaction between the body and the fluid, the magnitude of the friction depends on the characteristics of the body and the fluid. For the body, usually, a rough surface creates more friction compared to a smoother surface (however, in a turbulent flow, specific types of roughness in a surface can decrease the skin friction). For the fluid, Reynolds number affects the friction (NASA Glenn Research Center, n.d.).

Form drag (pressure drag) is a force that occurs due to the pressure difference over a moving body in a fluid environment. Local pressure changes as the object moves through a fluid environment and this pressure difference imposes the form drag on the object. Form drag depends on the shape of the object (NASA Glenn Research Center, n.d.).

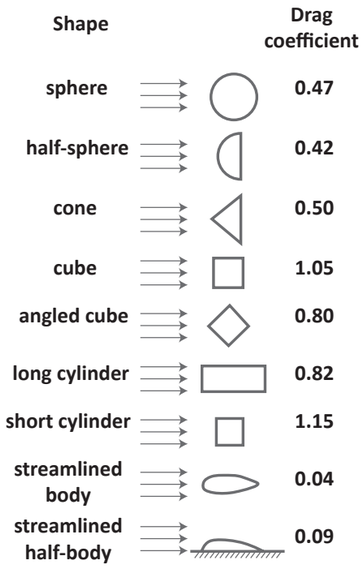

Figure 51: Measured drag coefficients. Source: www.scienceforums.net

When drag force is dominated by the viscous drag (friction drag), the body is streamlined and when the drag force is dominated by the form drag (pressure drag), the body is called a bluff. Whether a flow is form-drag dominated or friction-drag dominated depends on the shape of the object. As it is clear in figure 52, streamlined bodies have smaller form drag compared to bluff bodies because the pressure difference over the body is smaller.

4.1.1.7 Total length of the path

The length of the passage is one of the factors that can affect the outflow. The longer the length of the path, the larger its effect on the airflow velocity and pattern.

4.1.1.8 Speed of response of the fluid-structure (for the future steps)

The optimal goal of this thesis is to achieve a fluid microstructure that can adapt its geometry based on the pressure drop over the system. Therefore, the microstructure would perform as a flow regulator,

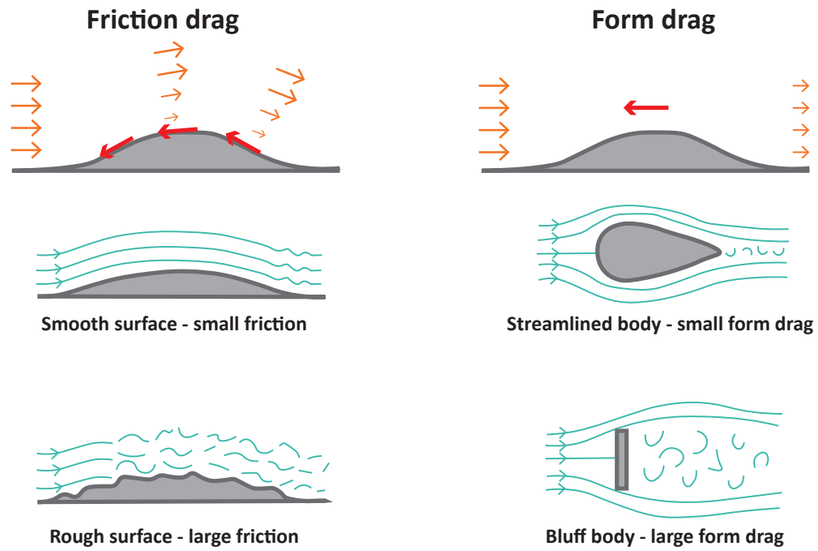

Figure 52: Form drag and friction drag over different bodies and surfaces. Source: http://people.oregonstate.edu/

making the airflow rate independent of pressure difference. In this approach, it is critical how fast this structure can respond to the environmental stimuli, to keep the performance of the system at its optimum.

4.1.1.9 The inlet to outlet ratio

Looking at the designed geometries in this thesis, the cross-sectional area at each given point is different. Therefore, each section has a different average Reynolds number. Based on the laws of conservation, the flow in each section is the same, therefore the velocity in each section area changes as an inverse function of the area. By increasing the section area, the velocity decreases (with a faster rate), resulting in a lower Reynolds number.

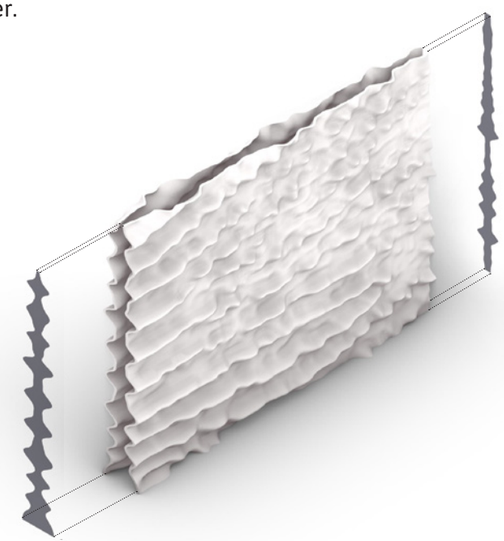

Figure 53: The inlet and outlet in these geometries do not have the same shape and cross section. Along with other factors, the ratio of inlet to outlet plays a role on the airflow velocity. Source: Author

4.1.2 Basic principles of the relationship between environmental conditions and airflow

4.1.2.1 Pressure gradient

Pressure difference over a distance is called an air pressure gradient. Pressure gradient induces the air to flow, always from an area with high air pressure to a low pressure one.

4.1.2.2 Velocity

According to the equation below, the airflow rate depends on the surface area and air velocity. Therefore, higher air velocity leads to higher flow rates.

Q (air flow rate) = A (surface area) * V (air velocity)

4.2 Geometry selection criteria for the evaluation

The mentioned factors that can affect the airflow rate and pattern can be divided into two categories: texture-related and geometry-related parameters. Thus, the selection of geometries is done based on these factors.

4.2.1 Based on texture-related factors

During the selection of textures, it was observed that many of them display similar features and can potentially be characterized based on those criteria. This could also be useful for the next steps of the process, such as better control over the geometry based on the features that originate from the texture and evaluating the properties of the geometry. Therefore, the textures were categorized qualitatively based on the following criteria:

Intensity distribution

The ratio of black to white pixels in a texture demonstrates the intensity distribution in the texture. Pixels in a texture can have any color in the grayscale spectrum and depending on which side of the range they are oriented to, a texture can have a more white or more black tone.

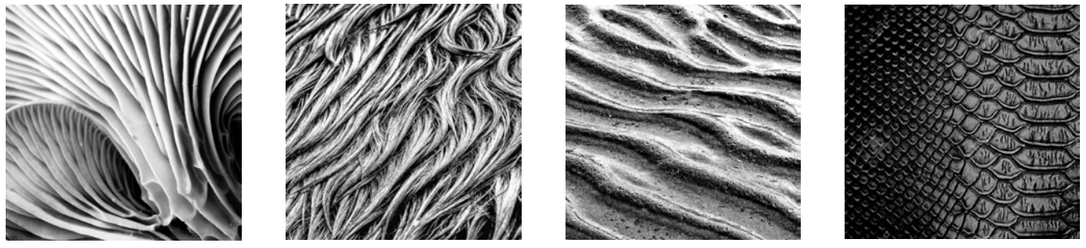

Figure 54: Textures with different intensity distributions. Sources for all texture can be found in the appendix.

Direction

A primary direction can be seen in a texture. If a texture is not direction-dominated, distribution type can be explored, for example, linear or radial distribution. Still, some textures can be direction-less.

Horizontal direction

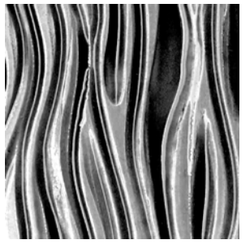

Vertical direction

Radial distribution

Linear distribution

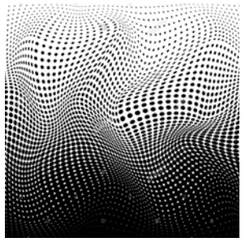

Direction-less

Direction-less

Figure 55: Textures can exhibit a primary direction, distribution type or can be direction-less. Sources for each texture can be found in the appendix.

Texture density

The density of a texture can be explored in two ways:

1- The density of a texture can be influenced by texture magnification. This means that by magnifying a texture, the elements' size can be changed, resulting in changing the density of the texture (Durgin & Proffitt, 1996).
2- Another method that can change the density in a texture is to keep the elements' size constant but alter the elements' frequency (Durgin & Proffitt, 1996).

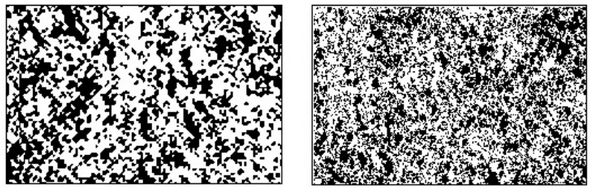

Figure 56: Different texture densities by magnifying the same texture. Source: Durgin & Proffitt, 1996.

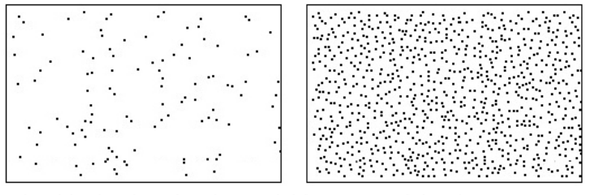

Figure 57: Different texture densities by changing the spatial frequency of the elements. Source: Durgin & Proffitt, 1996.

Placement of the cropping

A sample texture can be part of a bigger texture. Different sample textures can be extracted from a single texture, depending on the placement of the cropping. Therefore, different sample textures of the same texture can exhibit different properties (figure 58).

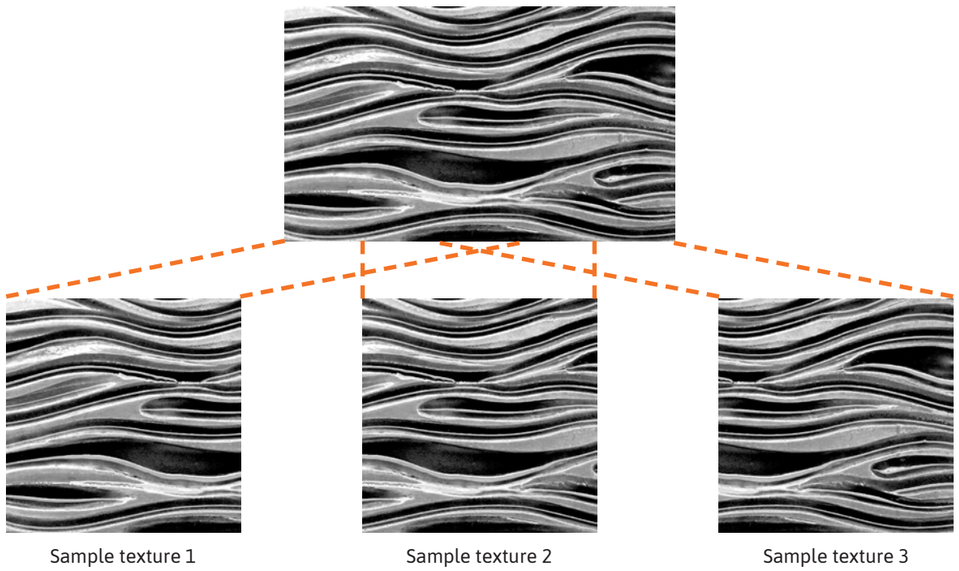

Figure 58: Different placement of the cropping can lead to different sample textures. Sources for all texture can be found in the appendix.

Repetitive patterns

A texture can be a single-piece or a multi-piece. A multi-piece texture has a repetitive pattern while a single-piece texture does not display repetitive patterns.

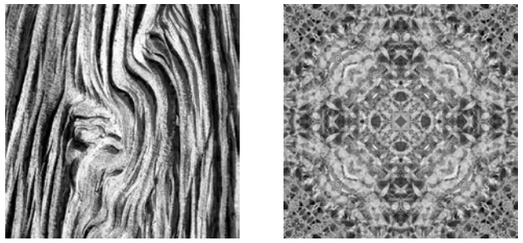

Figure 59: Left: A single-piece texture, right: a multi-piece texture. Sources for all texture can be found in the appendix.

4.2.2 Based on geometry-related factors

In addition to the effects that originate from the underlying texture and can influence the airflow in the geometry, some factors affect the geometry without being linked to the texture. These parameters include the cavity volume and the amount of surface roughness.

4.2.3 Relation between the choice of selected geometries and the principles

First, based on the texture-related parameters (texture properties), sample textures are selected. In this case, direction and intensity distribution are expected to have a higher impact on the airflow rate or pattern. A texture can have horizontal or vertical direction or can be direction-less which might alter the pattern of airflow. It is anticipated that geometries based on textures with horizontal direction have more uniform streamlines while the ones based on textures with vertical direction experience irregular and chaotic streamlines and high pressure drops.

Intensity distribution influences the contrast of the texture and affects the even or uneven distribution of surface roughness in the geometry. It is expected that textures with a high-intensity distribution result in geometries with higher surface roughness and more irregular streamlines in their cavity. A low contrast (low-intensity distribution) in the texture results in more even distribution of surface roughness and creates a smoother surface. Intensity distribution first shapes the surface roughness, which in turn affects the airflow behavior. Therefore, intensity distribution will be evaluated as part of the surface roughness in the geometry-related parameters.

Then, the geometries will be generated using the selected sample textures. Next, the influence of the geometry-related factors that are expected to be more dominant, would be investigated. This includes the cavity's width and surface roughness. Depending on the width of the cavity, the surface roughness affects the streamlines; the smaller the width of the cavity, the larger the influence of the surface roughness.

4.3 Design framework

Based on the obtained knowledge from the literature review and the initial part of the design through research process regarding the factors affecting airflow rate and pattern, a framework was set in which the design is defined.

An engineered geometry

Looking back on section 3.13, the designed geometries in this thesis are metamaterials that are based on textures as design primitive design elements to achieve specific performances.

Building envelope component

The designed geometry is the microstructure of a wall that will be integrated into a facade panel in the building envelope. The required area of the breathing parts of the wall will depend on the required flow rate (ventilation with outside air for air quality) and allowed average velocity. The flow rate and area of the breathing part will both influence local thermal comfort. By the means of additive manufacturing, the geometries can be printed opaque or translucent. This aspect is more related to aesthetics and was not explored in this thesis. However, as part of future development, this aspect certainly offers the potential to design envelope components with different visual features.

Target performance

In this system, a fluid (adaptive) microstructure allows the geometry to have a variable cavity volume depending on the induced pressure by the air velocity passing through the air channels. Thus, the airflow rate should become independent of the pressure difference over the facade. In a unit cell, the ratio of the cavity volume to the total volume represents the porosity of the unit cell. The easier the transmission of fluids in the unit cell, the higher its permeability. When the outside velocity induces low pressure on the geometry, the geometry has larger cavity volume; compared to when the exerted pressure is high, and the geometry needs to have a smaller cavity volume.

Material

Due to their high thermal resistance, water resistance, ease of manufacturing and relatively low cost, polymers are the selected material category for the fabrication process. The specific material can be selected considering the production technique, ease of printing, cost, time and final surface quality. This aspect was part of the initial design framework. However, due to Covid-19 and the lockdown of the campus, the manufacturing part was not possible and the focus was shifted more towards the geometry generation and evaluation phase.

4.4 Digital workflow: geometry generation

Several papers on the topic of 3D Sampling were analyzed to understand the workflow and process that were used in those papers. The common process comprises several steps, among which the step of converting the texture into geometry is the most challenging one. Authors of those papers had created their codes using processing platforms, to be able to translate textures into geometries and have control over different parameters.

Since there was not a specific software to produce the expected results for the geometry generation part, different techniques had to be tested to find the most suitable one, such as using the height-field in Rhino or converting the texture into a 3D object in Photoshop 3D. Although both of these approaches might be valid, they were not the best techniques for this thesis as they didn't provide parametric control over the values embedded in creating the geometry. The technique that is selected as the final approach includes creating a code in Grasshopper that uses texture as input data which is then translated to a surface and allows for further modifications and parametric controls and changes. Details of each step will be discussed in the following sections.

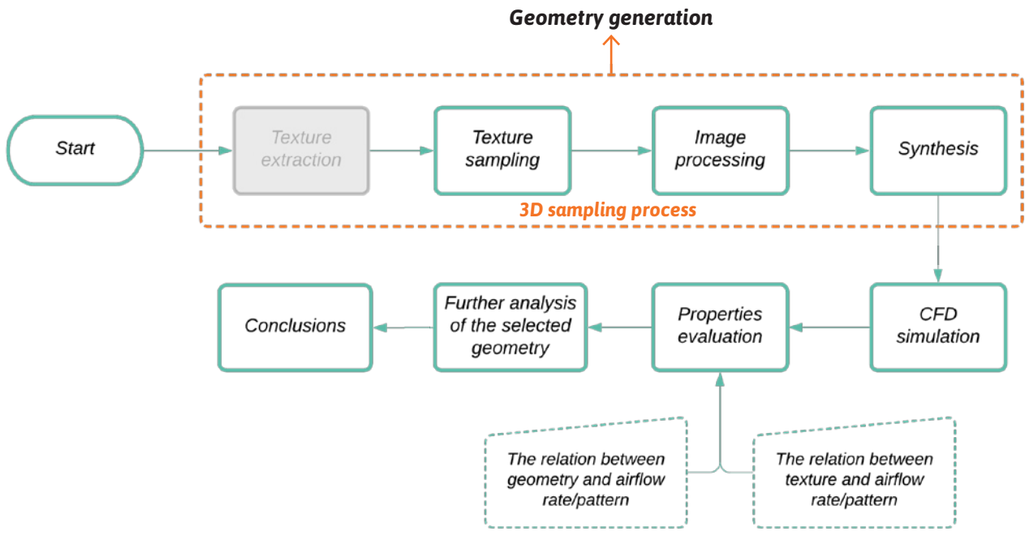

Figure 60: Digital workflow. Source: Author.

4.4.1 Texture extraction

Usually, the textures need to be extracted from 3D scanned models, especially if a particular texture is to be studied. However, the goal of this research is to explore the effect of different textures on airflow rate and pattern, rather than studying specific textures. Therefore, a large archive of textures is needed which is accessed via the online texture database.

4.4.2 Sampling

Using the online texture database, a wide range of different textures are selected. Then, they are filtered based on the features defined in section 4.2.1 and the selection is narrowed down to 30 textures. Some of them are shown below (the full selection can be seen in Appendix C).

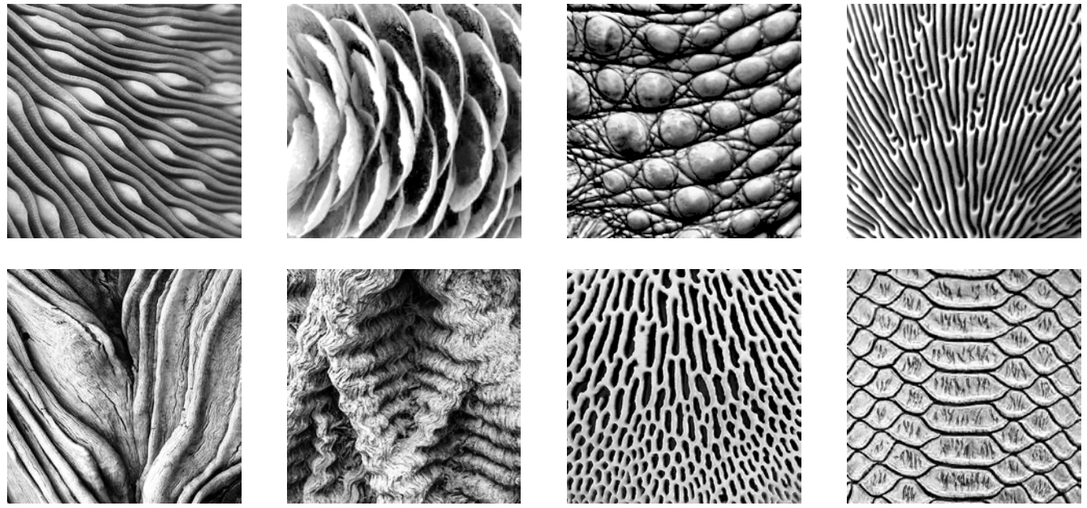

Figure 61: Some of the final selected textures. Sources for all texture can be found in the appendix.

4.4.3 Image processing

In this stage, the raw textures are edited to supply the final texture samples. If the texture is not black and white, then the first step is to convert the colored image into a black and white image. By doing this, the factor of color is eliminated and makes the comparison easier. Then, histogram equalization is used which is a technique that adjusts the intensities of the image to improve its contrast and provides better consistency in the sample textures. This is done by increasing the contrast of the grayscale texture through distributing intensities of the texture on the full grayscale spectrum. Depending on the texture, further steps can be taken to adjust the sample size of the texture, such as scaling and cropping.

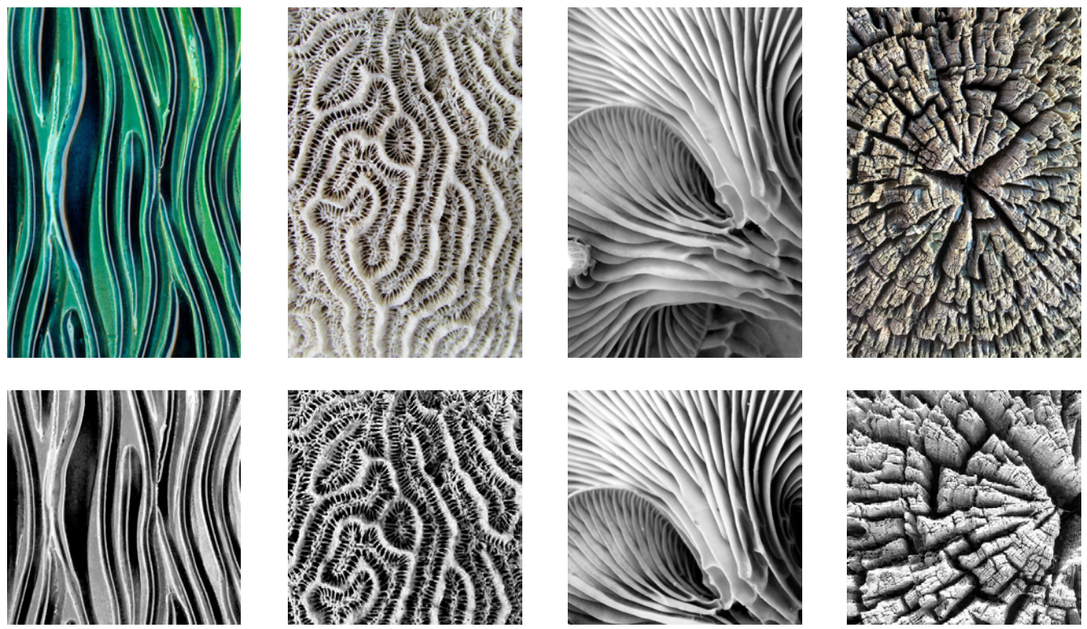

Figure 62: Up: raw textures, down: textures after image processing. Sources for all texture can be found in the appendix.

4.4.4 Synthesis

In this phase, a unit cell is synthesized. First, the sample texture is mapped onto a surface. The translation of the texture on the surface can be controlled by using the graph mapper component which is based on mathematical functions. The gap between each two unit-cell is closed so that when the geometry performs as a fluid-structure, its effect is not negated by the cavities which are not "designed" as the pores of the geometry.

At this point, some parts of the code are set manually, such as the graph type and input data used in the graph mapper, the thickness of the layers, the spacing in the unit cell, etc. However, as part of the future developments, the ideal approach is to have parametric control over these factors that could later allow for digital optimization of the geometry.

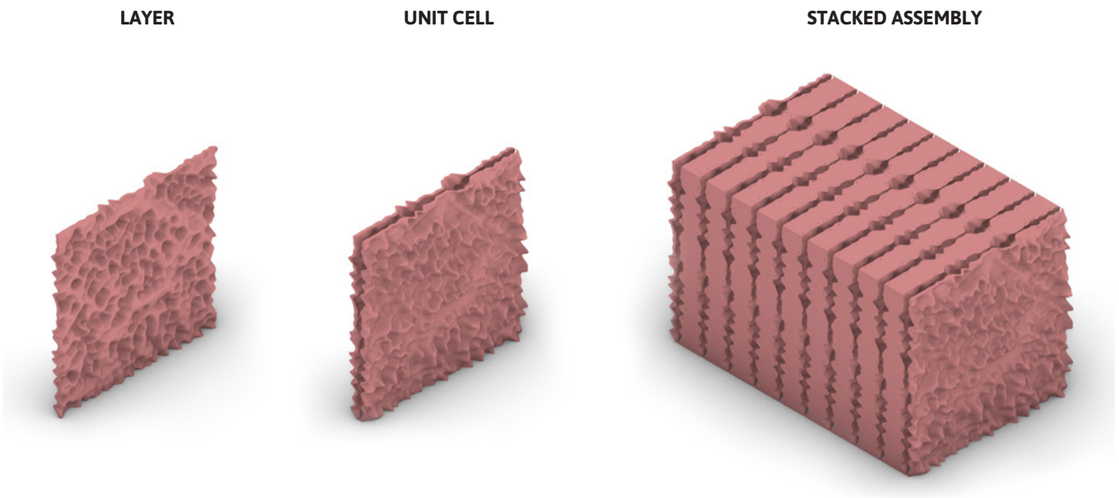

Figure 63: Unit-cell generation in Grasshopper. Source: Author.

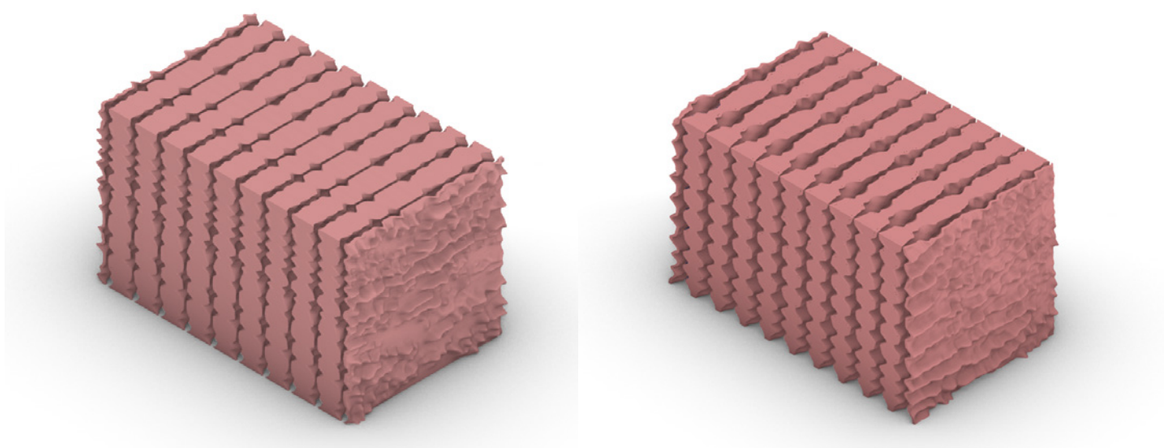

Figure 64: Geometry variations based on different sample textures. Source: Author.

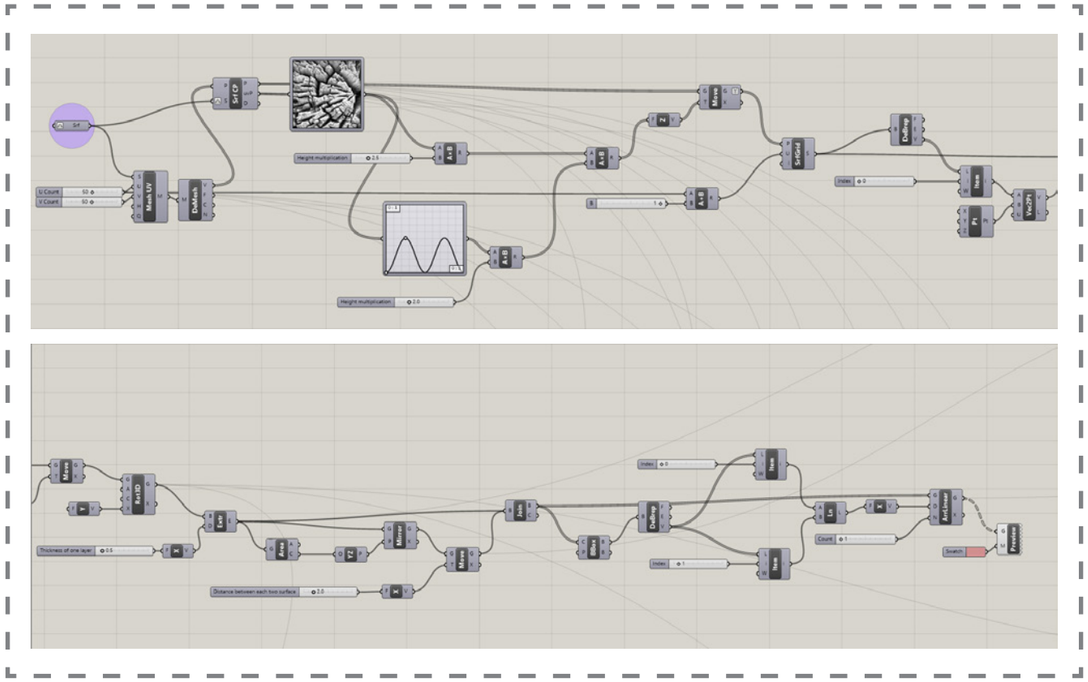

Figure 65: Geometry generation in Grasshopper. Source: Author.

The reason for choosing textures to generate geometries instead of using already existing structures such as Gyroid, Diamond or Schwarz P was a research approach. A texture gives an initial idea of how the airflow can move and be affected inside the geometry. Also, it gave more control and was simpler to envisage the expectations. This was proved in the CFD analysis.

4.5 Digital workflow: CFD simulation

Geometries that are selected for evaluation are based on the two categories of factors that can affect the airflow rate or pattern, which were introduced in section 4.2:

- Factors related to the texture
- Factors related to the geometry

From the geometry-related factors, surface roughness and volume of the cavity are expected to be more influential. Here, it is important how surface roughness is defined.

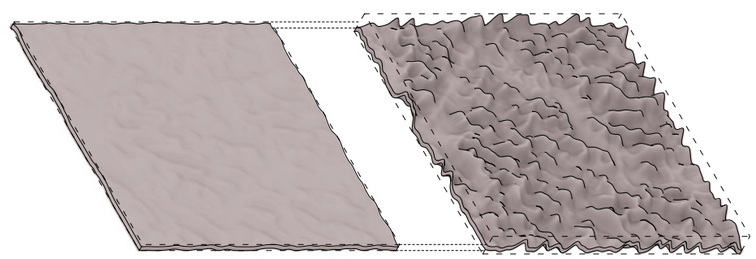

Figure 66: Assigning volume of the added mass to surface roughness. Source: Author.

Below, two approaches are presented that can result in the surface roughness of the geometry.

1- Calculating the volume of the added mass
2- Mass addition of distances from centroids of the modified mesh to the original mesh

The designed geometries in this thesis have a rather high surface roughness and thus, it is not possible to compare the obtained pressure drops from the CFD simulations to the values of the pressure loss chart. To make such a comparison, the obtained pressure drops have to be compared with the derived values from the Moody Chart (section 3.10.2). In this process, first, the surface roughness is calculated by the mass addition of the distances from centroids of the modified mesh to the original mesh. Then, the absolute surface roughness and relative surface roughness can be determined. Next, the friction factor can be obtained using the Moody chart. Finally, the pressure drop can be calculated based on the mentioned formula in the literature review.

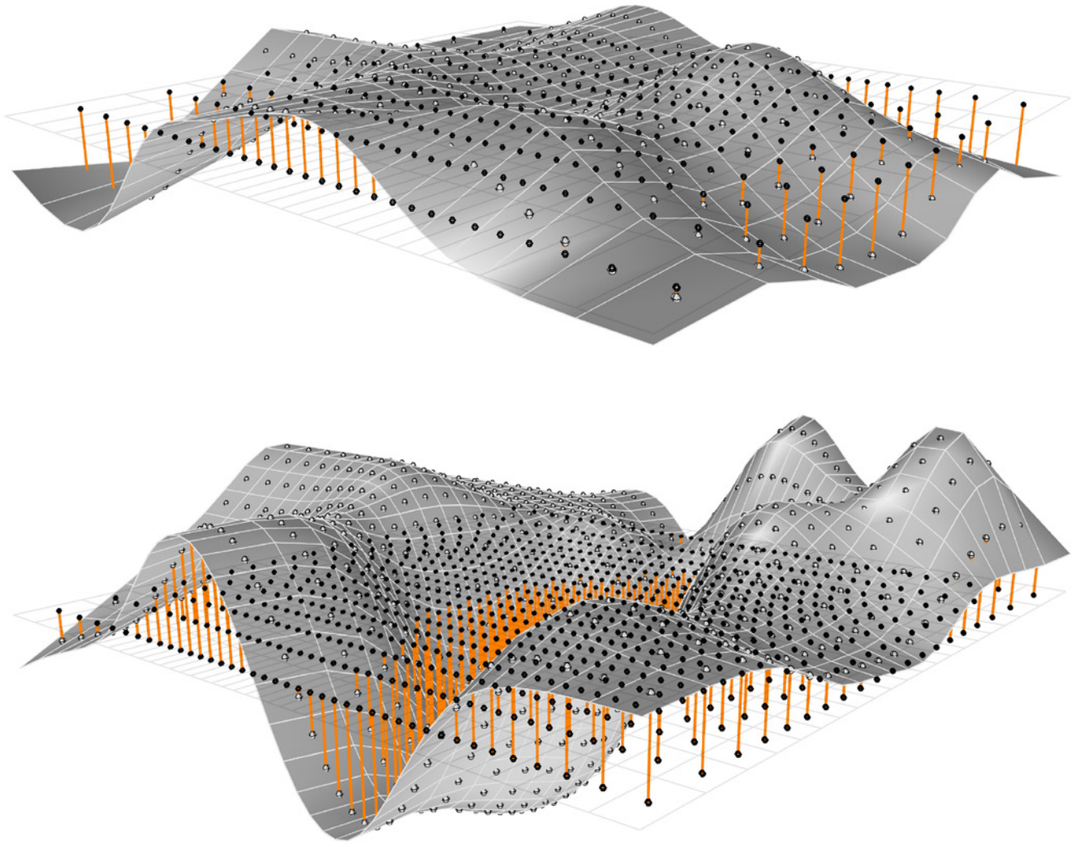

Figure 67: Assigning the mass addition of distances from centroids of the modified mesh
to the original mesh to the surface roughness, up: lower surface roughness, bottom: higher surface roughness.
Source: Author.

4.5.1 Simulation tool: Ansys Fluent

Simulation of the geometries is done using CFD (computational fluid dynamics) analysis in Ansys Fluent. Fluent is a CFD solver that is part of the Ansys Workbench platform. This powerful tool is commonly used in the aerospace field and it allows for running laminar or turbulent flow simulations. Compared to other available software, the biggest advantage offered by Ansys Fluent is that it allows for simulations inside complex geometries as well.

Probably, the biggest technical challenge of this thesis was the part for CFD simulations. It was expected that after spending some time learning the software, the simulations could be set up. However, during the first 8 weeks spent on this phase, almost no results were achieved because the meshing step was far more complicated than expected.

To start the CFD analysis, the geometries were first extracted from the Grasshopper code. They were imported into Ansys Fluent as the input geometry and then the meshing was done in Fluent.

4.5.2 Analysis setup

The next step after meshing is the analysis setup. In the general tab, there are two types of solvers, pressure-based and density-based. The pressure-based solver is used for incompressible flow and the density-based solver is applied to compressible flow. Since the fluid material is air, the pressure-based solver is selected.

Whether the flow is steady or transient can be chosen here as the solution mode. Although the flows in all geometries here are steady turbulent flows, the transient solution mode is selected for them since the device behavior is not constant and changes with time. Different flow type models can be selected based on the geometry. SST K-omega is opted as the turbulence model for these geometries as it gives the most accurate results considering the complexity of the geometries. The K-epsilon model is avoided because it is known that it can be inaccurate for strong curvatures (eddies) in the flow.

To specify which materials are used in a region, cell zone conditions are applied. Air is assigned to the material of the fluid domain in the simulations.

Boundary conditions are applied to control the solutions at the internal and external boundaries. Different types are available to define the boundaries. Finally, to run the simulation, the number of iterations and time steps are defined.

Boundary conditions

To solve any computational fluid dynamics problem, boundary conditions have to be defined as they are an essential part of the mathematical model. In Ansys Fluent, boundary conditions such as inlet, outlet, walls, axis, periodic, symmetry, etc are available. The following settings are used as the boundary conditions for the simulations:

Inlet

- Type: Velocity - inlet
- Velocity specification Method: Magnitude, Normal to Boundary
- Velocity magnitude: 2 m/s

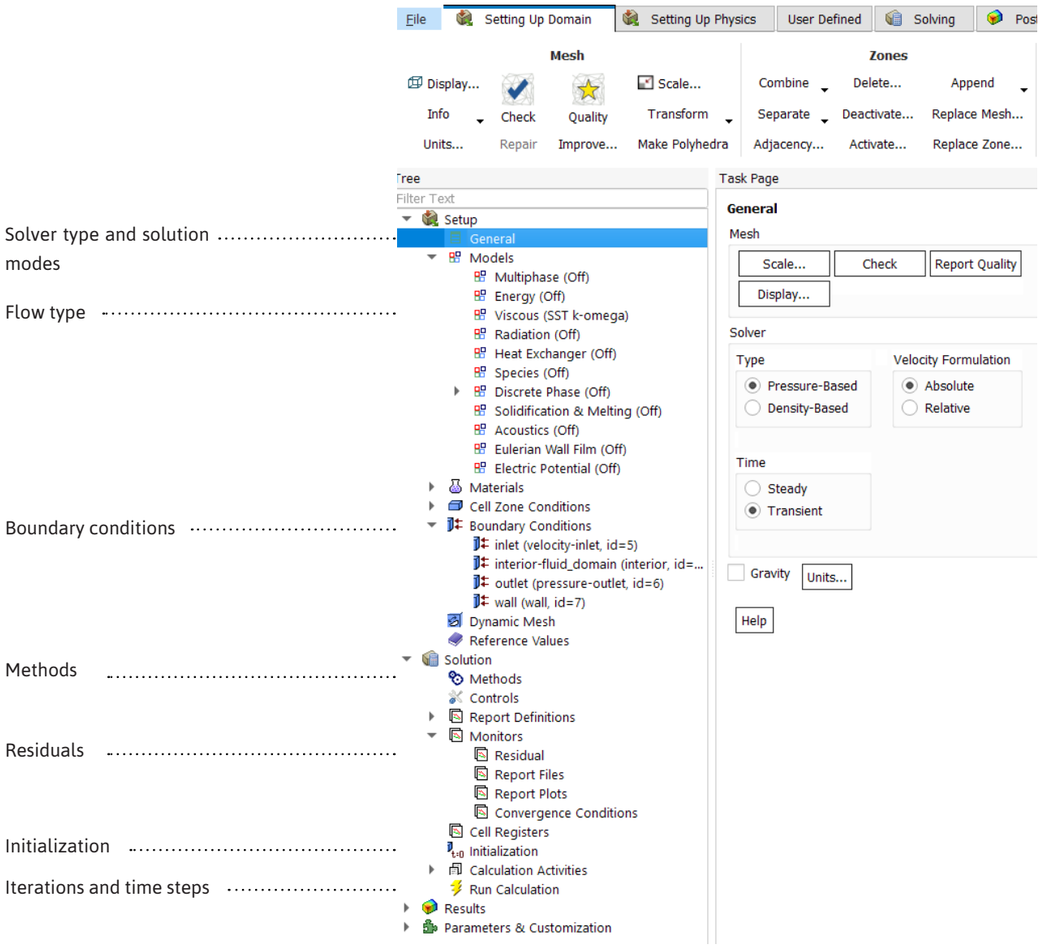

Figure 68: General settings used for CFD simulation in Ansys Fluent. Source: Author.

Velocity inlet boundary conditions are used for incompressible flow simulations.

Outlet

- Type: Pressure - outlet
- Gauge pressure: 0 Pascals
- Back-flow direction specification method: Normal to Boundary
- Back-flow pressure specification: Total pressure

Outlet boundary conditions set an outflow condition based on the flow pressure at the outlet.

Walls

- Type: Wall
- Wall motion: Stationary wall
- Shear condition: No slip

The no-slip condition sets the velocity near the solid parts to zero and defines the velocity profile.

Solution methods

The pressure-based solver chosen in the general tab allows for solving the flow problem in either a segregated or coupled approach. Ansys Fluent offers five options for pressure-velocity coupling algorithms: SIMPLE, SIMPLEC, PISO and Coupled. The segregated approach solves the continuity, momentum and energy equations (if needed) in a sequential manner. SIMPLE, SIMPLEC and PISO use this algorithm. However, in the coupled scheme, the continuity and momentum equations are solved together. Using a coupled algorithm is recommended for transient flows as it offers robust results and it uses fewer iterations to achieve the results compared to the other options.

Residuals and convergence

Residuals are an essential part of an iterative solution's convergence. In a CFD analysis, residuals measure the error in the obtained solution; meaning that the lower the residual, the more numerically accurate the solution is. Commonly, residual levels of 1e-04 are assessed to be loosely converged. Residual levels of 1e-05 show well-converged solutions and 1e-06 display tightly-converged solutions. 1e-06 is set for residuals criteria in the simulations of this section. However, it might not be possible to achieve such low residual levels in these complex geometries.

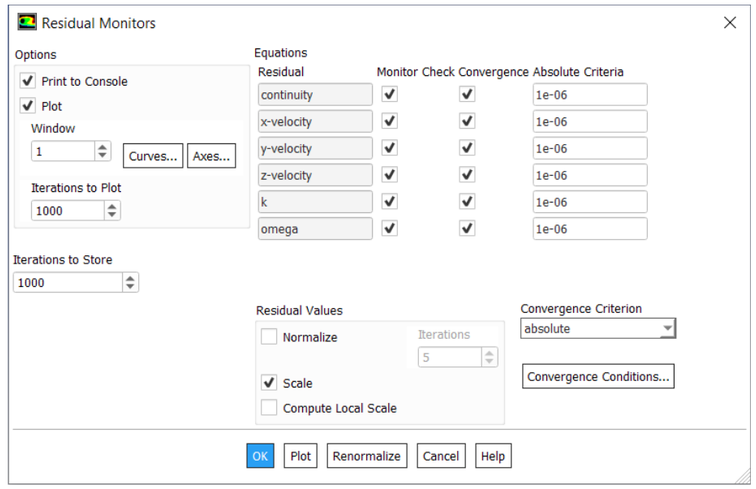

Figure 69: Residual monitors used for CFD simulation in Ansys Fluent. Source: Author.

4.5.3 Importance of meshing

The meshing of the geometry highly affects the accuracy of the obtained results. In the meshing process, the geometry is translated into mesh faces. Using a high number of mesh elements makes the transition between the faces smoother. Therefore, the translation of the geometry is more precise and closer to the real geometry. However, the student version of Ansys Fluent has a limit of 512000 for the number of mesh elements. If the number of mesh elements is higher than the limit, the mesh is generated but it cannot be used in the next steps. So the number needs to be reduced to proceed to next steps.

Although this number (512K) can be easily achieved for simple geometries, it was quite a low number for the complex geometries which were designed in this thesis. This made the meshing process very challenging.

Among aerospace students, meshing is somehow considered as an art. It requires a lot of experience and knowledge to be able to do the meshing correctly in the first attempts. Since the settings which are used in an analysis depend on the geometry and its features and complexity, there are not certain steps to follow to achieve a fine correct mesh. Usually, settings which are used in an analysis for a specific geometry cannot be used for another geometry. There needs to be changes and alterations according to the new geometry. This made the meshing step even more difficult because Ansys Fluent is not commonly used among building technology students and the author did not have any guidelines to follow for this step.

Considering the limitations of the student version of Ansys, complexity of the geometries, inherent difficulty of the meshing process and lack of fixed rules or guidelines to follow, this was the most challenging and time-consuming step of the CFD analysis.

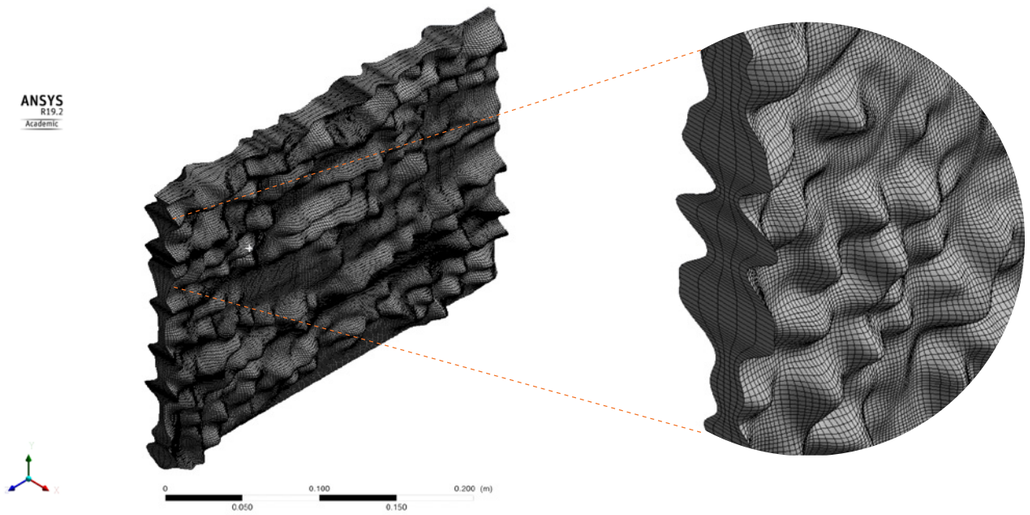

Figure 70: Prism meshing for geometry 1, with a number of mesh elements of 205920. Source: Author.

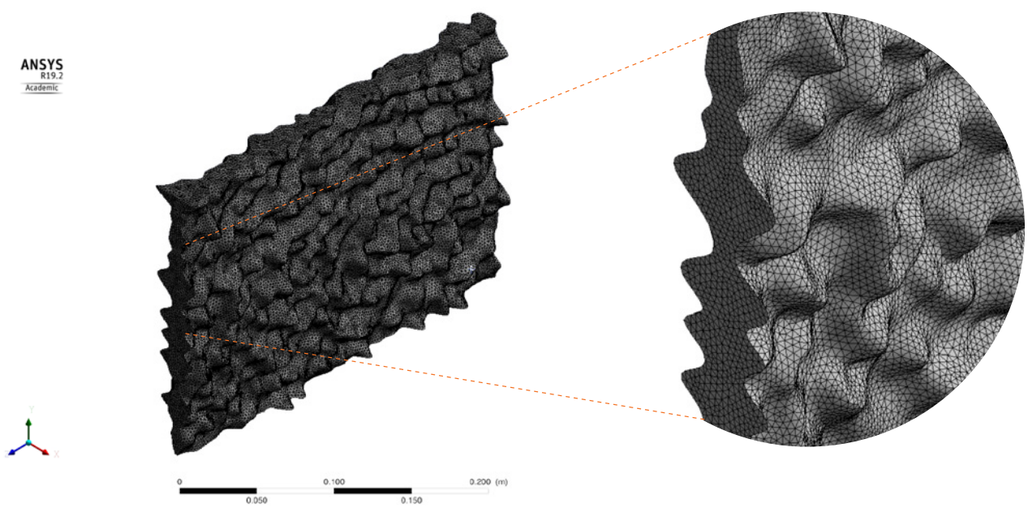

Figure 71: Tetrahedral mesh for geometry 3, with a number of mesh elements of 315100. Source: Author.

4.6 Digital workflow: Properties evaluation

The simulated geometries in this section represent the cavity in the unit-cell, as the cavity corresponds to the fluid domain in the CFD analysis. Another approach was to use the unit cell itself and define the two layers as solids and set the cavity in between as the fluid domain. However, due to the limitation of the student version of the software regarding the number of mesh elements, the first approach is utilized as it only simulates the cavity as the fluid domain and therefore results in less number of mesh elements.

As mentioned before, the ideal goal of this design is to have an adaptive microstructure that can regulate the flow rate. However, simulating a fluid-structure interaction (FSI) is highly complicated and beyond the limits of the master thesis. Therefore, to be able to envisage the performance of the geometry in such a system, a different approach was taken that could resemble the fluid-structure interaction. To do so, three scenarios were defined for each tested geometry:

- The main geometry (the initial state)
- A smaller cavity volume: this variation has a lower permeability compared to the main geometry and resembles the design in high-velocity scenarios, as the geometry is expected to become less permeable and less open to the outside air.
- A larger cavity volume: this variation offers a higher permeability compared to the initial state and corresponds to the low-velocity scenarios. In this variation, the geometry becomes more open to the outside air, to allow more air into the room.

It has to be noted that there are more positions for each geometry and these three scenarios are just representatives of the fluidity of the structure.

Simulations of the smaller cavities were done at a later stage due to technical challenges and for this specific scenario, the research version of Ansys was used, as it was impossible to stay below the meshing limit of the student version for such complex geometries with holes. Also, manual adjustments had to be done for these specific variations. This included adding 1-2 mm to the width of the cavity in the middle because it was found that Fluent could not place mesh faces in places where the two surfaces would meet as the distance between them was too small.

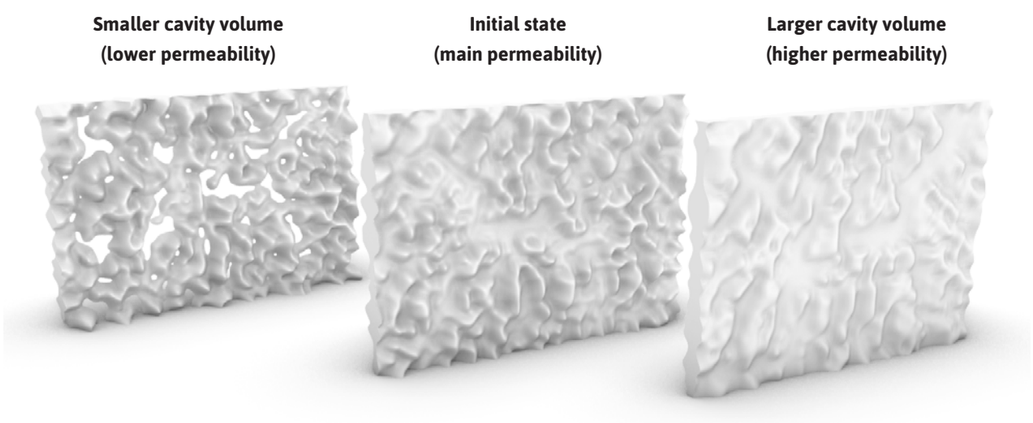

Figure 72: Three scenarios of a geometry, to resemble how the fluidity of the structure would be. Source: Author.

4.6.1 Geometry 1 - (G1)

Geometry 1 is based on texture 10 (Appendix B), which does not have a dominant direction but rather has a pattern of radial distribution. Figure 74 depicts the fluid domain in this geometry. The geometry was imported from Grasshopper into Ansys Workbench as ACIS file and the meshing was done in Ansys Fluent. The method used for the meshing implemented prism layers and resulted in 205920 mesh elements (mesh faces). The ratio of inlet area to the outlet area was 1.45.

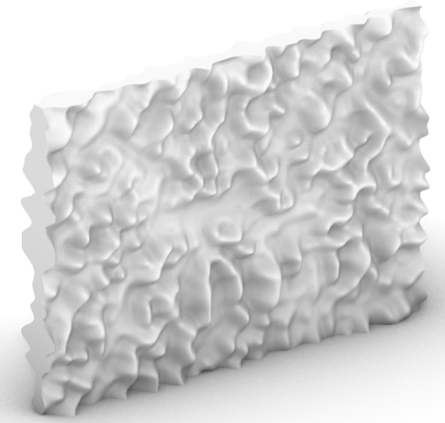

Figure 74: Geometry 1 used for CFD simulation in Ansys Fluent. Source: Author.

By defining the velocity at the inlet boundary, the resultant total pressure drop was 31.53 Pa; with the average inlet pressure of 38.61 Pa and average outlet pressure of 7.08 Pa. The values in the legends of figure 78 show the maximum and minimum limits inside the whole domain. Usually, there are local zones inside the domain where the pressure can be much higher (stagnation zones) and other parts where the pressure can be much less (separation zones). Therefore, the pressure drop is normalized with the inlet pressure to allow for a better comparison between the geometries.

$$\textbf{Normalized pressure drop} = (P_{in}-P_{out})/P_{in}$$

Thus, the normalized pressure drop was 0.81.

Figure 75 displays the velocity streamlines in the cavity as a snapshot in time. The average outlet velocity over the outflow boundary was 3.16 m/s which was higher compared to the 2 m/s inlet velocity. Before the simulation, it was expected that the geometries based on direction-less textures would have chaotic streamlines in their fluid domain. However, this did not occur. Nonetheless, this might be different in geometries based on other direction-less textures. Additionally, the influence of direction-less textures could be more intensified when the width of the cavity is smaller.

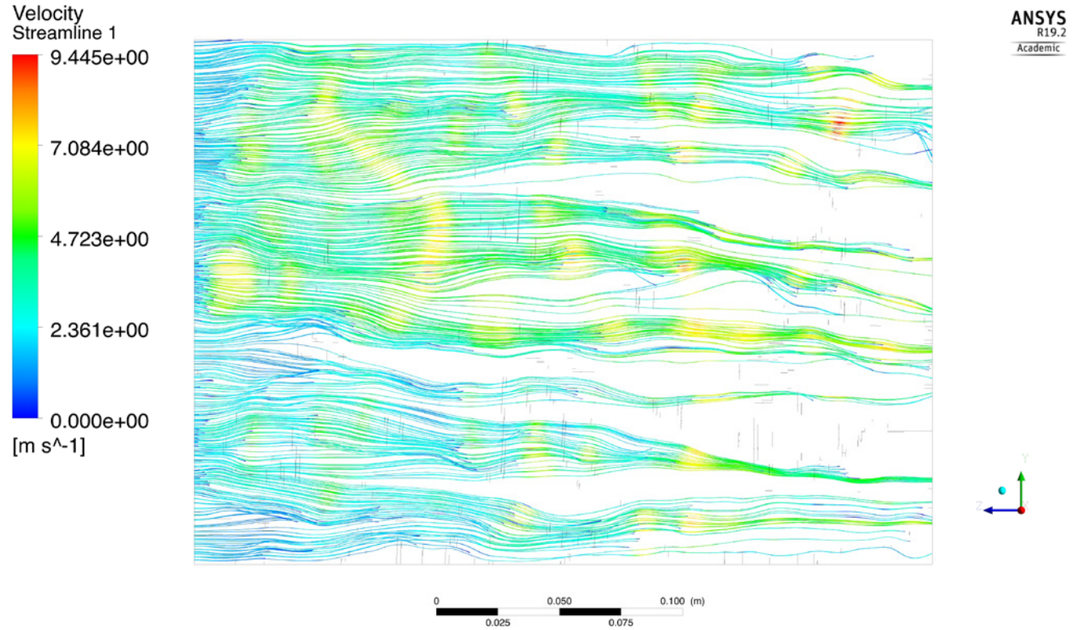

Figure 75: Velocity streamlines in Geometry 1, high velocities appear in cross-sectional areas corresponding to the black parts of the base texture. Source: Author.

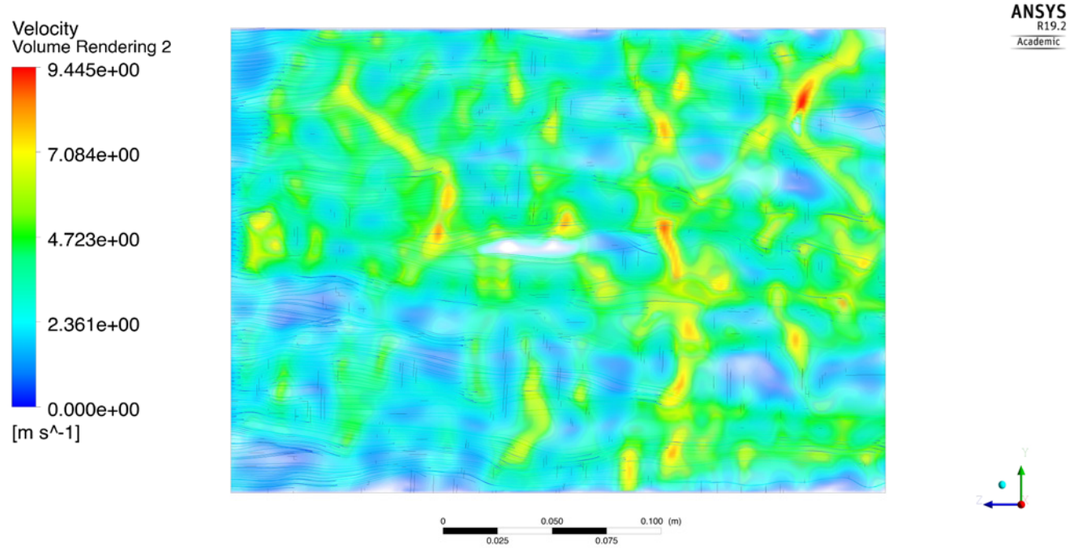

Figure 76: The radial distribution pattern of the base texture can be identified based on the high-velocity areas. Source: Author.

High velocities (red areas in the above figure) occurred in parts of the geometry which were corresponding to the black areas of the base texture. The reason behind this was clear, because the white parts of the texture were considered positive in the surface height and the black parts as negative (This approach is discussed in detail in section 4.1.1.4). Therefore, black parts of the texture would correspond to smaller cross sectional areas, thus having higher velocities, as seen in figure 76.

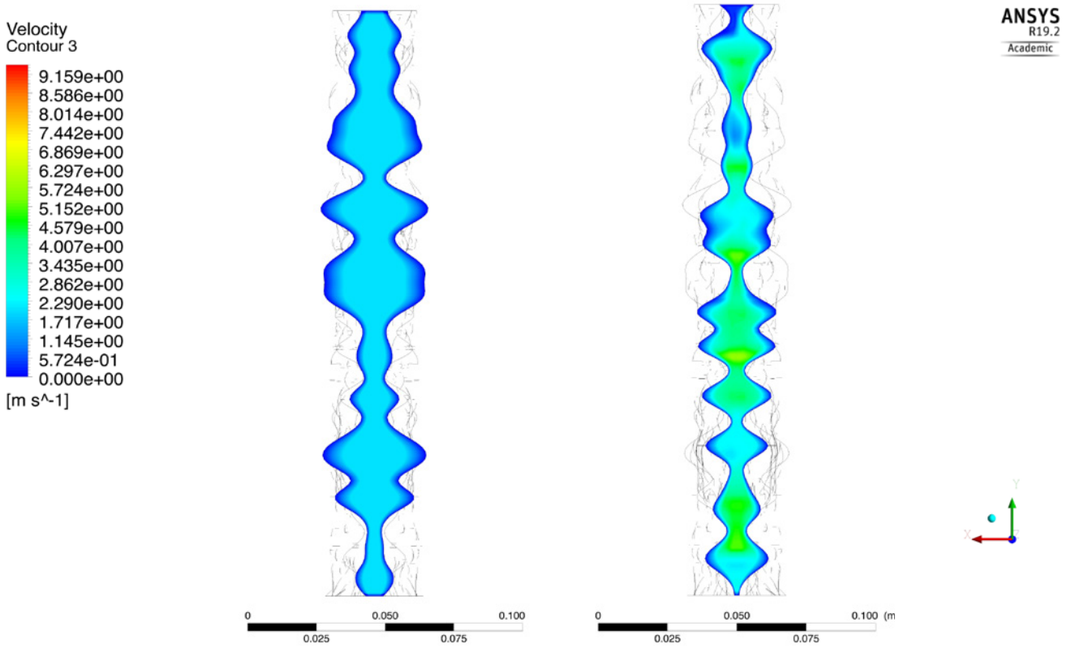

Figure 77: Left: Velocity contour at the inlet. Right: Velocity contour at the outlet, showing non-uniform and higher average outlet velocity compared to the inlet velocity. Source: Author.

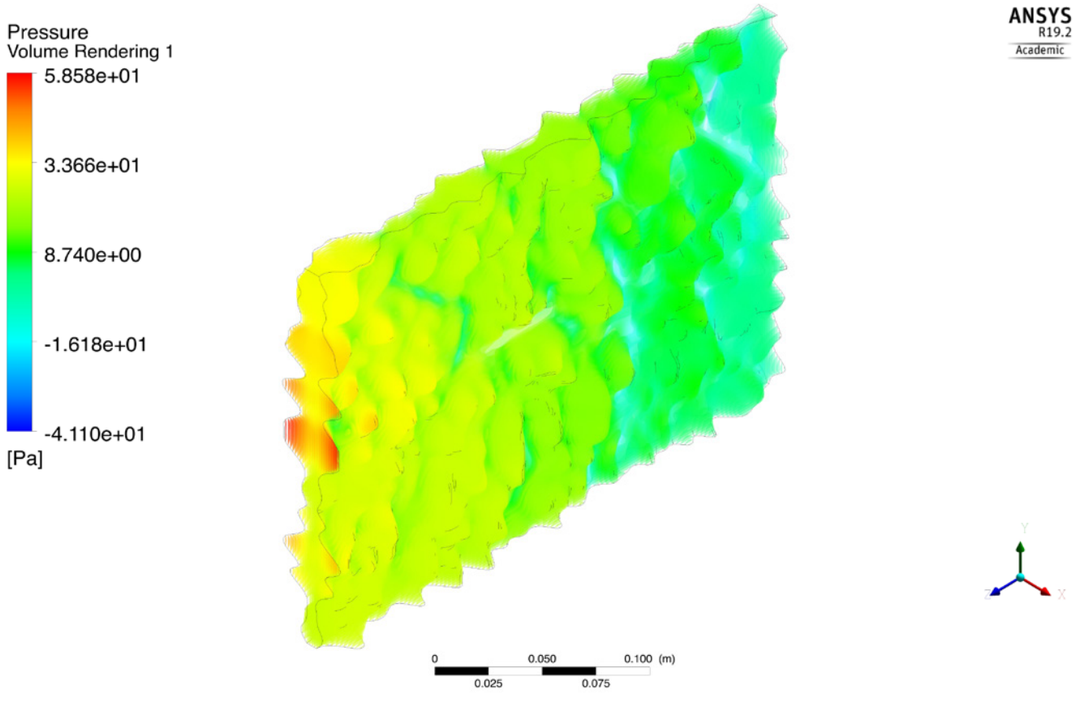

Figure 78: Pressure volume rendering in G1. Source: Author.

Variation A - Larger cavity volume (G1-A)

This variation had a slightly larger cavity volume (949 cm^3) compared to the main geometry (898 cm^3). The meshing was done using prism layers and resulted in 47000 mesh elements. The ratio of the inlet area to the outlet area was 1.01.

The average inlet and outlet pressure had much lower values compared to the main geometry, with the values of 6.43 Pa and 2.65 Pa respectively. The normalized pressure drop in this variation was 0.58 Pa.

Although the volume of the cavity in this variation was marginally larger, the velocity range in this geometry was almost one-third of the velocity range in the main geometry. In the main geometry, maximum velocity reached 9.44 m/s while it was 3.74 m/s in variation A. As expected, due to larger cavity volume and bigger inlet and outlet area, the velocity contour at the outlet was as uniform as the velocity contour at the inlet.

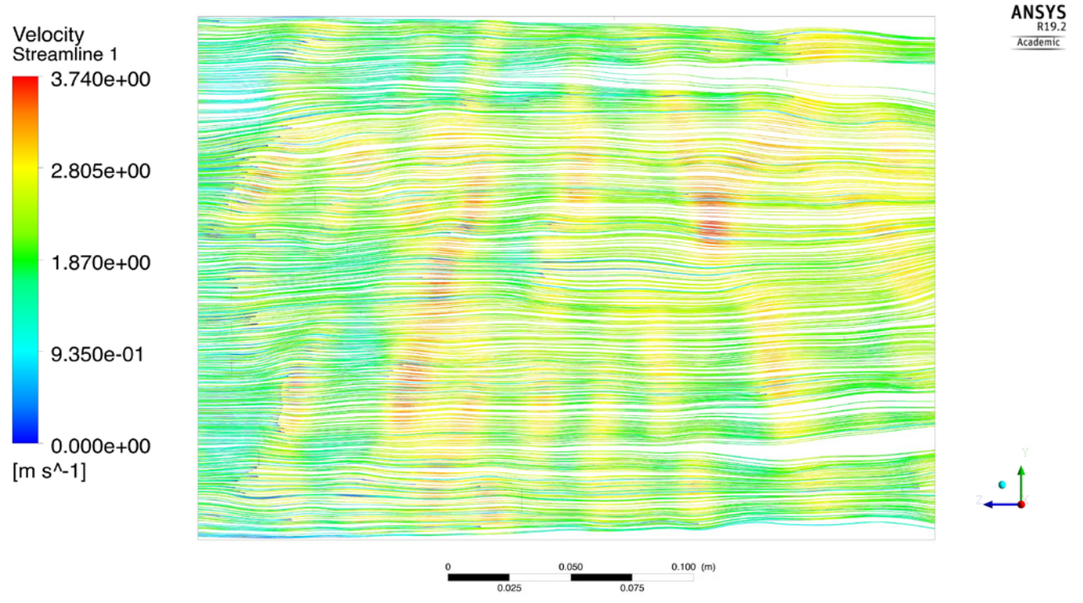

Figure 79: Velocity streamlines in variation A, with a smaller velocity range compared to the main geometry. Source: Author.

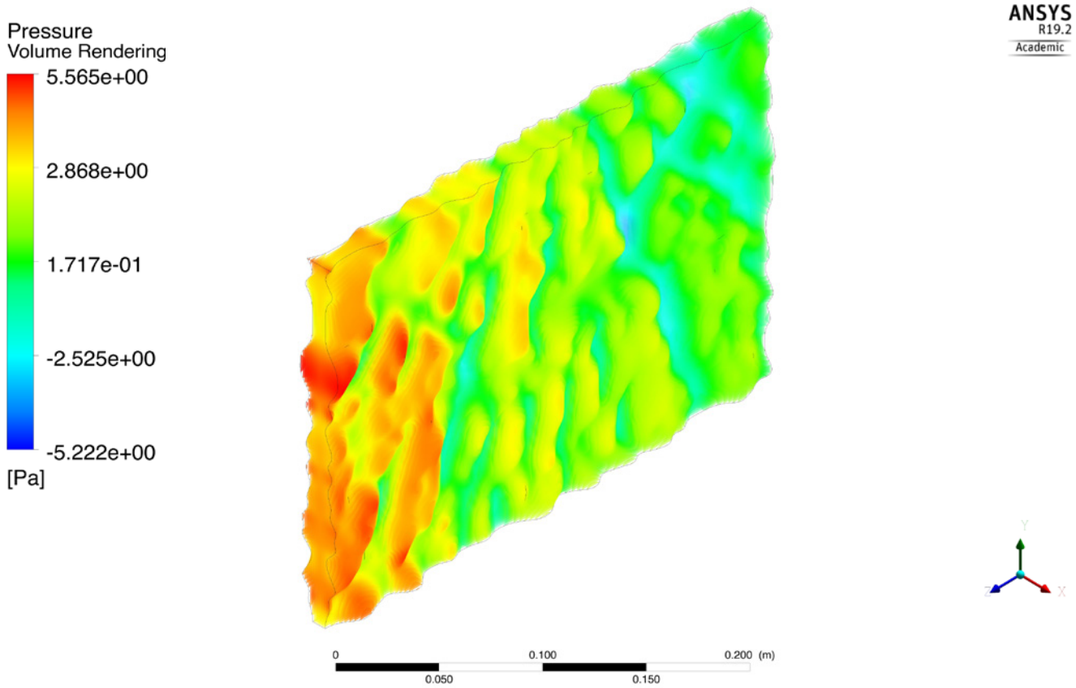

Figure 80: Pressure volume rendering in G1-A. Source: Author.

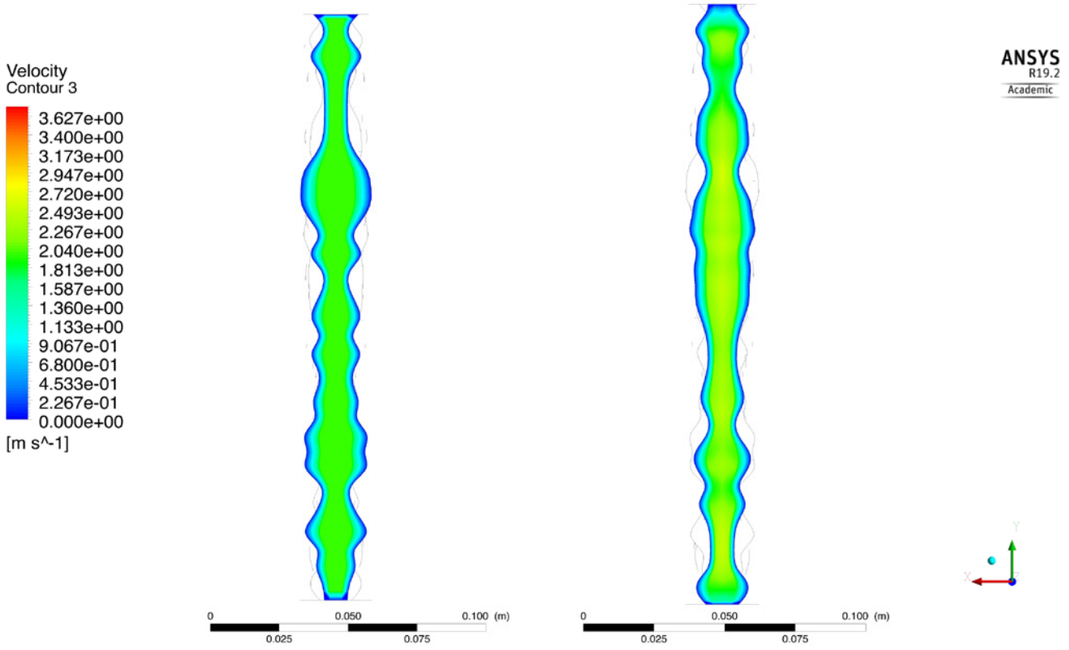

Figure 81: Left: Velocity contour at inlet, right: Velocity contour at outlet. The average outlet velocity is slightly higher and they both have an almost evenly distribution of velocity. Source: Author.

Variation B - Smaller cavity volume (G1-B)

The cavity volume in this variation was 823 cm^3. This variation is intended for when the outside velocity is high and therefore, the two layers in the unit cell have to become closer to permeate less air into the room. As a result, the parts that are taken out of the cavity in figure 82, show the parts where the two layers in the unit-cell intersect with each other. The meshing method used tetrahedrons and had 2698752 mesh elements. The ratio of the inlet area to outlet area was 1.09.

The normalized pressure drop in this variation was 0.98 which was the highest compared to G1 and G1-A. This was the result of the eddies and backflows that occurred in the geometry. The induced inlet velocity of 3.5 m/s reached to an average outlet velocity of 5.1 m/s .

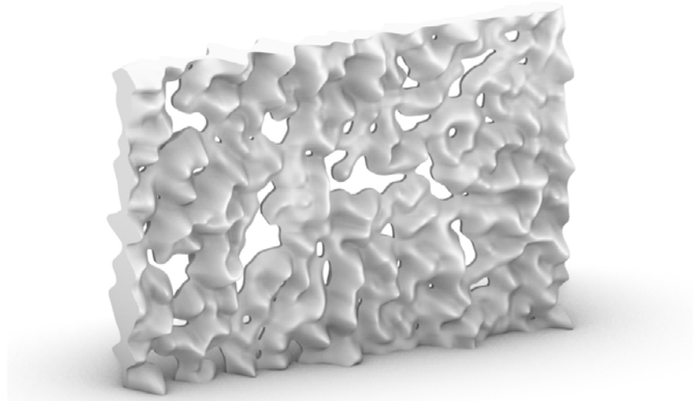

Figure 82: Variation B with smaller cavity volume. Source: Author.

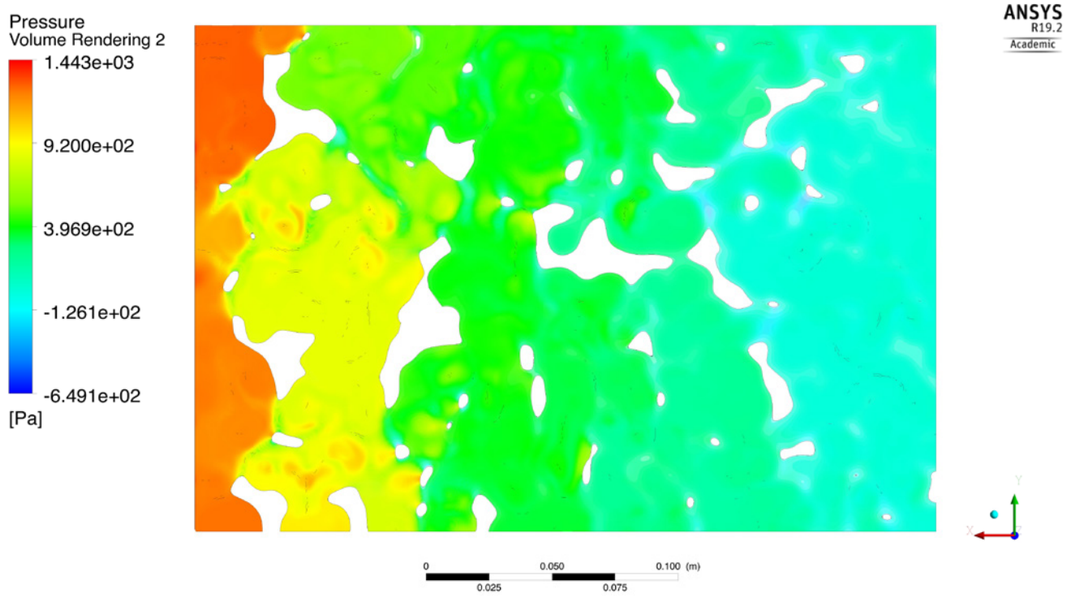

Figure 83: Distinct and high pressure-drops in the direction of fluid movement between large intersection areas of the geometry. Source: Author.

From the pressure volume rendering in figure 83, it was clear that the intersection areas (holes in the geometry) which were more vertically-directed (similar to a bluff body), induced major form drags, resulting in large changes of pressure along the direction of the flow. Distinct borderlines could be drawn between the vertical holes, representing areas with different pressures. However, where the intersections were more horizontal and similar to a streamlined body, the form drag was much less and therefore, the pressure drop was lower.

In figure 84, there are different recirculation regions, mostly placed between the bigger intersection areas of the two layers of the unit-cell. It was evident that the larger the intersection area, the higher its impact on the streamlines. Also, backflows occurred where the distance between the intersection areas was wide.

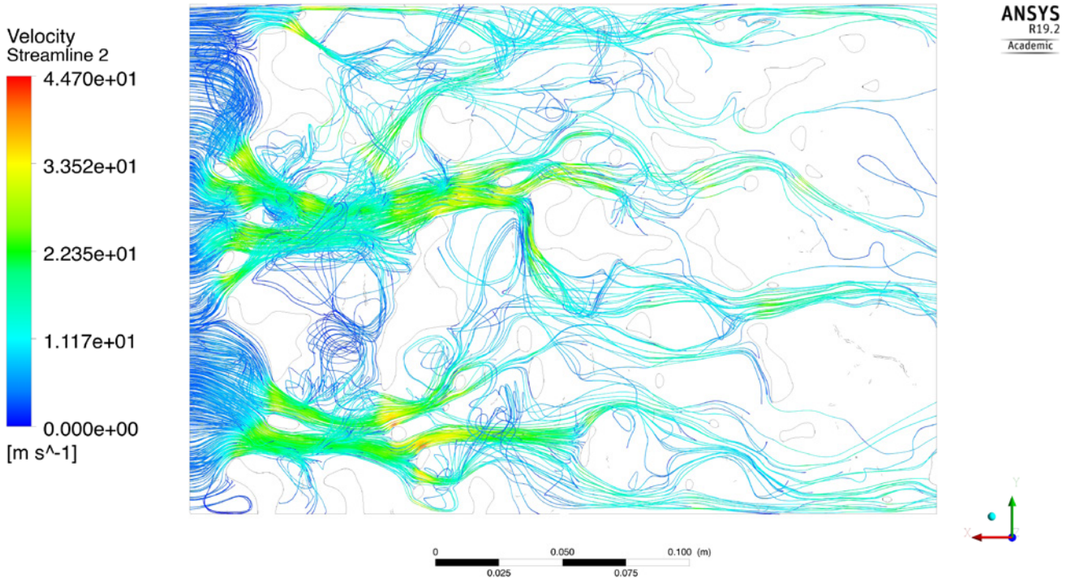

Figure 84: Velocity streamlines in variation B, turbulent flow shows eddies and recirculation of streamlines in different areas. Source: Author.

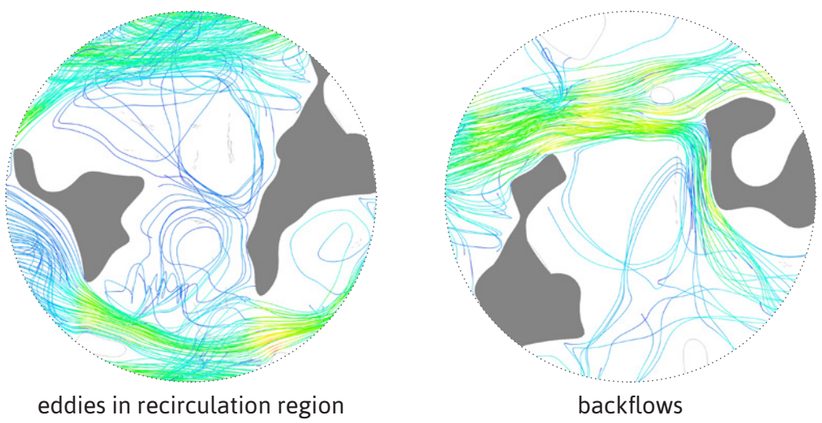

Figure 85: Eddies and backflow between the large intersection areas of the geometry. The grey areas show the intersection parts between the two layers of the unit-cell which correspond to the holes in the geometry. Source: Author.

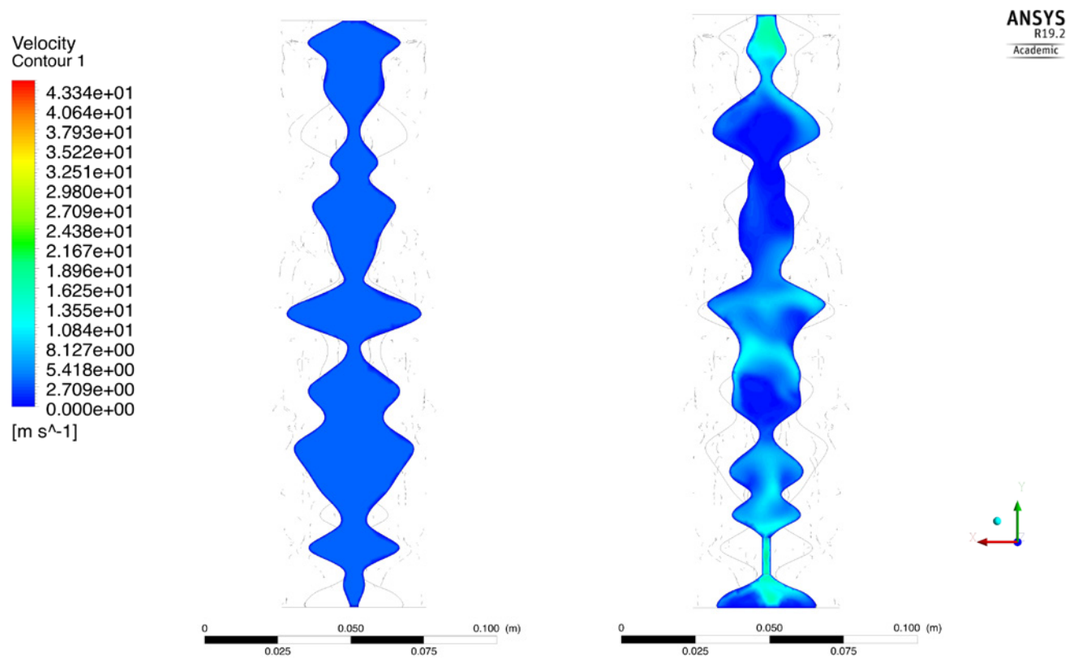

Figure 86: Left: Uniform velocity contour at inlet, right: Non-uniform velocity contour at outlet with a higher average outlet velocity. Source: Author.

Variation A and variation B had similar inlet to outlet ratios. However, the normalized pressure-drop in variation B was much higher than the main geometry and variation A. This was the result of vertical holes in the geometry, acting as obstacles along with the fluid flow and inducing large form drags. As expected, the larger the normalized pressure-drop, the higher the average outlet velocity was.

It was also noticed that the influence of texture in this geometry was not discernible and cavity volume as a geometry-related factor had a much higher impact on the pressure-drop and the average outlet velocity.

Geometry 1	Larger cavity volume (G1-A)	Main geometry (G1)	Smaller cavity volume (G1-B)
Cavity volume (cm^3)	949	898	823
Inlet to outlet ratio	1.01	1.45	1.09
Average inlet pressure (Pa)	6.43	38.61	1238.53
Average outlet pressure (Pa)	2.65	7.08	26
Normalized pressure drop ($\Delta P/P_{inlet}$)	0.58	0.81	0.98
Inlet velocity (m/s)	2	2	3.5
Average outlet velocity (m/s)	2.07	3.16	5.1

Table 5: Comparison among Geometry 1 and its variations with larger and smaller cavity volumes. Source: Author.

4.6.2 Geometry 2 (G2)

Geometry 2 is based on texture 12 (appendix B). Similar to texture 10, texture 12 is also direction-less. However, it does not have a dominant pattern of distribution. The geometry of the cavity which was used as the fluid domain can be seen in figure 87. The meshing was done using the tetrahedron method and resulted in 435719 mesh elements. The ratio of inlet area to the outlet area was 1.07. Similar to Geometry 1, geometry-related factors such as cavity volume had a larger impact compared to texture-related factors such as having no direction.

Here the average inlet pressure was 26.70 Pa and the average outlet pressure was 4.31, resulting in a normalized pressure-drop of 0.83. The pressure dropped almost linearly along with the flow. The average outlet velocity, 2.41 m/s, was slightly higher than the induced inlet velocity. Compared to the velocity contour at the inlet, the velocity contour at the outlet was not uniform.

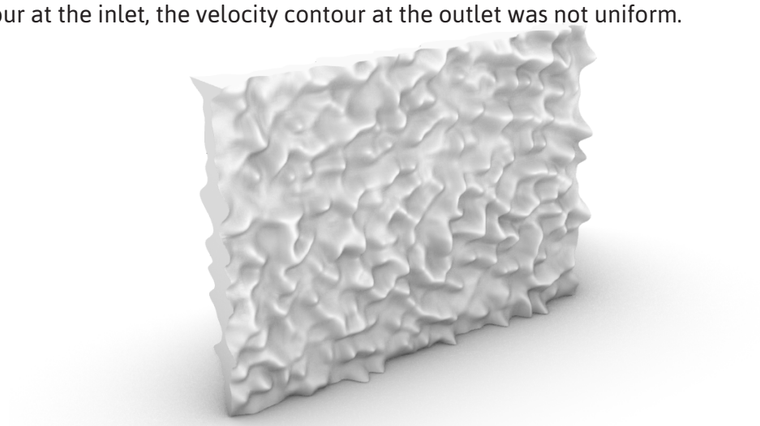

Figure 87: Geometry 2 used for CFD simulation in Ansys Fluent. Source: Author.

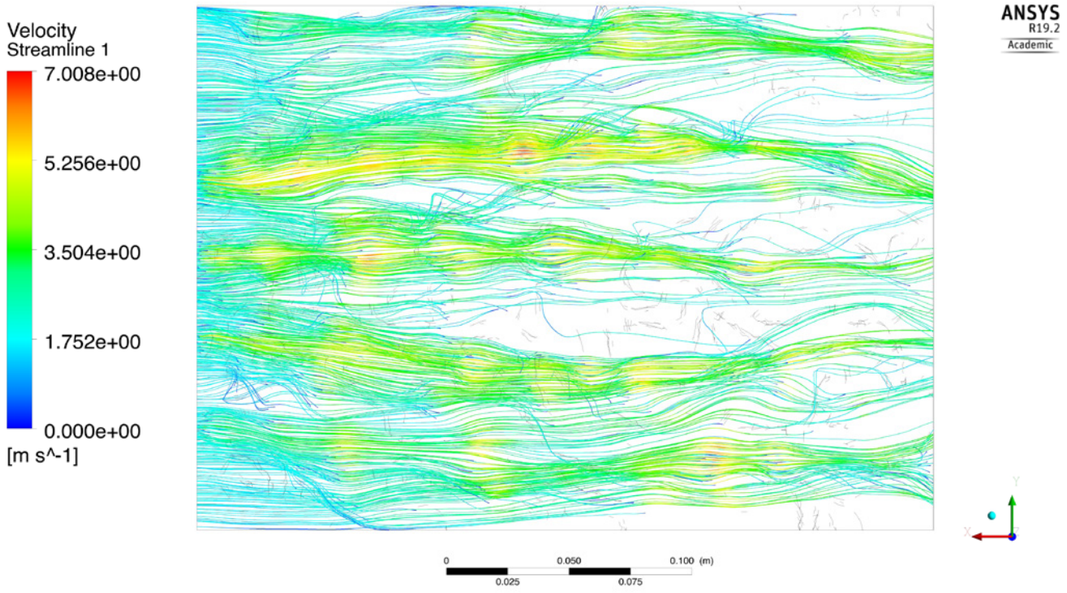

Figure 88: Velocity streamlines in Geometry 2. Since the base texture was direction-less, a distinct change in the velocity streamlines could not be identified. Source: Author.

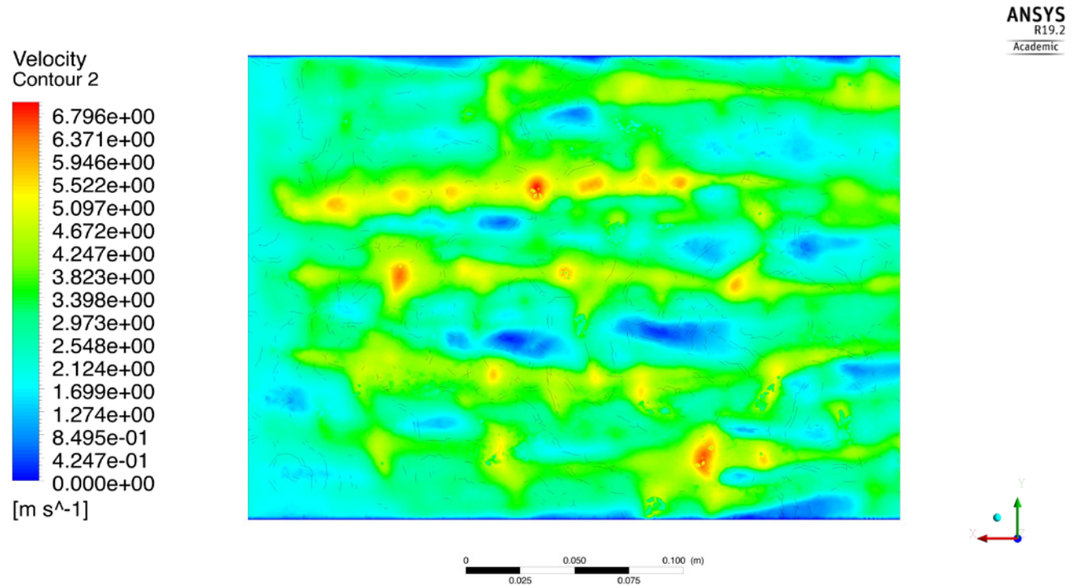

Figure 89: The base texture could not be traced based on the velocity contour. Source: Author.

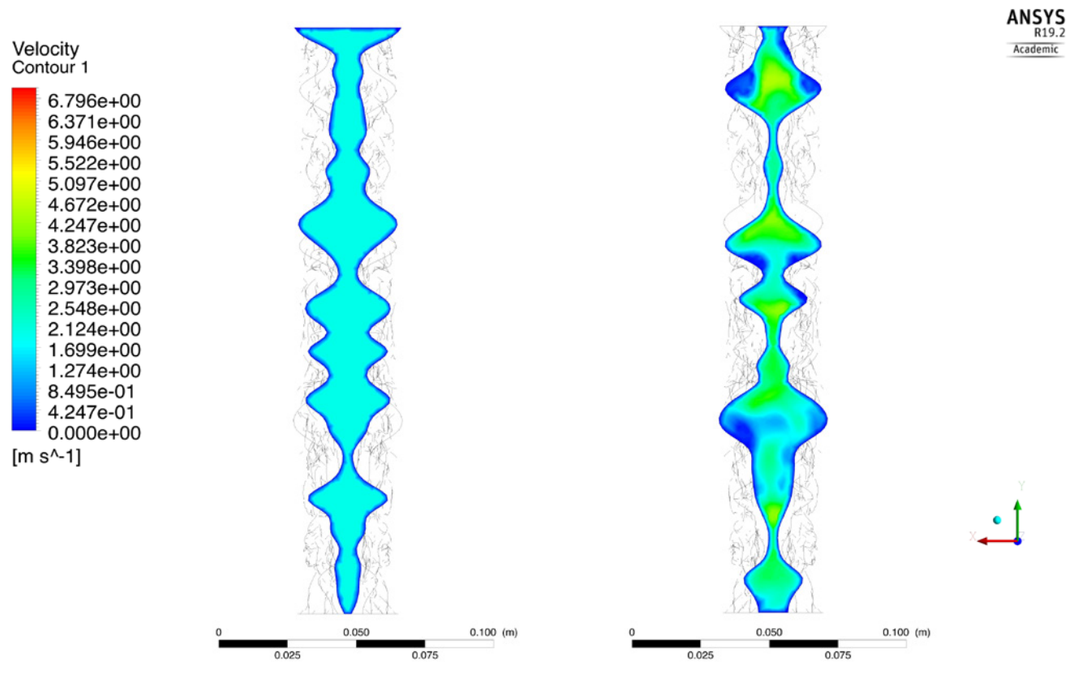

Figure 90: Left: Velocity contour at the inlet. Right: Velocity contour at the outlet with slightly higher average velocity compared to the inlet. Despite the inlet, the velocity contour at the outlet was not evenly distributed. Source: Author.

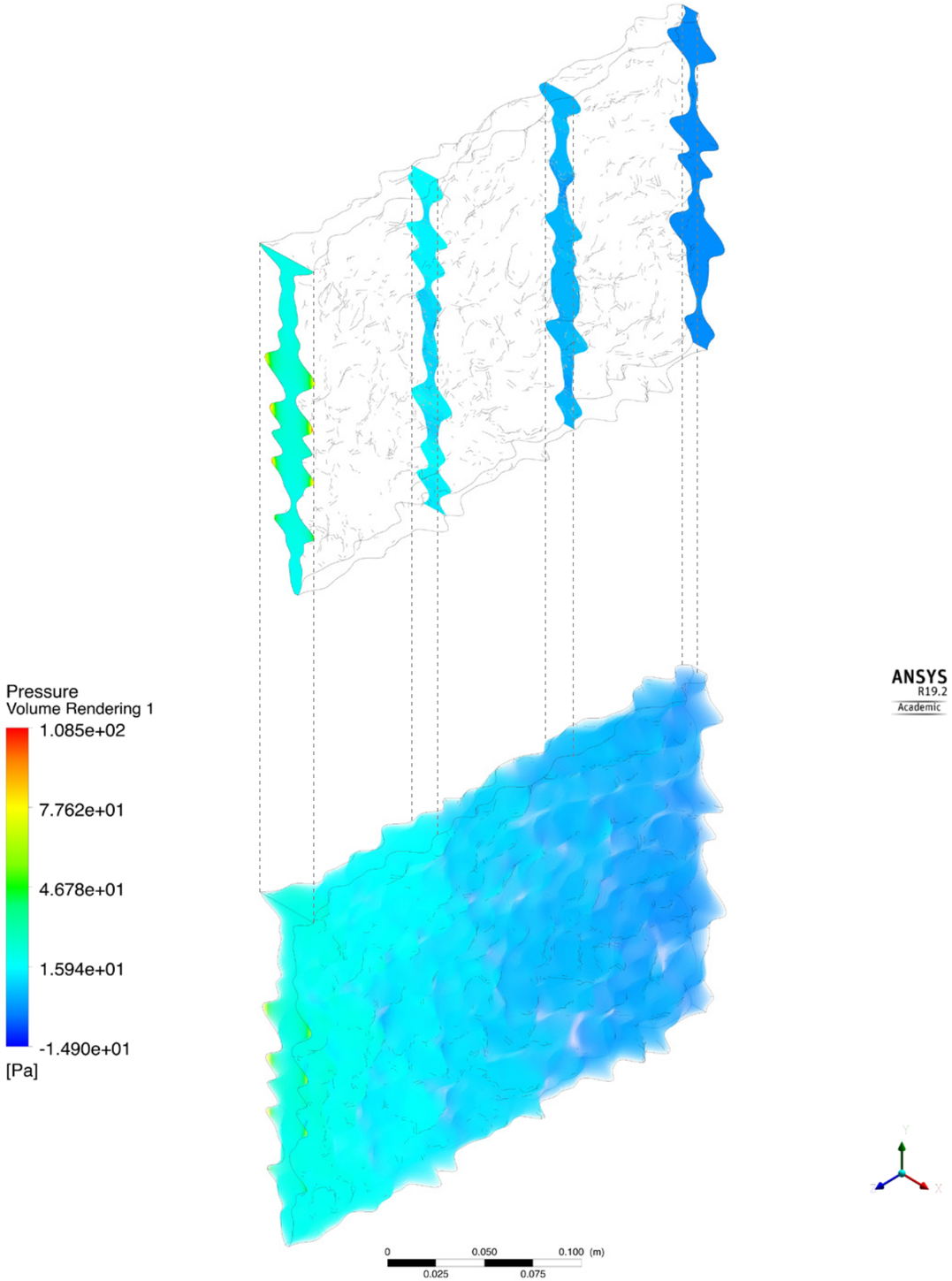

Figure 91: Pressure volume rendering in Geometry 2. Similar to velocity streamlines, there were no particular areas with too high or too low pressures. Source: Author.

Variation A - Larger cavity volume (G2-A)

The volume of the cavity in G2-A was 953 cm^3 which was 27cm^3 larger than the volume of the cavity in G2. Prisms were used in the meshing and resulted in 64260 mesh elements. The ratio of the inlet area to the outlet area was 0.99.

The normalized pressure-drop in this variation was 0.48 Pa, with an average inlet pressure of 4.90 Pa and an average outlet pressure of 2.52 Pa.

Similar to G1-A, G2-A also had a smaller velocity range compared to its main geometry G2. The velocity range in G2-A was almost one-third of the velocity range in the main geometry. In the main geometry, maximum velocity reached 7 m/s while it was 2.94 m/s in the G2-A variation. The average outlet velocity, 1.9 m/s, was slightly lower than the induced inlet velocity. As expected, due to larger cavity volume and bigger inlet and outlet area, the velocity contour at the outlet was as uniform as the velocity contour at the inlet.

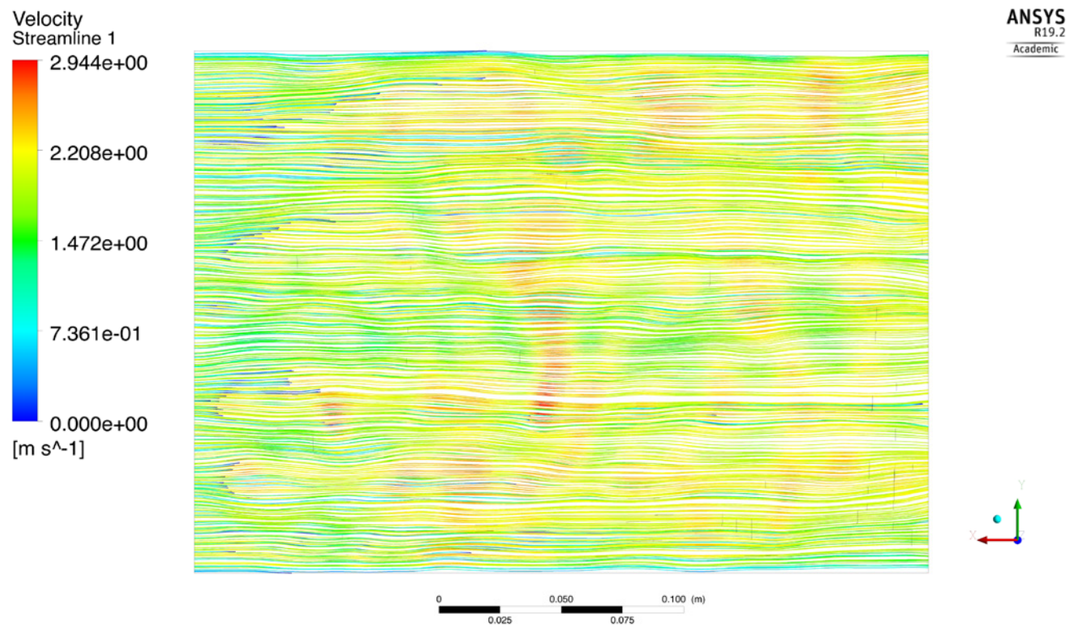

Figure 92: Velocity streamlines in G2-A, with a smaller velocity range compared to the main geometry. Source: Author.

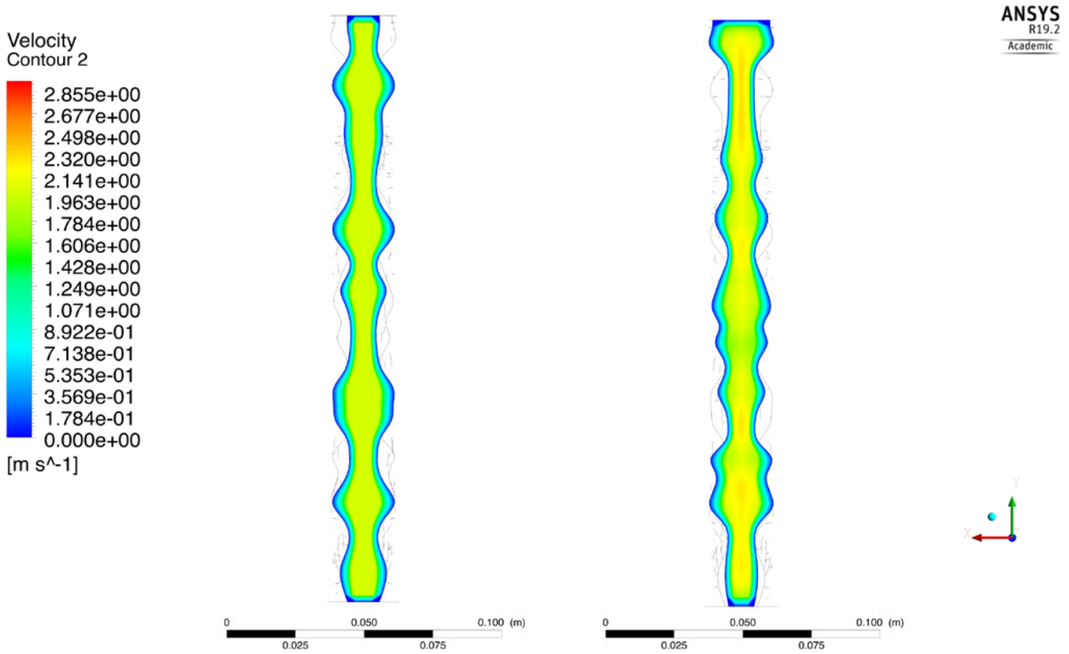

Figure 93: Left: Velocity contour at the inlet. Right: Velocity contour at the outlet. Velocity contours at both inlet and outlet are almost evenly distributed and more uniform compared to G2. Source: Author.

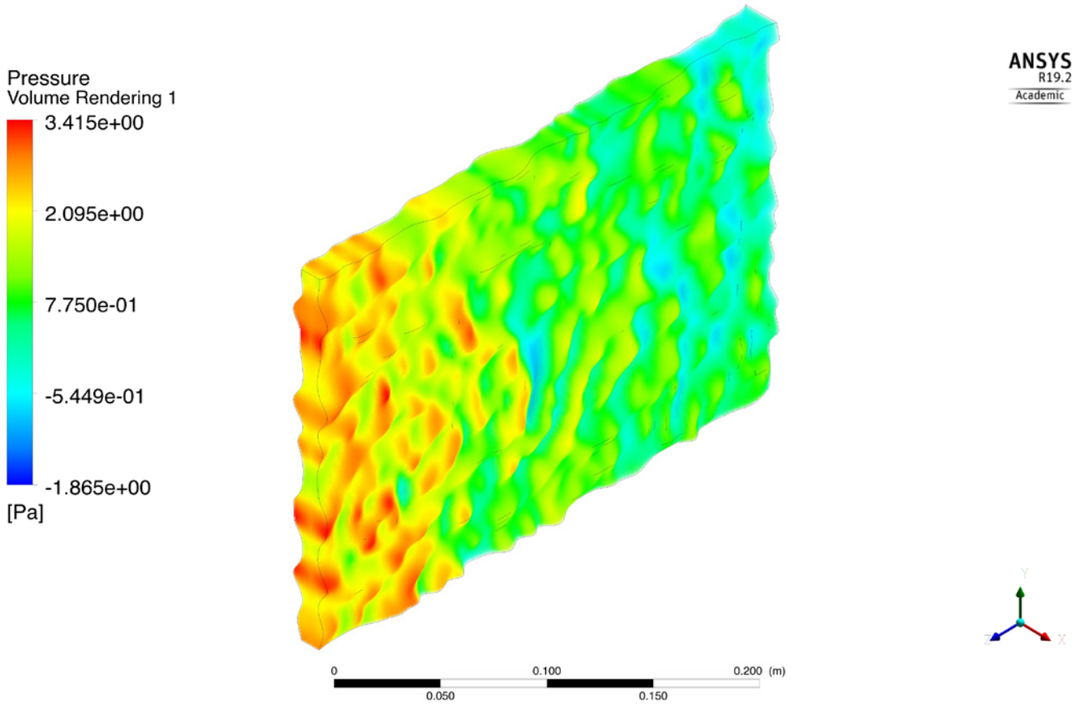

Figure 94: G2-A with smaller pressure range and lower normalized pressure-drop compared to G2. Source: Author.

Variation B - Smaller cavity volume (G2-B)

This variation had a cavity volume of 898 cm^3. Similar to G1-B, the parts that are taken out of the cavity in figure 95, show the areas where the two layers in the unit cell intersect with each other. The meshing method used tetrahedrons and had 2702954 mesh elements. The ratio of the inlet area to the outlet area was 0.97.

The average inlet pressure was 94.66 Pa and the average outlet pressure was 11.68 Pa. As expected, the normalized pressure drop in this case, 0.87 Pa, was the highest among G2 and G2-A due to backflows and eddies. The induced inlet velocity of 3.5 m/s reached an average of 3.87 m/s at the outlet.

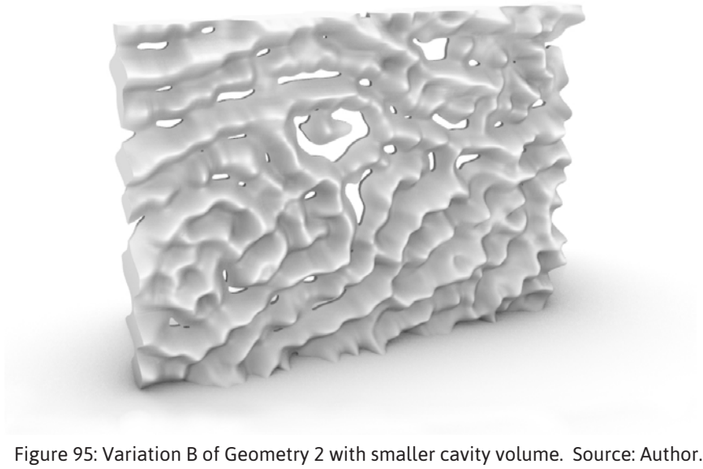

Figure 95: Variation B of Geometry 2 with smaller cavity volume. Source: Author.

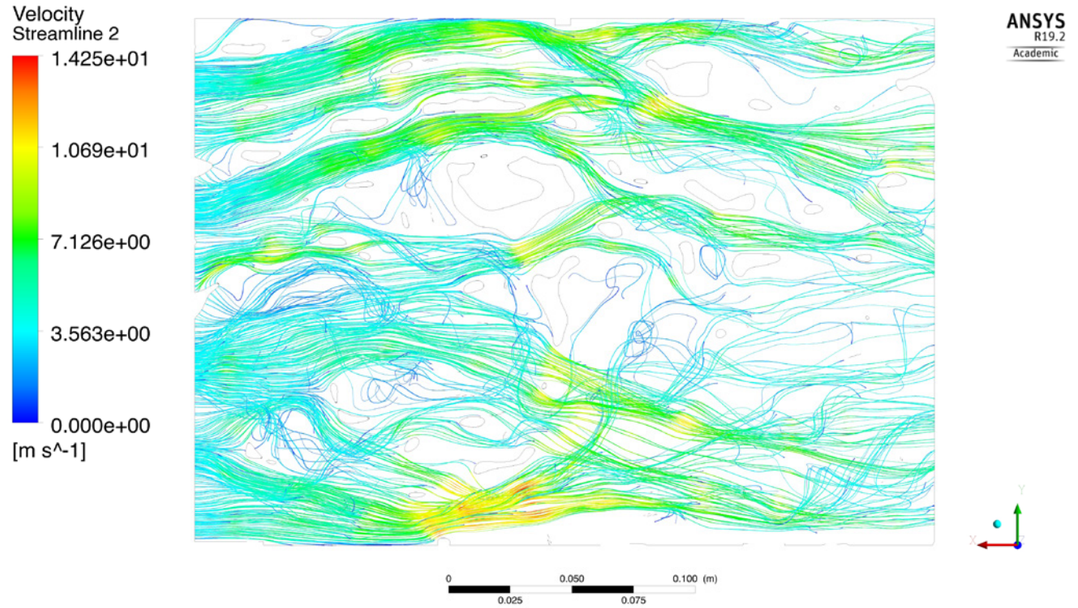

Figure 96: Velocity streamlines in G2-B, turbulent flow shows eddies and recirculation of streamlines in different areas. Source: Author.

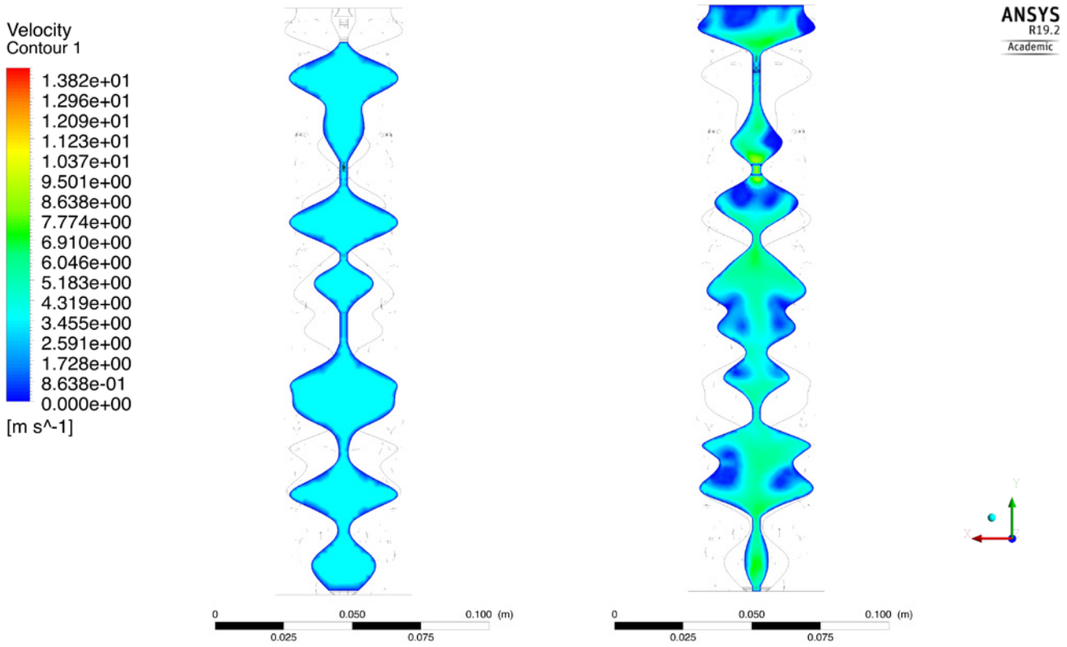

Figure 97: Left: Velocity contour at the inlet. Right: Velocity contour at the outlet. Despite the inlet, the velocity contour at the outlet was not evenly distributed. Source: Author.

Geometry 2	Larger cavity volume (G2-A)	Main geometry (G2)	Smaller cavity volume (G2-B)
Cavity volume (cm^3)	953	926	898
Inlet to outlet ratio	0.99	1.07	0.97
Average inlet pressure (Pa)	4.90	26.70	94.66
Average outlet pressure (Pa)	2.52	4.31	11.68
Normalized pressure drop ($\Delta P/P_{inlet}$)	0.48	0.83	0.87
Inlet velocity (m/s)	2	2	3.5
Average outlet velocity (m/s)	1.9	2.41	3.87

Table 6: Comparison among Geometry 2 and its variations with larger and smaller cavity volume. Source: Author.

Variations A and B had similar inlet to outlet ratios. However, the normalized pressure-drop in variation B was almost double the pressure-drop in variation A due to the eddies and backflows.

In Geometry 2, similar to Geometry 1, the cavity volume as a geometry-related factor had a much higher impact on the pressure-drop, compared to the influence of texture.

Comparison between Geometry 1 and Geometry 2

Geometry 1 and Geometry 2 both were direction-less. However, Geometry 1 had a radial distribution pattern, which impacted the pressure contours. Overall, in both main geometries, the effect of texture on the airflow distribution was not significant. Geometry 1 and Geometry 2 had similar cavity volumes. In their main geometries, Geometry 1 had a higher inlet to outlet ratio which could be the reason for the higher average outlet velocity (3.16 m/s) compared to Geometry 2 (2.41 m/s).

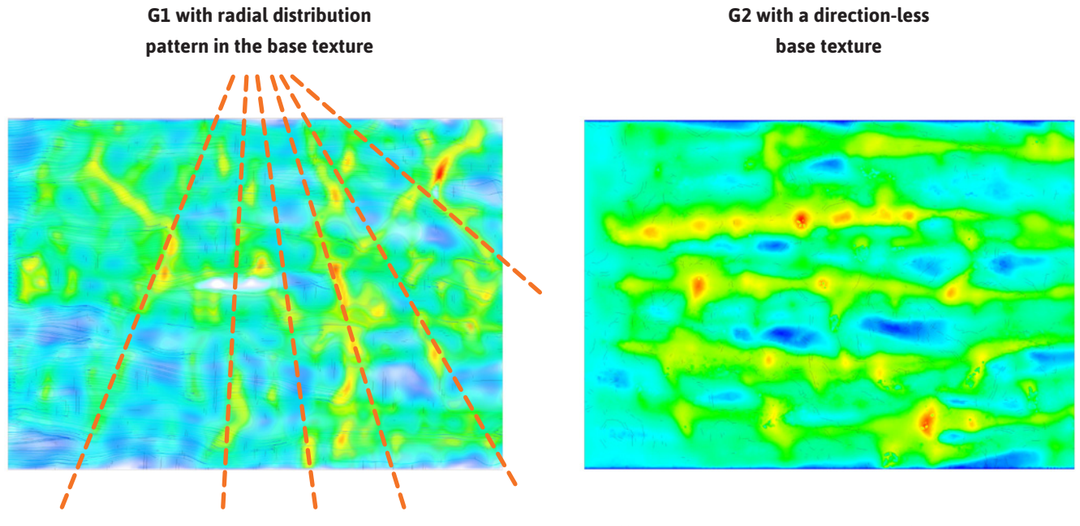

Figure 98: Velocity contour through the geometry at G1 and G2, the difference can display the pattern of the base texture. Source: Author.

Main geometry	Cavity volume (cm^3)	Inlet to outlet ratio	Average inlet pressure (Pa)	Average outlet pressure (Pa)	Normalized pressure drop ($\Delta P/P_{inlet}$)	Average outlet velocity (m/s)
Geometry 1	898	1.45	38.61	7.08	0.81	3.16
Geometry 2	926	1.07	26.70	4.31	0.83	2.41

Table 7: Comparison between G1 and G2, with the inlet velocity of 2m/s. Source: Author.

The variations with larger cavity volumes, G1-A and G2-A, also had similar cavity volumes. Their inlet to outlet ratio was quite similar and therefore, their average outlet velocity was not much different. It was 2.07 m/s in G1-A and 1.9 m/s in G2-A.

As expected, in all tables, the geometry with a higher inlet to outlet ratio had a higher average outlet velocity.

Similar to their main geometries, in G1-B and G2-B the influence of cavity volume as a geometry-related factor was more effective in airflow distribution than the one of the underlying texture. The impact of the base texture on airflow distribution could not be discovered in these variations.

Higher porosity	Cavity volume (cm^3)	Inlet to outlet ratio	Average inlet pressure (Pa)	Average outlet pressure (Pa)	Normalized pressure drop ($\Delta P/P_{inlet}$)	Average outlet velocity (m/s)
Geometry 1	949	1.01	6.43	2.65	0.58	2.07
Geometry 2	953	0.99	4.90	2.52	0.48	1.9

Table 8: Comparison between G1-A and G2-A, with the inlet velocity of 2m/s. Source: Author.

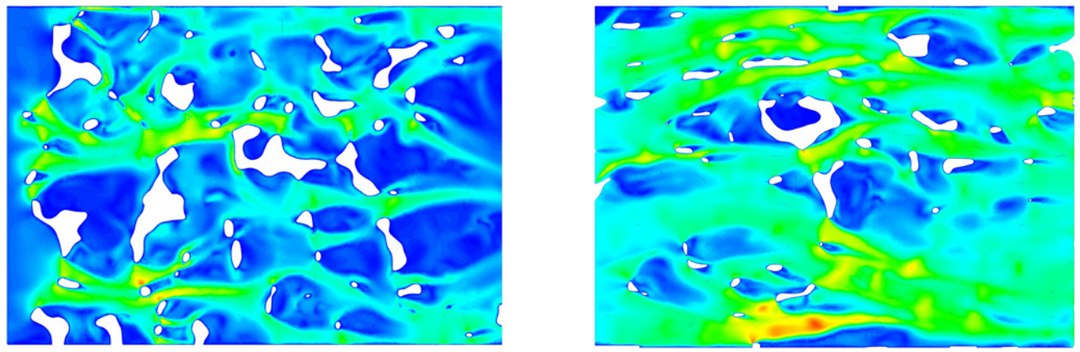

Figure 99: Velocity contour through the geometry at G1-B (right) and G2-B (left), with no distinct trace of the base texture. Source: Author.

Lower porosity	Cavity volume (cm^3)	Inlet to outlet ratio	Average inlet pressure (Pa	Average outlet pressure (Pa)	Normalized pressure drop ($\Delta P/P_{inlet}$)	Average outlet velocity (m/s)
Geometry 1	823	1.09	1238.53	26	0.98	5.1
Geometry 2	898	0.97	94.66	11.68	0.87	3.87

Table 9: Comparison between G1-B and G2-B, with the inlet velocity of 3.5m/s. Source: Author.

The obtained simulation results of Geometry 1, Geometry 2 and their variations suggest that when the base texture is direction-less, the airflow distribution is predominantly controlled by geometry-related factors including cavity volume and the inlet to outlet ratio rather than the base texture. However, fixed conclusions cannot be drawn as the tested geometries are limited and also other underlying textures may result in different effects in the geometry. More investigation and exploration have to be conducted over a larger group of sample textures to draw solid conclusions.

4.6.3 Geometry 3 (G3)

Geometry 3 is based on texture 22 (Appendix B). Since the base texture displays a dominant direction, it can be implemented horizontally or vertically in the process of geometry generation. Therefore, to evaluate the influence of direction in the base texture on airflow pattern in the geometry, two geometry variations are derived from this texture, one with horizontal channels and one with vertical channels.

With horizontal channels

The meshing in this variation used prism layers and resulted in 315100 mesh elements. The ratio of inlet area to the outlet area was 1.11.

With vertical channels

Meshing of the geometry with vertical direction also used prism layers and resulted in 409920 mesh elements. The ratio of inlet area to the outlet area was 1.88.

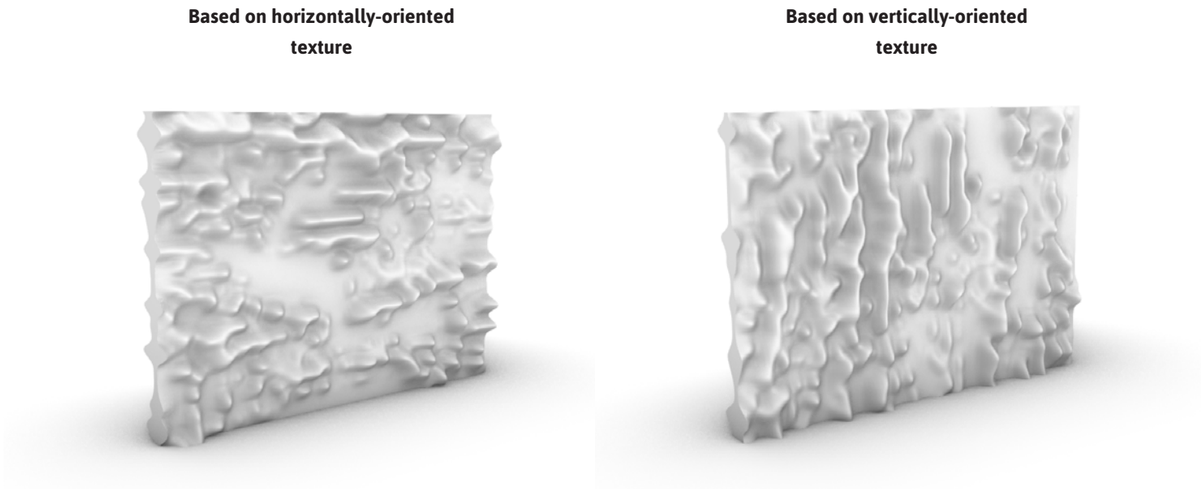

Figure 100: Geometry 3 with two variations, used for CFD simulation in Ansys Fluent. Source: Author.

As can be seen from figures 101 and 102, the horizontal channels accelerated the airflow rate and unified the streamlines, which resulted in an evenly-distributed velocity contour at the outlet. However, the geometry with vertical channels interrupted the streamlines and resulted in fluctuating streamlines. These turbulent lines mostly occurred in cross-sections with vertical channels, based on the vertical direction of the underlying texture.

Although the average outlet velocity in the geometry with vertical channels (3.8 m/s) was much higher compared to the other geometry (2.34 m/s), the volume flow rate was larger in the geometry with horizontal channels (22.89 m^3/h) due to the larger outlet area. The volume flow rate in the geometry with vertical channels was 16.96 m^3/h.

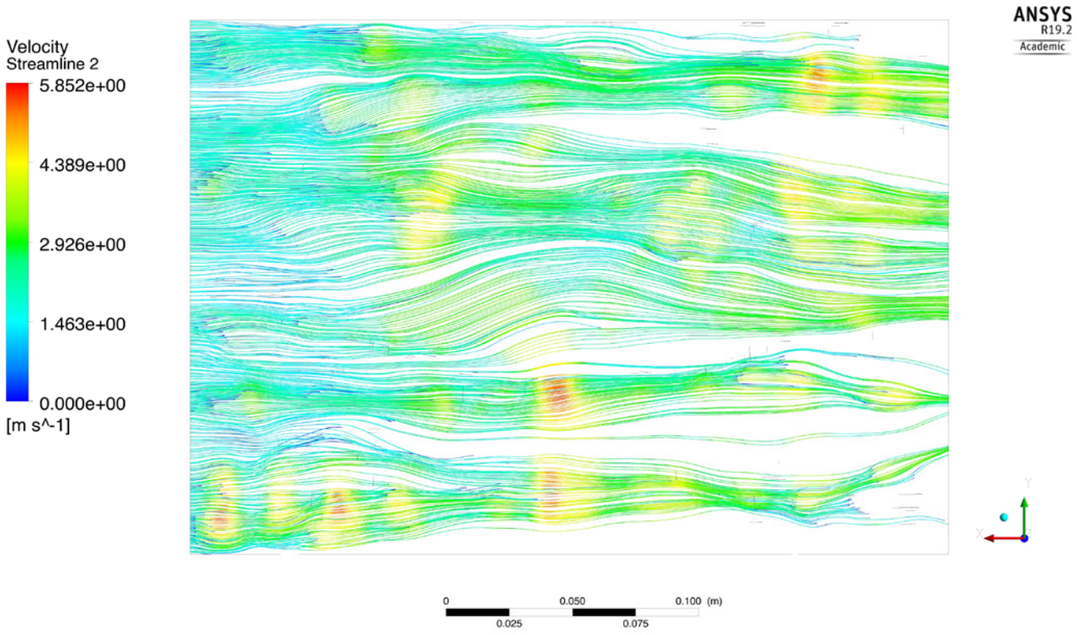

Figure 101: Velocity streamlines in geometry 3 with horizontal channels are almost regular. Source: Author.

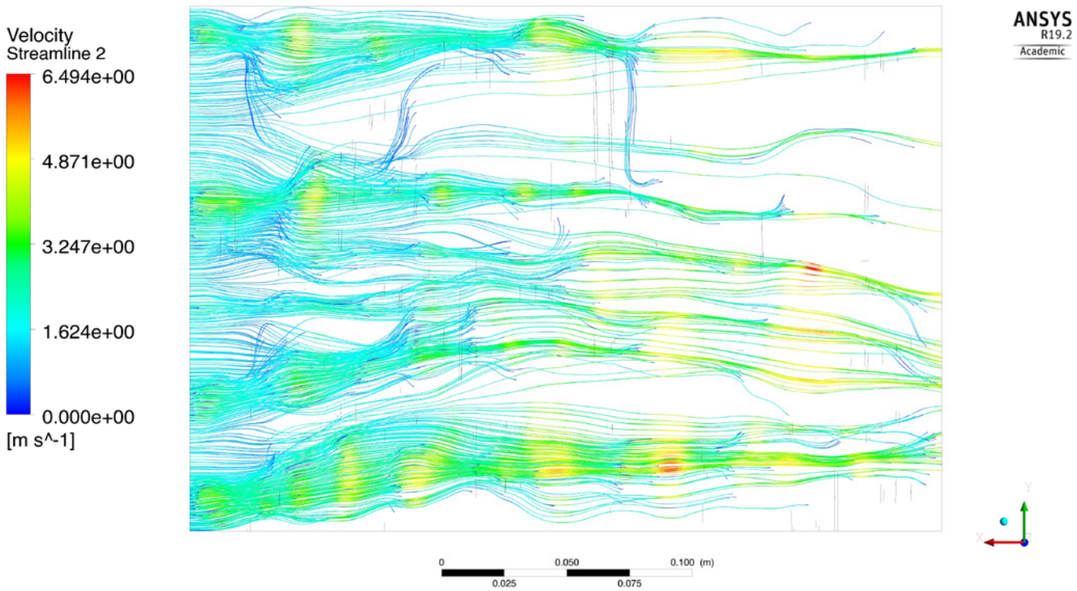

Figure 102: Velocity streamlines in geometry 3 with vertical channels exhibit turbulent behavior. Source: Author.

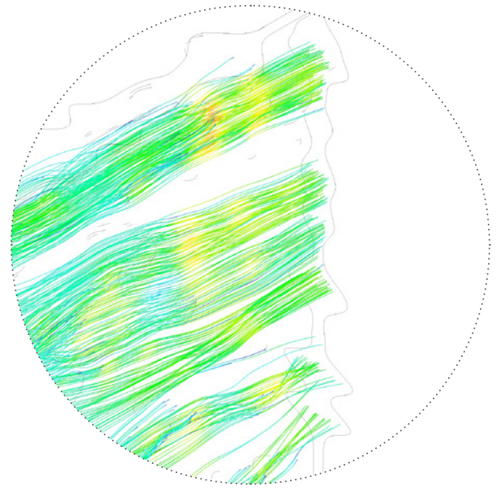

Figure 103: Almost parallel and uniform streamlines in geometry with horizontal channels. Source: Author.

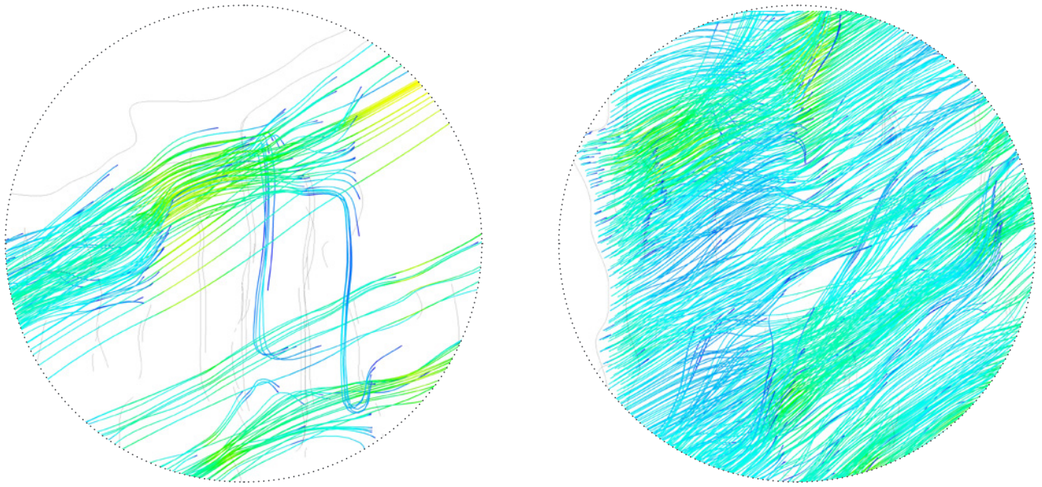

Figure 104: Turbulent streamlines in geometry with vertical channels. Source: Author.

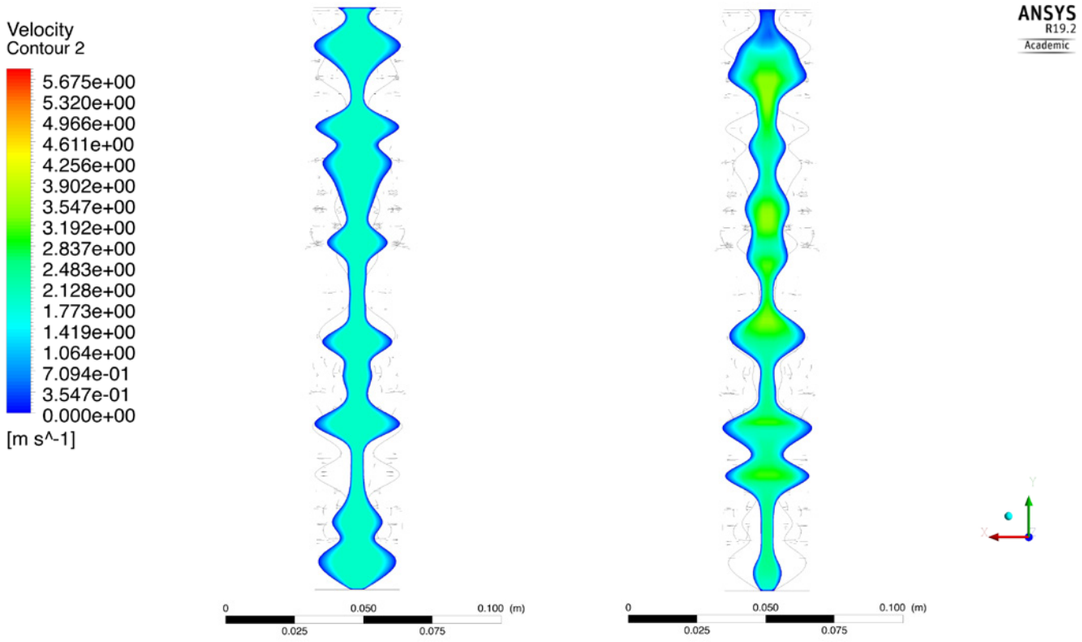

Figure 105: Left: Velocity contour at the inlet. Right: Velocity contour at the outlet. Variation of geometry 3 with horizontal channels. Source: Author.

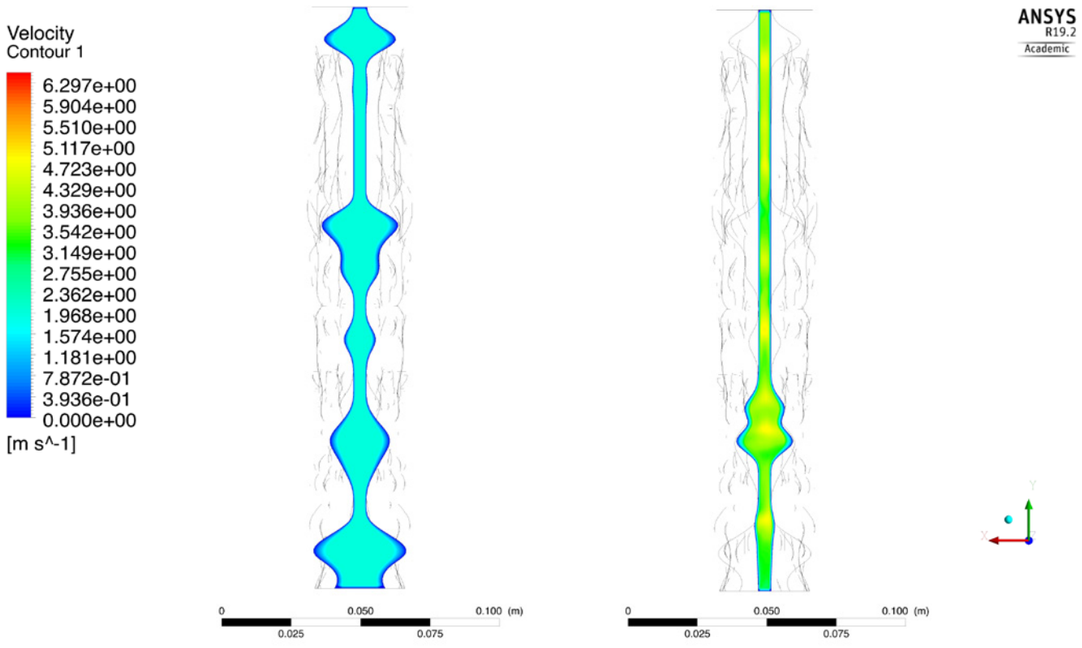

Figure 106: Left: Velocity contour at the inlet. Right: Velocity contour at the outlet. Variation of geometry 3 with vertical channels. Source: Author.

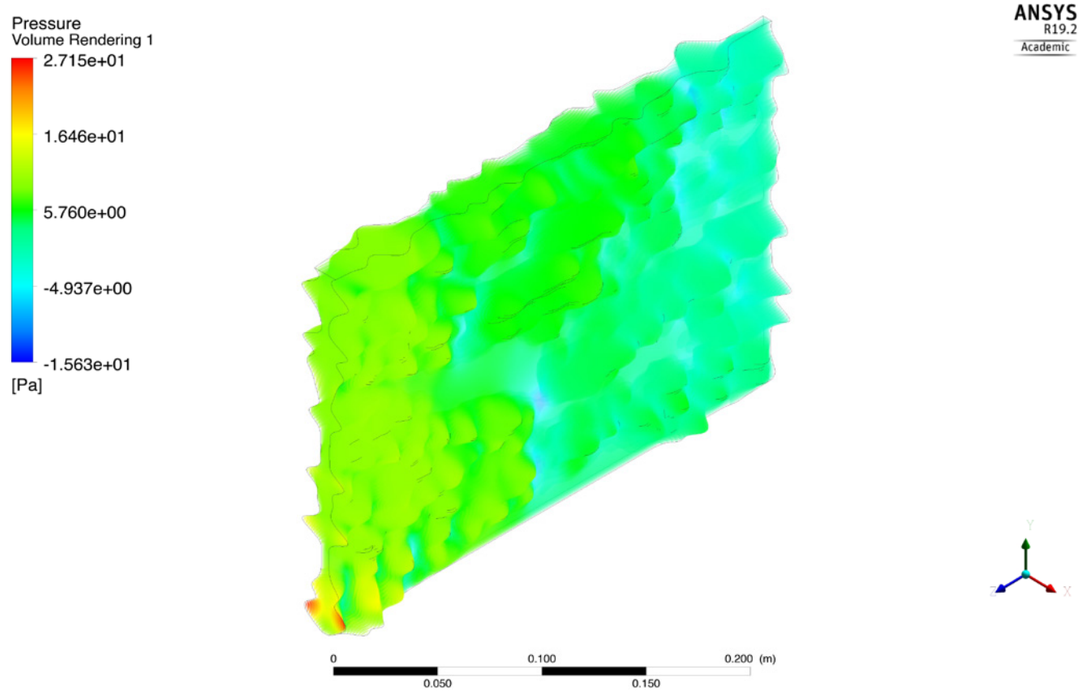

Figure 107: Pressure volume rendering in the geometry variation with horizontal channels showed more of a gradual change in the pressure drop over the geometry. Source: Author.

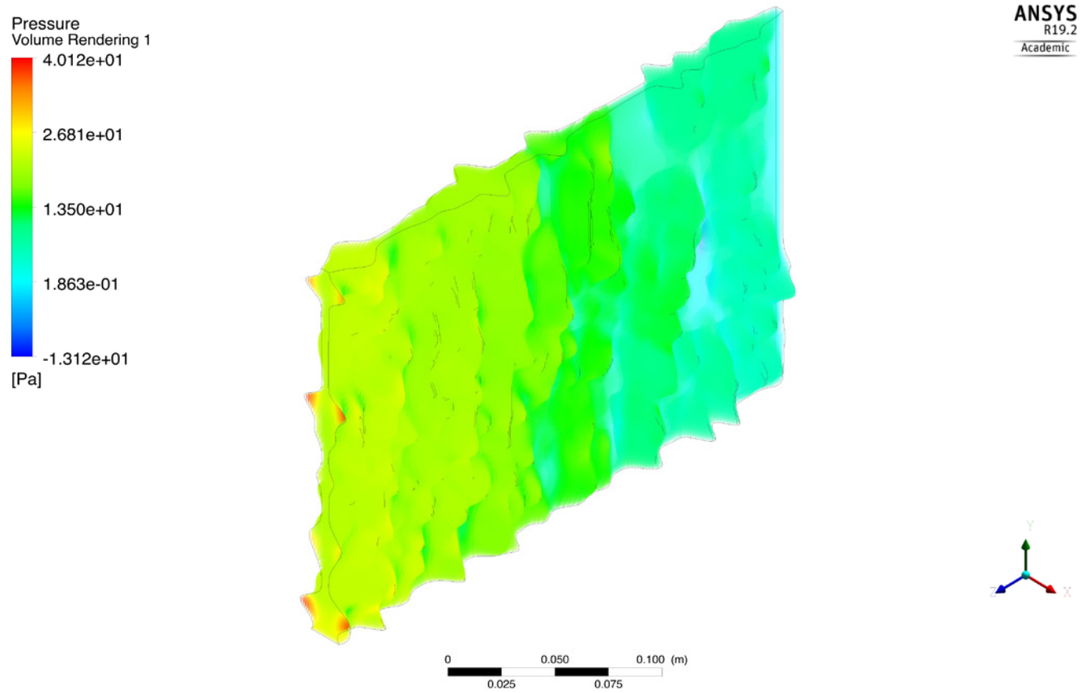

Figure 108: Pressure volume rendering in the geometry variation with vertical channels. Pressure dropped faster along the flow compared to the variation with horizontal channels. Source: Author.

The normalized pressure-drop in variation with horizontal channels was 0.73 Pa, with an average inlet pressure of 13.49 Pa and an average outlet pressure of 3.58 Pa.

In variation with vertical channels, the average inlet pressure was 26.48 Pa and the average outlet pressure was 9.43 Pa. The normalized pressure-drop was 0.64 Pa.

Due to the vertical directions of the channels, it was expected that this variation would have a higher pressure-drop compared to the variation with horizontal channels. However, the results did not confirm this which could be due to the larger inlet to outlet ratio in this variation.

Geometry 3	Horizontal direction	Vertical direction
Cavity volume (cm^3)	826	884
Inlet to outlet ratio	1.11	1.88
Average inlet pressure (Pa)	13.49	26.48
Average outlet pressure (Pa)	3.58	9.43
Normalized pressure drop ($\Delta P/P_{inlet}$)	0.73	0.64
Inlet velocity (m/s)	2	2
Average outlet velocity (m/s)	2.34	3.8

Table 10: Two variations of geometry 3, with horizontal and vertical channels . Source: Author.

Based on the obtained results from the two variations of geometry 3, it was clear that geometry with vertical channels should be avoided as they created chaotic and turbulent streamlines and affected the flow pattern.

Based on the previous simulations, it was evident that in the geometries with larger cavity volumes, the effect of texture was less significant compared to the ones with smaller cavity volume. Furthermore, in the ones with larger cavity volume, both velocity contours at the inlet and outlet were almost evenly distributed. However, in the variations with smaller cavity volume, the outlet velocity contour confirmed the uneven distribution of the velocity due to the more irregular form of the cavity.

Thus, as the results of the variation with larger cavity volume were more predictable, it was decided to only simulate the variations with smaller cavity volume in Geometry 3 and Geometry 4 with horizontal air channels.

Variation B - Smaller cavity volume (G3-B)

This variation of Geometry 3 with horizontal direction had a cavity volume of 830 cm^3. The meshing in this geometry was done using tetrahedrons and the resultant number of mesh elements was 2121232. The inlet to outlet ratio was 1.28.

With the average inlet pressure of 394.84 Pa and the average outlet pressure of 31 Pa, the normalized pressure-drop in this variation was 0.92. Similar to the previous variations with smaller cavity volume, this high pressure-drop was the result of eddies and backflows in several parts of the geometry.

The induced inlet velocity of 3.5 m/s reached an average of 5.42 m/s at the outlet.

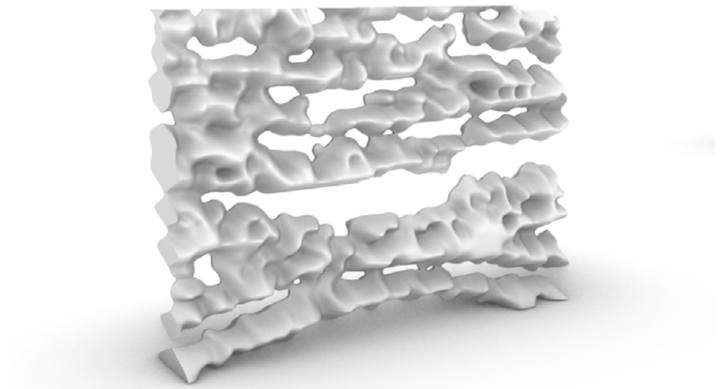

Figure 109: Variation with smaller cavity volume with horizontal air channels. Source: Author.

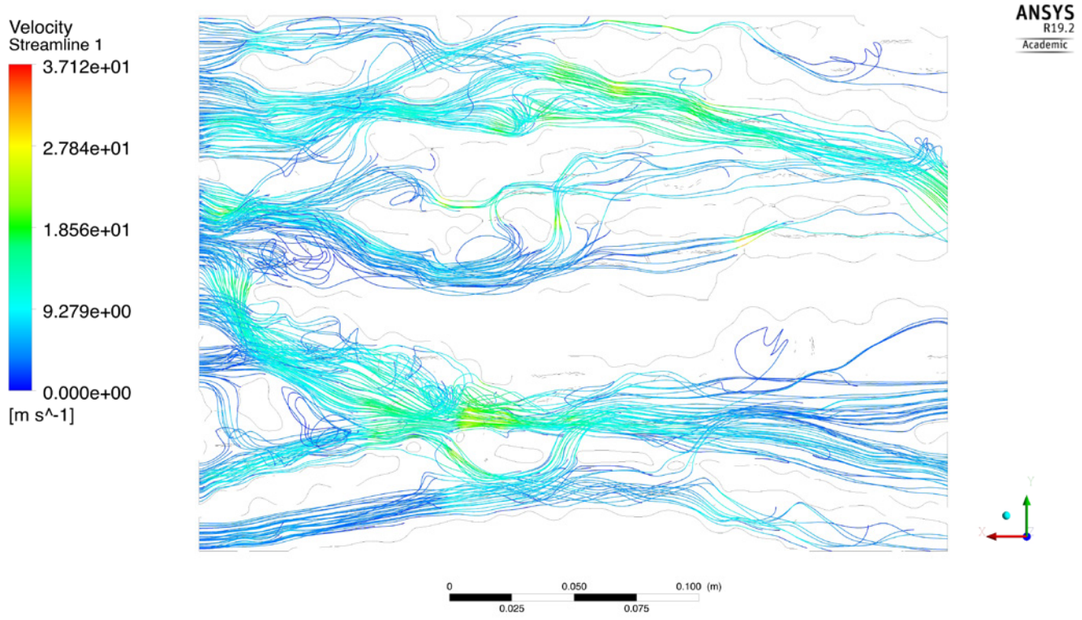

Figure 110: Velocity streamlines in this variation are turbulent and eddies appear along the movement of the air's particles. Source: Author.

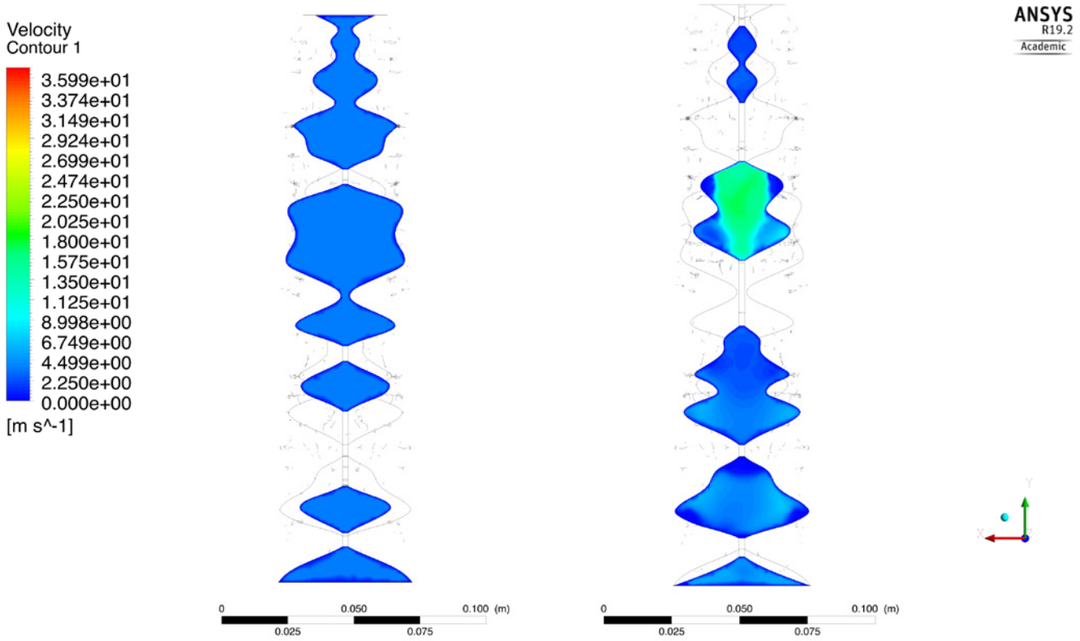

Figure 111: Left: Velocity contour at the inlet. Right: Velocity contour at the outlet. Source: Author.

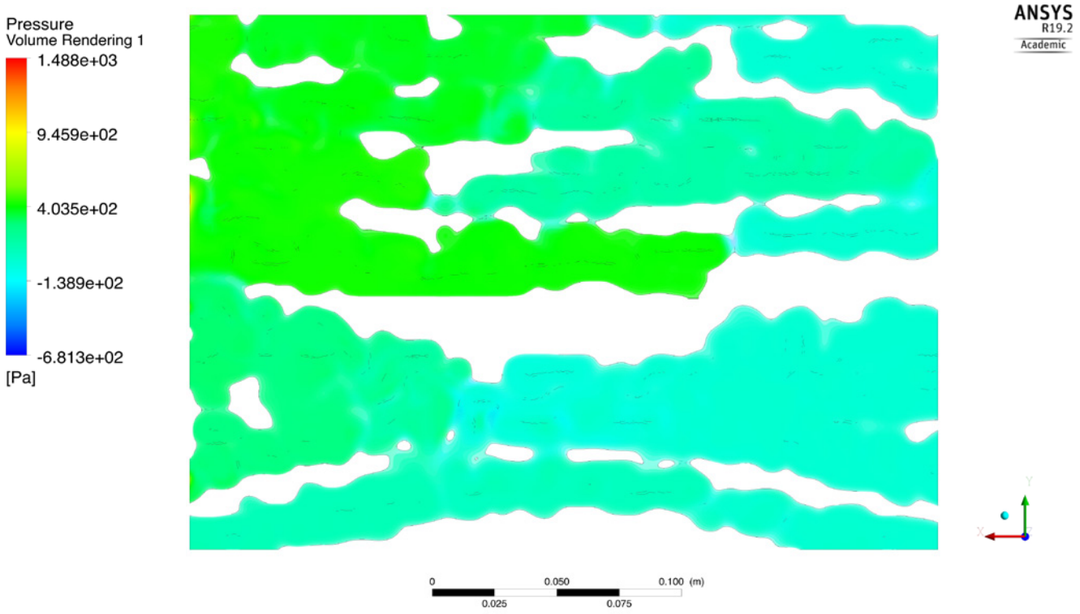

Figure 112: Pressure volume rendering in the geometry displayed major pressure-drops along the smaller cross-sectional areas . Source: Author.

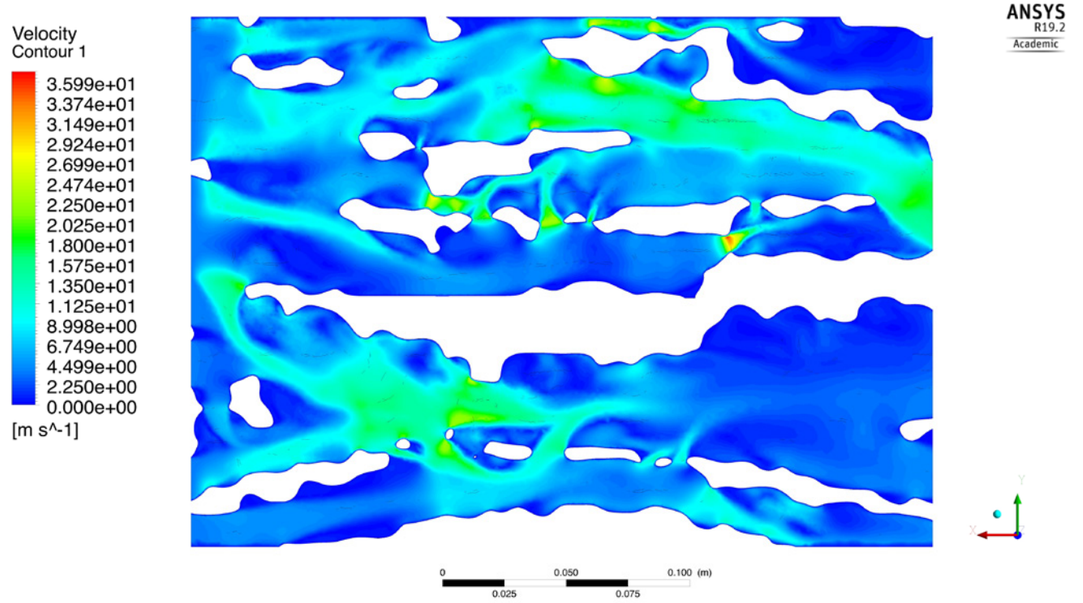

Figure 113: Velocity contour through the geometry showed evident impact of the underlying texture in distributing the flow. Source: Author.

Geometry 3 - horizontal direction	Main geometry (G3)	Smaller cavity volume (G3-B)
Cavity volume (cm^3)	874	830
Inlet to outlet ratio	1.11	1.28
Average inlet pressure (Pa)	13.49	394.84
Average outlet pressure (Pa)	3.58	31
Normalized pressure drop ($\Delta P/P_{inlet}$)	0.73	0.92
Inlet velocity (m/s)	2	3.5
Average outlet velocity (m/s)	2.34	5.42

Table 11: Comparison between Geometry 3 and its variation with a smaller cavity volume. Source: Author.

The impact of the underlying texture was substantial in the variation with smaller cavity volume, as it influenced the formation of the horizontal channels and gave a clear direction for the flow distribution. However, due to large channels' width in some areas, the occurrence of eddies was observed which was more due to the dimensions of the channel rather than its horizontal direction.

4.6.4 Geometry 4 (G4)

Geometry 4 is based on texture 30 (Appendix B). Similar to Geometry 3, two variations are derived from this texture, one with horizontal channels and one with vertical channels.

With horizontal direction

This geometry is based on texture with a horizontal direction. The meshing was done using the tetrahedron method and resulted in 415800 mesh elements. The ratio of the inlet area to the outlet area was 2.39.

With vertical direction

The meshing of the geometry with vertical direction also used tetrahedrons and resulted in 508120 mesh elements. The ratio of the inlet area to the outlet area was 1.1.

Based on horizontally-oriented texture

Based on vertically-oriented texture

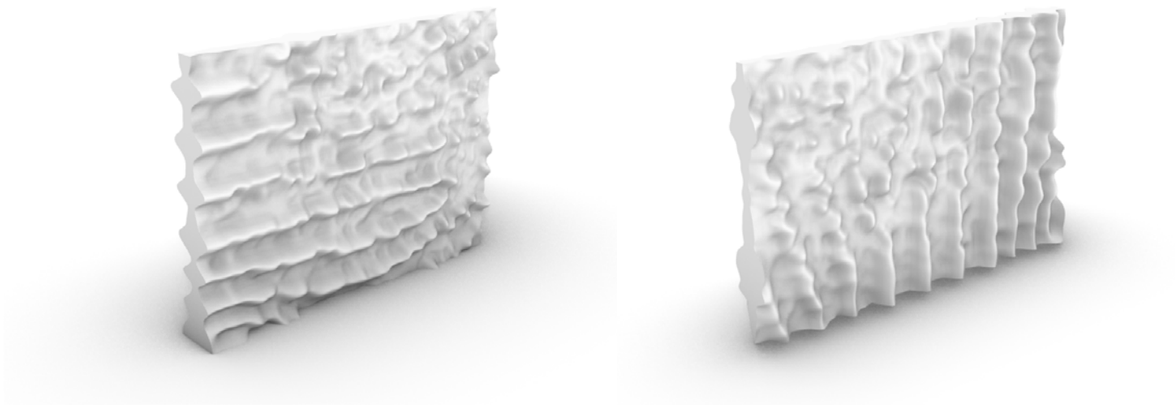

Figure 114: Geometry 4 with two variations, used for CFD simulation in Ansys Fluent. Source: Author.

The clear horizontal lines in the base texture distributed the streamlines almost evenly. In the geometry with vertical channels, the flow distribution was not uniform and the influence of the vertical channels was more significant at the bottom part of the geometry due to the larger channel size. Also, eddies occurred in some regions.

Contrary to Geometry 3, the average outlet velocity in Geometry 4 with horizontal channels (5.31 m/s) was higher compared to both its induced inlet velocity (2 m/s) and the average outlet velocity of the geometry with vertical channels (2.63 m/s) (Appendix K and L for comparison of the velocity contours).

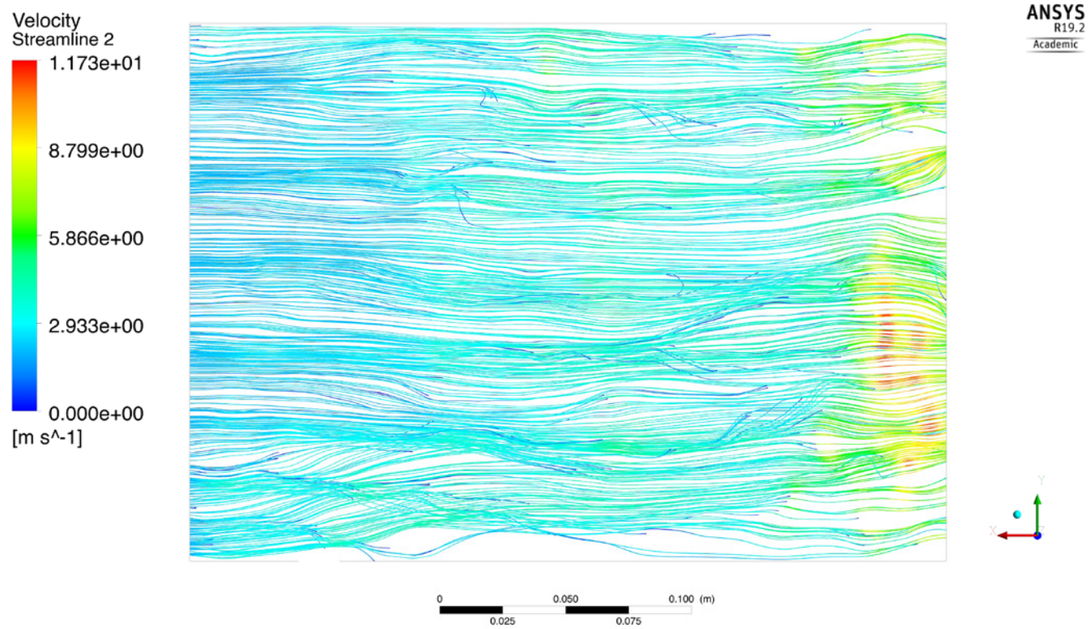

Figure 115: Velocity streamlines in geometry 4 with horizontal channels display a uniform distribution. Source: Author.

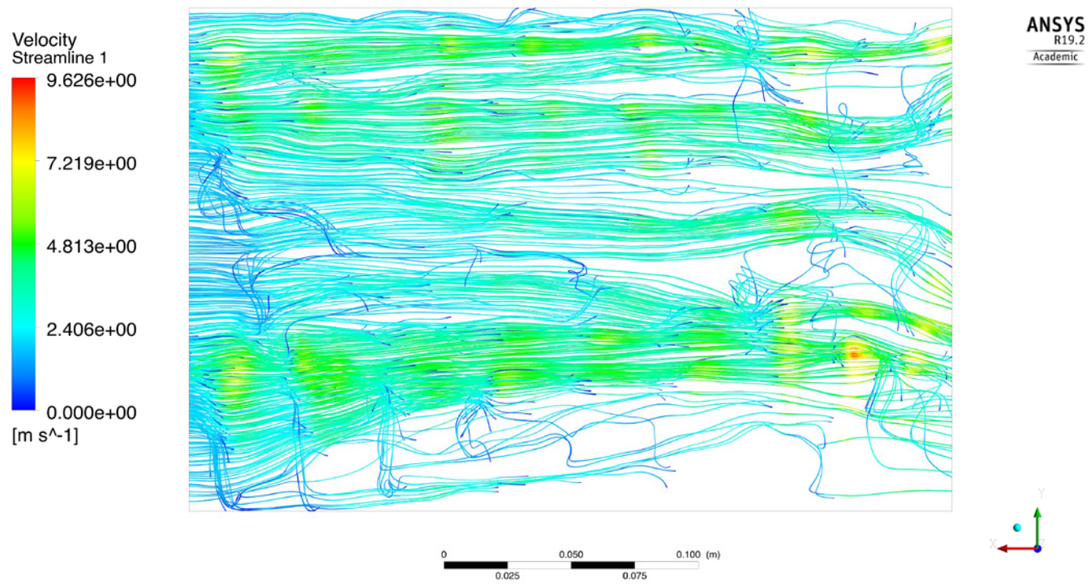

Figure 116: Velocity streamlines in geometry 4 with vertical channels. Change of the flow paths mostly occurred in the cross-sectional areas of the vertical channels, with eddies in some parts. Source: Author.

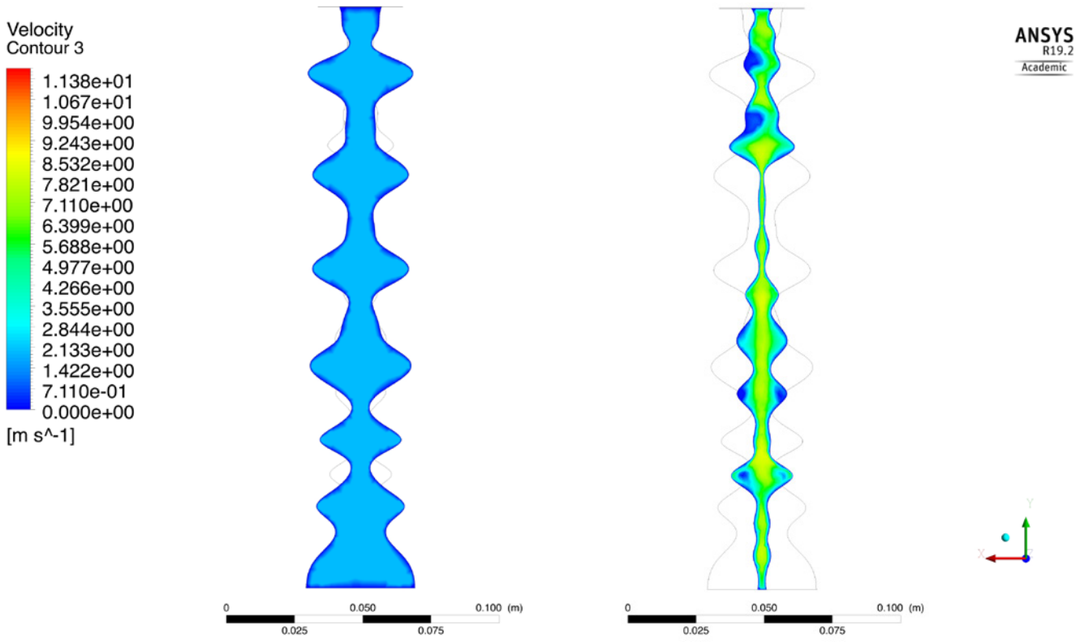

Figure 117: Left: Velocity contour at the inlet. Right: Velocity contour at the outlet. Variation of Geometry 4 with horizontal channels, with non-uniform distribution of velocity at the outlet. Source: Author.

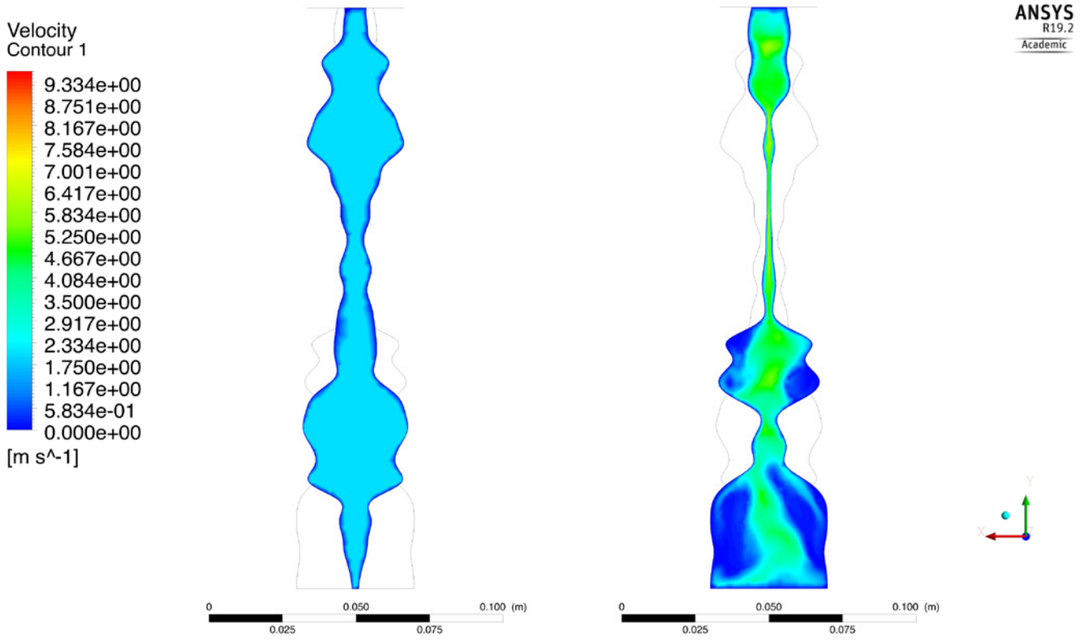

Figure 118: Left: Velocity contour at the inlet. Right: Velocity contour at the outlet. Variation of Geometry 4 with vertical channels, with non-uniform distribution of velocity at the outlet. Source: Author.

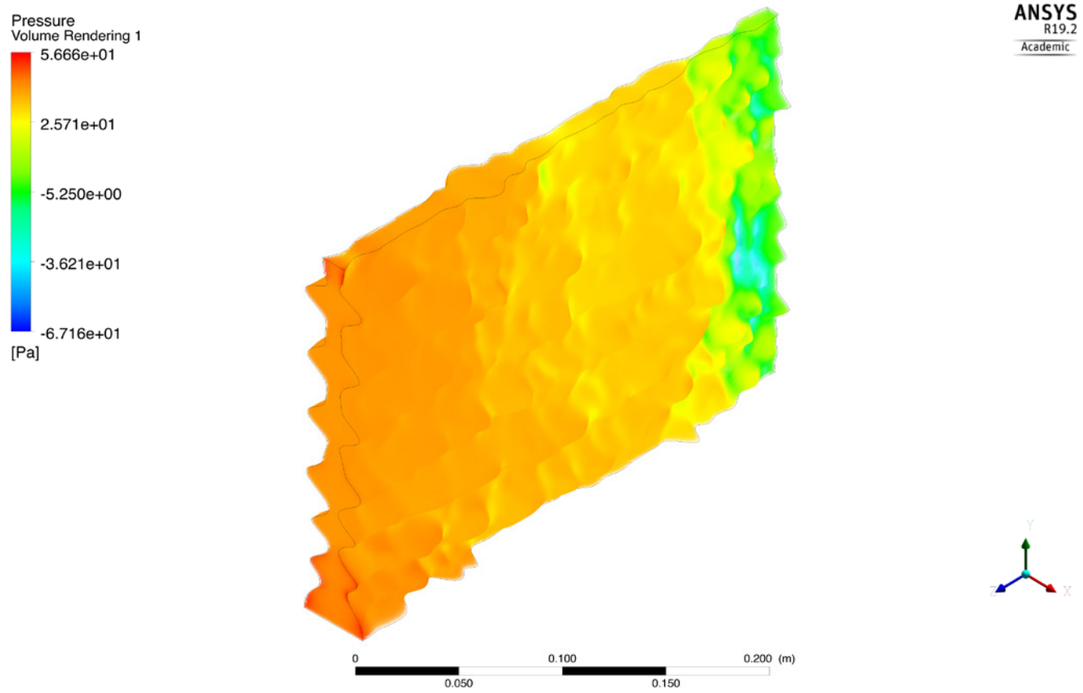

Figure 119: Pressure volume rendering in the variation with horizontal channels. Source: Author.

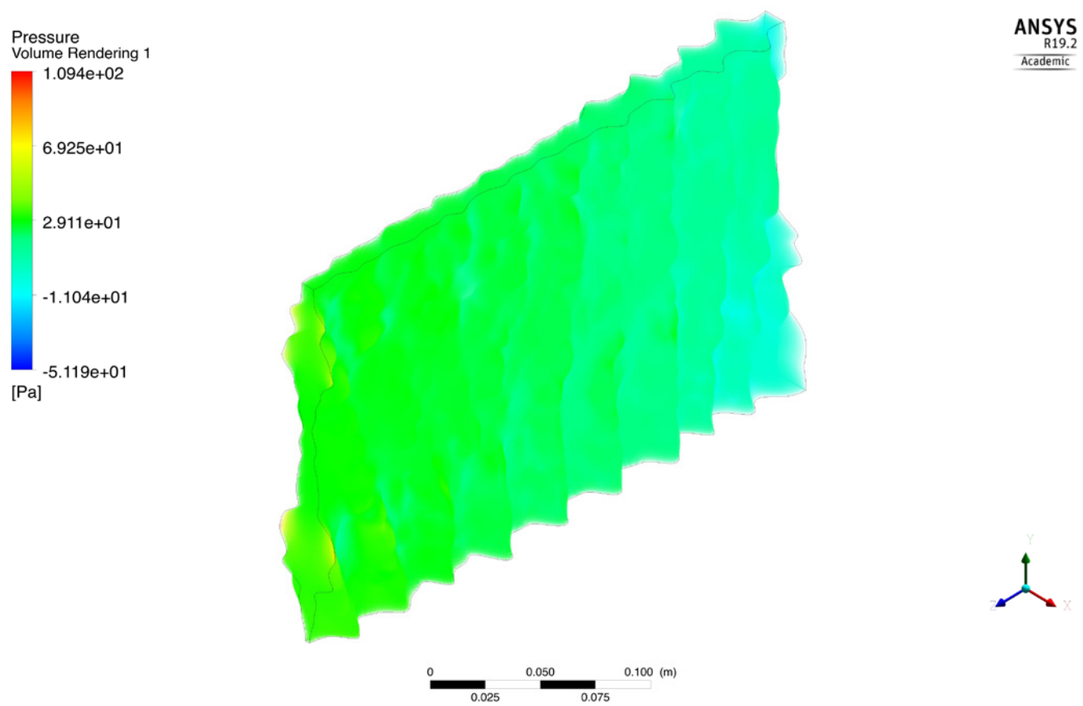

Figure 120: Pressure volume rendering in the variation with vertical channels. Source: Author.

The normalized pressure-drop in the variation with horizontal channels was 0.55 Pa, with an average inlet pressure of 45.02 Pa and an average outlet pressure of 20.25 Pa.

The geometry with the vertical channels had an average inlet pressure of 37.58 Pa and an average outlet pressure of 6.25 Pa. The normalized pressure-drop was 0.83 Pa, higher than the other variation, as expected.

Geometry 4	Horizontal direction	Vertical direction
Cavity volume (cm^3)	930	947
Inlet to outlet ratio	2.39	1.1
Average Inlet pressure (Pa)	45.02	37.58
Average outlet pressure (Pa)	20.25	6.25
Normalized pressure drop ($\Delta P/P_{inlet}$)	0.55	0.83
Inlet velocity (m/s)	2	2
Average outlet velocity (m/s)	5.31	2.63

Table 12: Two variations of geometry 4, with horizontal and vertical direction . Source: Author.

Variation B - Smaller cavity volume (G4-B)

This variation had a smaller cavity volume compared to Geometry 4 with a horizontal direction. The meshing used tetrahedrons and the resultant number of mesh elements was 1660878. The inlet to the outlet ratio was 0.6, much lower than the main geometry.

Here the normalized pressure-drop was 0.89 Pa, with an average inlet pressure of 55.36 Pa and an average outlet pressure of 6.07 Pa.

Contrary to G3-B which had a higher average outlet velocity compared to its inlet, the average outlet velocity in G4-B was lower than its inlet velocity. Here the average outlet velocity was 2.48 m/s. The velocity contour through the geometry can be found in Appendix M.

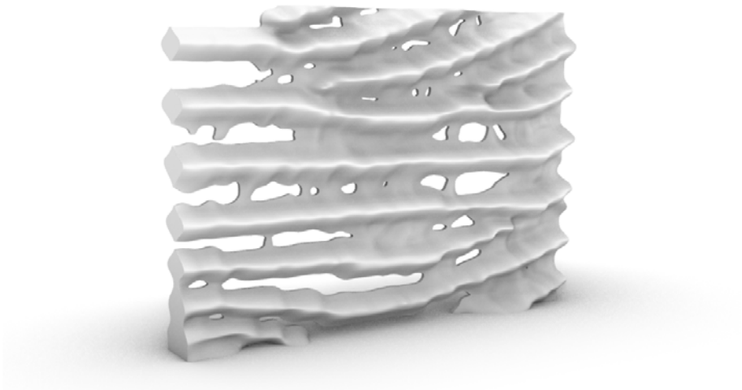

Figure 121: Variation of Geometry 4 with horizontal air channels with a smaller cavity volume. Source: Author.

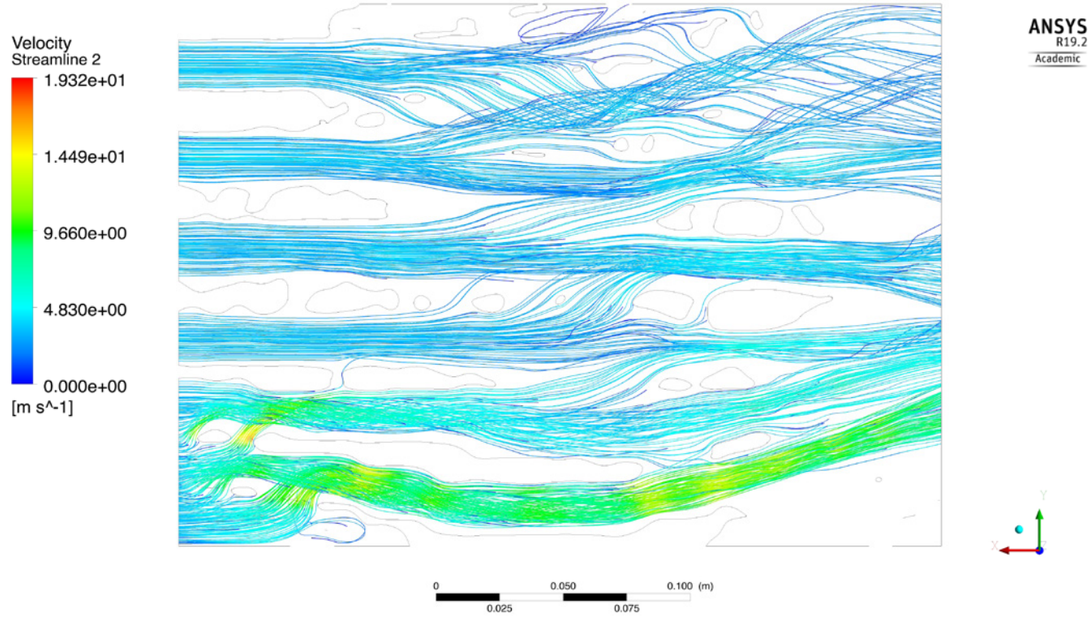

Figure 122: Velocity streamlines in this variation were mainly affected and distributed by the horizontal channels in the geometry. Source: Author.

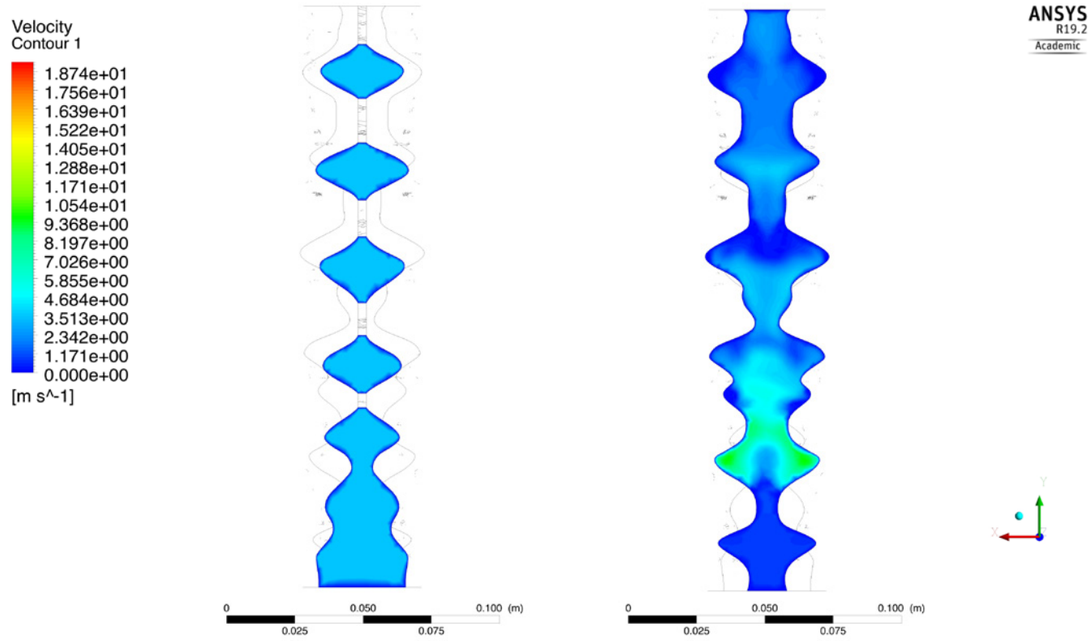

Figure 123: Left: Velocity contour at the inlet. Right: Velocity contour at the outlet. Source: Author.

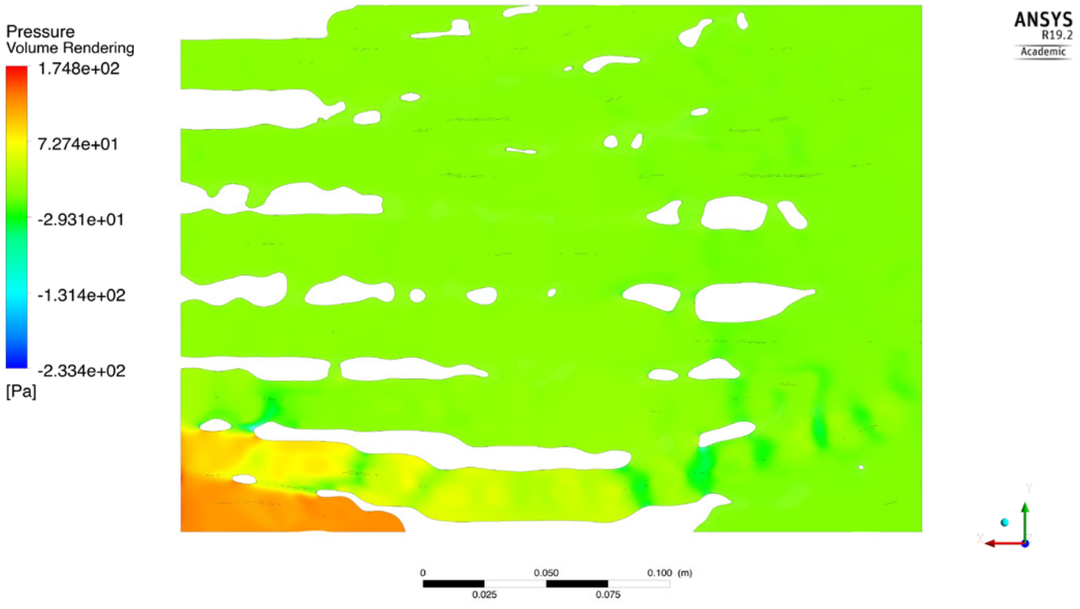

Figure 124: Pressure volume rendering in the geometry. Source: Author.

Geometry 4 - horizontal direction	Main geometry (G4)	Smaller cavity volume (G4-B)
Cavity volume (cm^3)	930	866.52
Inlet to outlet ratio	2.39	0.6
Average inlet pressure (Pa)	45.02	55.36
Average outlet pressure (Pa)	20.25	6.07
Normalized pressure drop ($\Delta P/P_{inlet}$)	0.55	0.89
Inlet velocity (m/s)	2	3.5
Average outlet velocity (m/s)	5.31	2.48

Table 13: Comparison between Geometry 4 and its variation with a smaller cavity volume. Source: Author.

Compared to G3-B, the average outlet velocity in G4-B was lower than its defined inlet velocity. The reason for this was that the outlet shape in G3-B was more diffused and branched. While in G4-B, this was not the case and the form at the outlet was more uniform and concentrated.

4.7 Further analysis

To grasp a better understanding of the relation between different factors such as the average outlet velocity, the pressure-drop and the volume of the cavity, geometry 4 with the horizontal channels was selected for further analysis. The reason for choosing this geometry was as following:

- The horizontal direction of the underlying pattern made a significant impact on guiding the streamlines especially in the variation with a smaller cavity volume.
- The normalized pressure-drops in this geometry with the variations of horizontal and vertical channels were as expected and the one with vertical channels had a larger pressure-drop (This was also expected in Geometry 3 but it did not occur).

As part of the further analysis, first Geometry 4 was used in 6 simulations with 6 different induced inlet velocities with a fixed interval between them. Figure 125 illustrates the changes in the average outlet velocity and pressure-drop as the inlet velocity changes.

With the increase of the inlet velocity, both the pressure-drop and the average outlet velocity increased. However, the changes in the pressure-drop were much larger and faster compared to the changes in the average outlet velocity. The changes of both parameters as a function of the inlet velocity was not linear.

It has to be noted that these obtained results would probably be different for the other geometries that were tested in the evaluation phase.

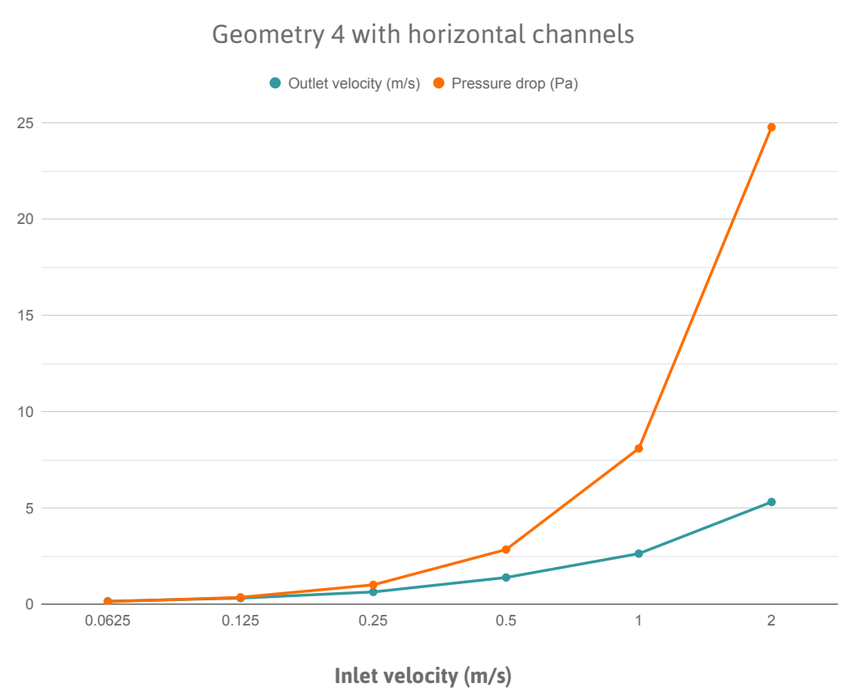

Figure 125: Comparison between the pressure-drop and the average outlet velocity over different inlet velocities. Source: Author.

Figure 126 displays the relation between the volume flow rate and the pressure-drop. Similar to figure 125, the values in the graph are shown for inlet velocities starting from 0.0625 m/s, doubling up at each interval until 2 m/s. While the volume flow rate almost doubled with each increase of the inlet velocity, the change of the pressure drop was not linear. More details of this simulation can be found in Appendix N.

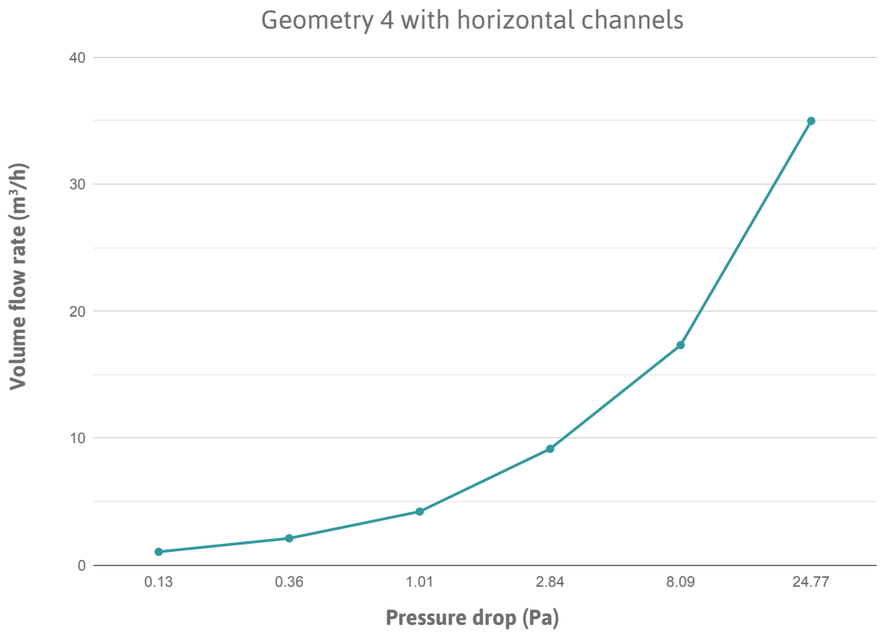

Figure 126: The relation between pressure drop and the volume flow rate in Geometry 4 was not linear. Source: Author.

Next, to evaluate the effect of the volume of the cavity on the pressure-drop and average outlet velocity, the same underlying texture of Geometry 4 was used to generate 8 new geometries with different cavity sizes. The width of the cavity is based on the width of the geometry with no surface roughness.

A defined inlet velocity of 1 m/s was used for all of the variations. Due to the changes in the geometry, normalized pressure-drops were calculated for better comparison among the variations.

Width (cm)	1.6	1.8	2	2.2	2.4	2.6	2.8	3
Average inlet pressure (Pa)	4.9	3.62	3.03	2.57	2.32	2.07	1.98	1.79
Average outlet pressure (Pa)	1.52	1.35	1.18	1.15	1.14	1.05	0.97	0.96
Pressure drop (Pa)	3.38	2.27	1.85	1.42	1.18	1.02	1.01	0.83
Normalized pressure drop	0.69	0.63	0.61	0.55	0.51	0.49	0.51	0.46
Inlet velocity (m/s)	1	1	1	1	1	1	1	1
Average outlet velocity (m/s)	1.46	1.39	1.35	1.31	1.28	1.25	1.23	1.21

Table 14: Results of simulations for 8 geometries with different cavity sizes. Source: Author.

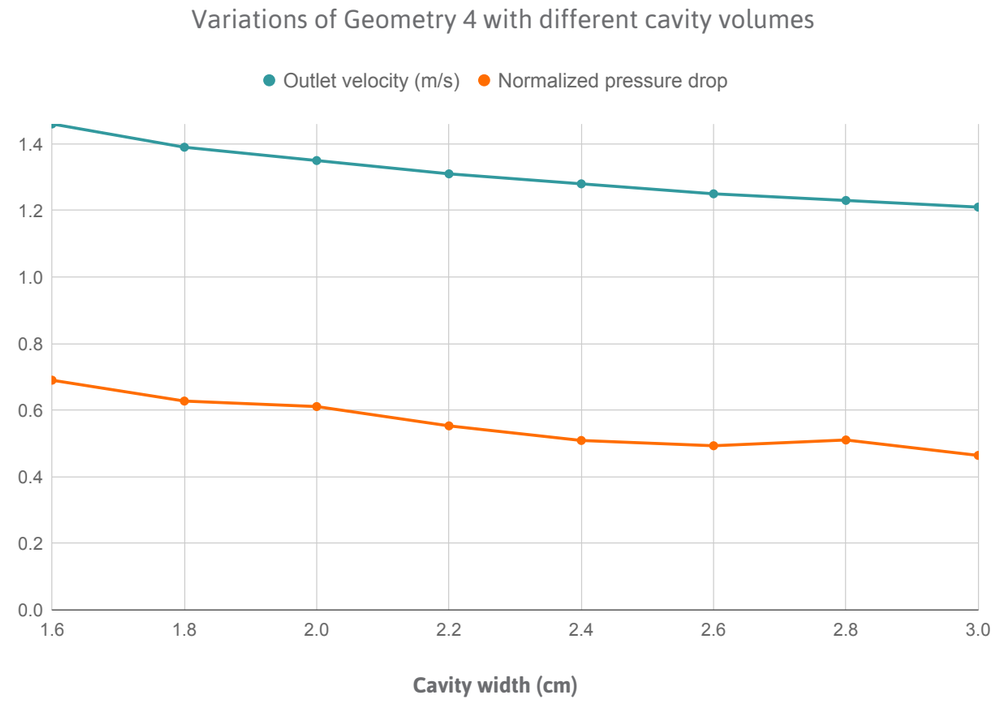

Figure 127: Normalized pressure-drops and outlet velocities based on 8 different cavity widths. Source: Author.

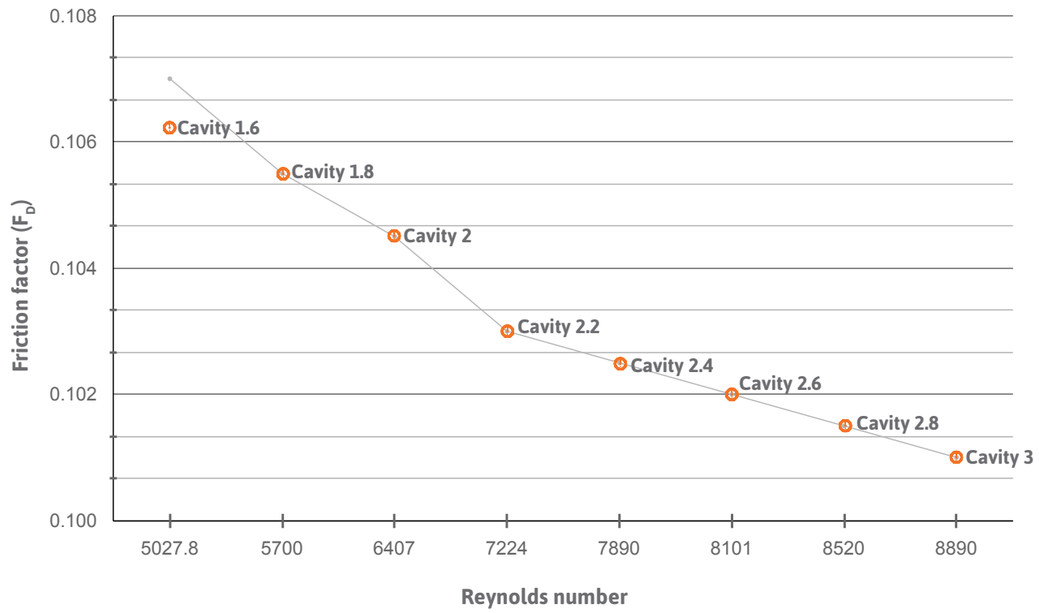

Figure 128: Comparison of friction factors and Reynolds number for each simulated cavity. Source: Author.

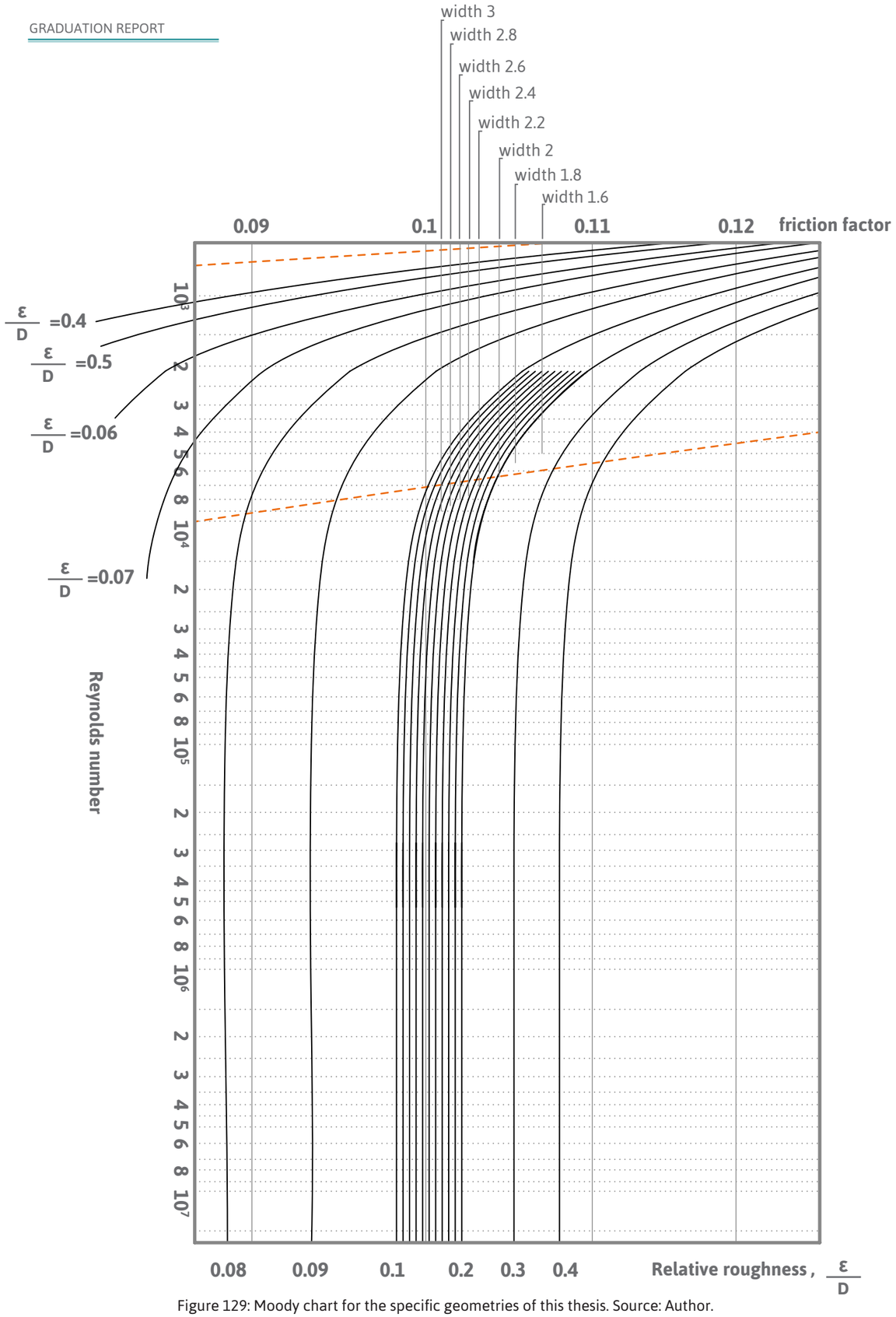

Figure 129: Moody chart for the specific geometries of this thesis. Source: Author.

4.8 Validation of the results

To validate the pressure-drop values from the simulations, they had to be compared with the values from the literature. Since the geometries had surface roughness, the Moody chart had to be used which includes relative roughness and friction factor. Due to high relative roughness, the friction factors in the geometries were very close, almost 0.1. Using the Moody chart, the pressure drops were calculated for each geometry (however, the relative roughness of the geometries were much higher than the values of the axis). Yet, the values from the chart and the ones from the simulations had a large difference.

Literature	
absolute roughness (cm)	0.25
diameter (cm)	1.49
relative roughness (Ɛ)	0.16
Reynolds number	4748.71
friction factor	0.1
length (m)	0.3
Pressure drop (Pa)	4.83

CFD simulation	
Inlet pressure (Pa)	26.7
Outlet pressure (Pa)	4.31
Pressure drop (Pa)	22.39

Table 15: Geometry 2, comparison of pressure drops from the CFD simulation and the literature. Source: Author.

Literature	
absolute roughness (cm)	0.31
diameter (cm)	1.45
relative roughness (Ɛ)	0.21
Reynolds number	4516.92
friction factor	0.1
length (m)	0.3
Pressure drop (Pa)	4.96

CFD simulation	
Inlet pressure (Pa)	13.49
Outlet pressure (Pa)	3.58
Pressure drop (Pa)	9.91

Table 16: Geometry 3, comparison of pressure drops from the CFD simulation and the literature. Source: Author.

Literature	
absolute roughness (cm)	0.3
diameter (cm)	1.54
relative roughness (Ɛ)	0.19
Reynolds number	6037.33
friction factor	0.1
length (m)	0.3
Pressure drop (Pa)	4.67

CFD simulation	
Inlet pressure (Pa)	45.02
Outlet pressure (Pa)	20.25
Pressure drop (Pa)	24.77

Table 17: Geometry 4, comparison of pressure drops from the CFD simulation and the literature. Source: Author.

To ensure the results from Ansys Fluent were valid, a simulation was run for a straight smooth channel with the same dimensions of the corresponding complex geometry. With the same settings as in the simulations of complex geometries, in this simple geometry, the average inlet pressure was 4.18 Pa and the average outlet 2.56 Pa. The pressure drop was 1.62 Pa. This pressure drop was very close to the calculated number based on the theory which was 1.6 Pa (https://goodcalculators.com/friction-loss-calculator/). In this simulation, the pressure dropped linearly along with the flow. This outcome confirmed the validity of the collected results from the simulations of the complex geometries.

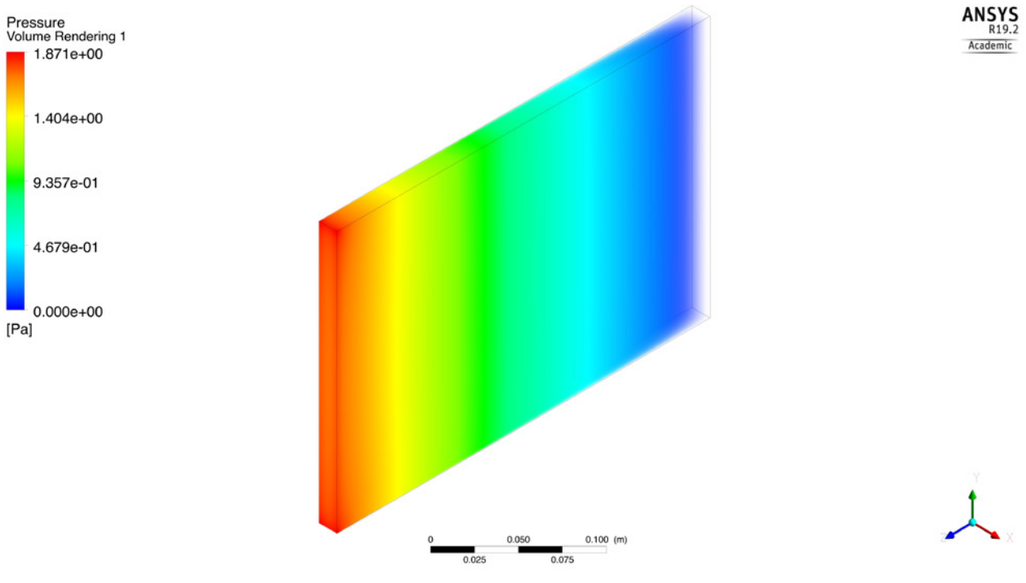

Figure 130: Pressure volume rendering in a straight smooth channel with the dimensions of the corresponding complex geometry. Pressure drop was linear along the flow as expected. Source: Author.

Based on the obtained results, the data suggest that the difference in the pressure drops of the simulations and literature is expected to be due to the backflows and eddies that occur as a result of the very high surface roughness in the geometries. These eddies were observed in the CFD analysis of the complex geometries. Additionally, the changing shape of the inlet might also play a role in this.

4.9 Next steps

For further development of the research, the focus has to be on several aspects.

First, the fluid-structure interaction, as it would be in the real-life application, has to be simulated. This allows the designer to evaluate and adjust the geometries, based on the simulation results. For this process, it is ideal to create a digital workflow that integrates the design phase and the CFD analysis within one platform. In the carried out research, geometry generation was done in Grasshopper and CFD analysis was done in Ansys Workbench. Although adjusting the geometries based on the CFD results was possible, it was not the most efficient way. Having an iterative loop within one platform facilitates the evaluation and optimization. Once a promising design solution is identified, automatic optimizations can be performed. The optimization loops are intended to allow both identifying the optimal design configuration and studying relations between geometric features and performances.

As for the manufacturing of the fluid-structure, the material and the fabrication technique has to be explored in detail. The outcome of the initial research suggests that shape memory polymers are the most promising solution for this function. In addition to their lower price, shape memory polymers display a better shape memory effect with larger deformations compared to shape memory alloys. In general, polymers are widely used in the 3D printing industry due to their relatively low cost, the possibility of mass-customization and rapid prototyping and their low thermal conductivity makes them a promising choice of material for the application of insulations. Furthermore, based on the performance and aesthetics requirements, using materials with different visual properties can also be an option, such as using translucent or opaque materials. To achieve a deformable and (possibly) multi-material geometry, 4D printing is a promising technique.

For the real-life application of these geometries as dynamic insulation, the required permeable area in the wall will depend on the required flow rate (ventilation with outside air for air quality) and allowed average velocity. The flow rate and area of the breathing part will both influence local thermal comfort.

Finally, the geometries can be printed with opaque or translucent materials. As part of future development, this aspect certainly offers the potential to design envelope components with different visual features.

4.10 Future vision

As the future vision, the target is to develop the used design-through-research method into a design toolkit based on a texture database. This provides the designer with a platform in which a wide range of textures are categorized according to their properties and their respective performance features. Depending on the target functionality, each texture can also be modified to adjust the resultant performance.

CONCLUSION

This thesis was developed to answer the following main research question:

How can complex microscale geometries contribute to regulating the air flow rate and pattern inside dynamic insulation, using the potentials of additive manufacturing?

To answer the main research question, several sub-questions were defined that helped to focus on different aspects of the main topic and shaping the research outcome.

1. What are the complex geometries? How can they be generated and how can their properties be evaluated?

In the presented research, complexity has been addressed based on the following aspects:

Functional complexity

As part of the building envelope, dynamic insulation can be used in the design of the walls and has to adapt itself to the continuous changes of the outdoor environment while providing comfort for the occupants. The velocity and direction of the outside air always change. Therefore, integrating static pores with a specific path (conventional design of dynamic insulation) for the air to permeate through might not be an efficient design and in scenarios where the outside velocity is too high or too low, the performance of the system is affected.

For the dynamic insulation to be able to respond to the outside velocity, it has to have a variable ventilation performance by having an adaptive cavity volume. This goal can be achieved by integrating a self-regulating system within the geometry and introducing a fluid-structure. Since CFD evaluation of a fluid-structure is beyond the limits of a master thesis, multiple static scenarios are simulated during the evaluation phase, to roughly represent how the fluid-structure would perform. However, the exact simulations of the fluid-structure interaction are part of the future developments of this thesis.

In the proposed design, permeability is not constant. It is not only dependent on position but also on another parameter that can be controlled, airflow rate. By doing so, the airflow rate can become independent of the pressure difference and ensures that the flow passes through the geometry regardless of the pressure difference over the facade.

The engineered geometries are texture-based metamaterials with cavities. The reason behind the title is that the implemented design principles are based on the concept of metamaterials, in which the microstructural units are designed and assembled to create the material. Using textures as the foundation of the geometries is simply the author's choice to explore a research method. The cavities of the geometries represent the pores in a conventional porous material and transportation of fluids is done through the cavities. By changing the shape or size of the unit-cells, various geometries can be obtained.

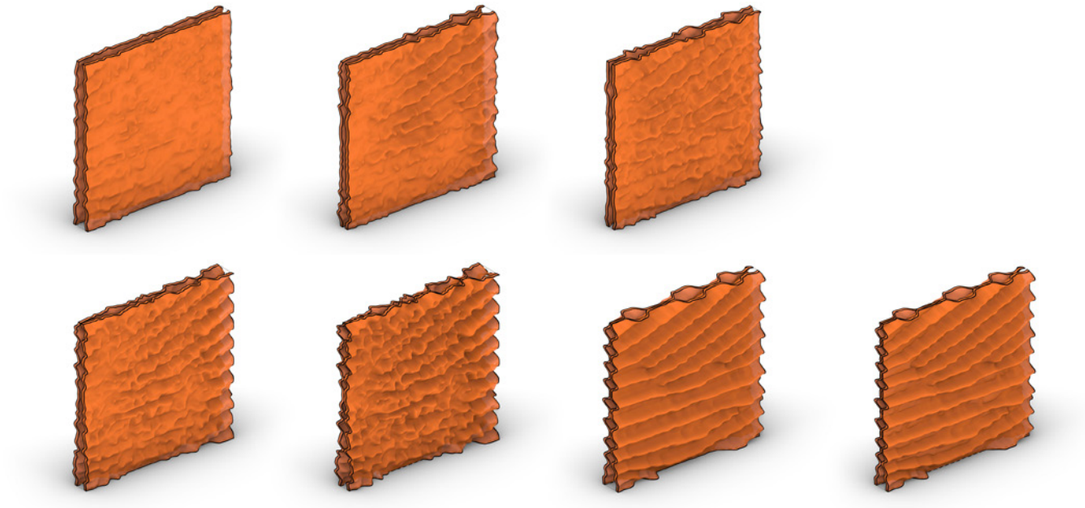

Figure 131: Adaptation of the unit cell in response to the outside velocity. Source: Author.

As a self-regulating system, it is expected that when the pressure drop over the system is low, the microstructure is smooth with minimum surface roughness and large cavity volume. With the increase of pressure drop, the microstructure has to provide a lower permeability to keep an almost constant airflow rate, prevent user discomfort, and decrease in the performance of the system by allowing less air permeate through the wall. Thus, the two layers in each unit-cell come closer together, intersecting in some areas and as a result, reducing the volume of the cavity. Compared to the initial position, higher surface roughness leads to smaller cavity volume in the geometry and lower overall permeability.

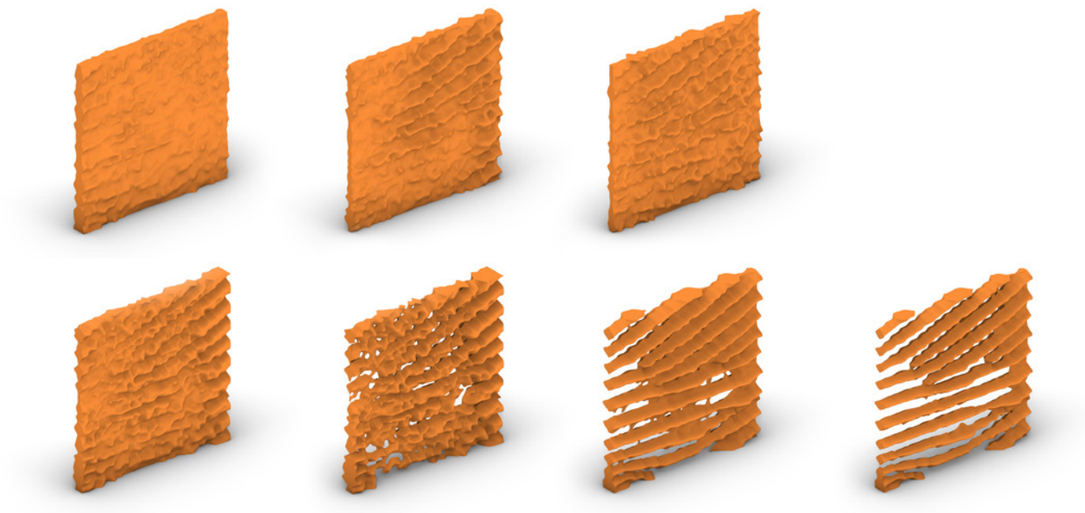

Figure 132: Adaptation of the cavity in response to the outside velocity. Source: Author.

Shape complexity

While functionally graded materials (FGMs) have gradually-changing porosity, microstructure or chemical composition over the entire volume of the material, the engineered geometries in this thesis have **gradually-changing cavity volume, over time,** in response to the exerted pressure by the outside velocity as the stimuli of the system. In FGMs, the varying properties of the material depend on the spatial position in the geometry, whereas in the obtained engineered geometries, the changing outside velocity is the determinant parameter of the variation of properties over time. Compared to the static geometry of functionally graded materials, the varying properties in the engineered geometry is offered by its fluid-structure.

Material complexity

Common porous materials contain pores in the form of channels or cavities. The properties of porous materials depend on several factors such as the porosity, and the form and size of the pores. The designed engineered geometry **performs as a material** that cannot be described as a conventional microscopic porous medium. Using the 3D Sampling technique as part of the design-through-research method allows generating various geometries based on different textures. To achieve the aesthetics preferences or structural targets, multi-material 3D printing could also be considered as an option.

2. Why implementing complex geometries in the design of dynamic insulation could offer a potential contribution to the performance of the system?

Based on the availability of the literature focusing on dynamic insulation, it can be said that this topic is still evolving and has unknown areas that require investigation and research. Most research papers are based on the principles of this system and have tried to explore it with new components such as using different materials (concrete, wood, etc) or using water circuits to induce temperature change. However, they have only explored the system using geometries with static circular pores. Therefore, it became evident that the use of complex geometries is not yet investigated. Since the proposed geometries have varying cavity volume over time, they can offer various functionalities in response to the outside air and have the potential to improve the performance of dynamic insulation compared to using static geometries.

3. What is the effect of texture on air flow rate and pattern?

Textures exhibit various features such as a dominant direction, intensity distribution, density, etc. The obtained data from the CFD simulations suggest that a texture with horizontal direction can result in unifying the streamlines and relatively low pressure-drops in the geometry. However, textures with vertical direction lead to turbulent and chaotic streamlines, the occurrence of eddies and backflows in the cavity and high pressure-drops. This effect is intensified when the outside velocity is high, as the geometry has to adapt to having a smaller cavity volume; thus, the presence of an underlying texture becomes more highlighted. Overall, textures with a horizontal or vertical direction had a large impact on the airflow behavior in the designed geometries, whereas the influence of direction-less textures was not as significant as the ones with a dominant direction.

Intensity distribution influences the contrast of the texture and affects the even or uneven distribution of surface roughness in the geometry. Textures with a high intensity-distribution result

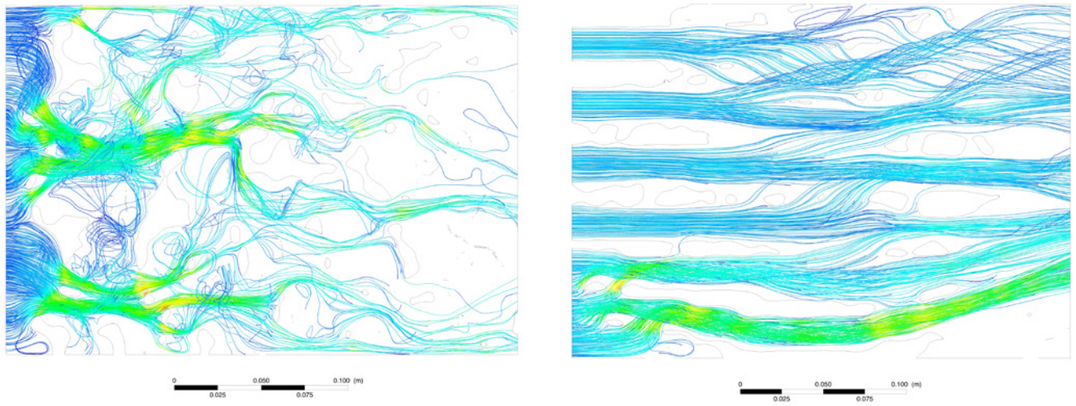

Figure 133: Comparison for better understanding of the impact of textures with different dominant directions. Geometry 2 based on a direction-less texture experiences eddies and backflows (right), while Geometry 4 based on a texture with horizontal direction experiences unified streamlines and almost no eddies. Source: Author.

in geometries with higher surface roughness and more irregular streamlines in their cavity. Low intensity-distribution in the texture results in more even distribution of surface roughness in the geometry and thus, a smoother surface. Geometries based on low-intensity textures have relatively parallel streamlines with almost no eddies (depending on the width of the cavity). The intensity distribution of the texture did not have a significant impact on the pressure-drops in the designed geometries.

Due to several reasons including the occurrence of backflows and eddies, and different inlet and outlet areas, the effect of texture on airflow rate was inconclusive.

Yet, the above-mentioned results are the outcome of simulations on a limited group of selected geometries and textures. To be able to draw definite conclusions, further tests and simulations on a larger sample group are required. As part of the next steps of this research, the intention is to create a platform in which a texture database is defined and based on the expected results, specific textures can be chosen as the underlying texture to generate the geometries.

4. What is the effect of surface roughness on the airflow rate and pattern?

In texture-based geometries, surface roughness can be influenced by the intensity distribution of its base texture, as a low contrast in the texture creates a smoother surface by evenly distributing the roughness over the surface. Depending on the width of the cavity, very high surface roughness can create eddies and turbulent streamlines. Also, as the width of the cavity increases, the influence of surface roughness on the middles areas of the flow is reduced.

Based on the surface roughness, the relative roughness of the cavity can be calculated which is the ratio of the absolute roughness to the diameter of the cavity. Relative roughness defines the roughness of the cavity's inner surface. By knowing the relative roughness of the cavity and the Reynolds number of the flow which passes through it, the friction factor (representing the frictional losses in the cavity) is obtained from the Moody chart (due to very high relative roughness, Moody

chart was customized for the designed geometries).

In the designed geometries, the flow is turbulent and the friction factor is highly dependent on the relative roughness of the cavity. The high surface roughness in these geometries results in high pressure-drops.

5. What is the effect of the geometry's changing cavity volume and morphology of the air channels on the airflow rate and pattern?

In conventional porous materials, transportation of fluids is done through the channels or pores of the material. This research uses 3D Sampling as the design through research method and generates texture-based metamaterials with cavities in which, the cavities represent the pores (air channels) of the material in the conventional design. Thus, with a constant volume of the solid parts, different cavity volumes result in different porosities of the geometry.

In this process, several parameters can influence the size or form of the cavity in the geometry:

- The amount of surface roughness of the layers in the unit cell
- The cavity width in the unit cell
- The direction in which a texture is translated to a geometry

Due to the complexity of fluid-structure interaction, and to resemble the fluidity of the system, different static states of each geometry is simulated. The smaller cavity-volume variation illustrates the geometry during the times when the exerted pressure by the outside velocity is high, whereas the larger cavity-volume variation depicts the reaction of the system to low outside velocities and low induced pressures. To achieve higher accuracy, more static states can be simulated.

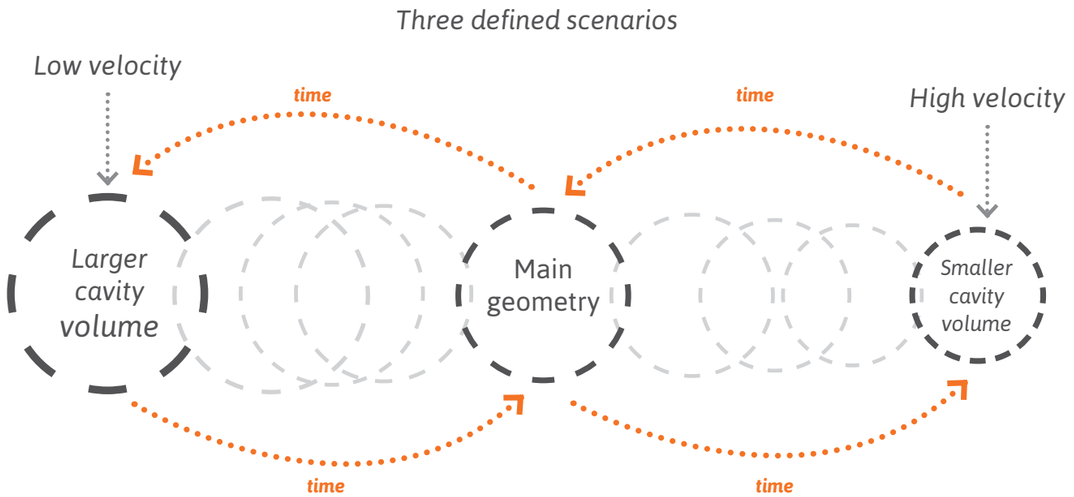

Figure 134: Due to the complexity of fluid-structure interaction, several static scenarios are defined that could resemble how the fluid-structure would work as part of the bigger picture of the research. Source: Author.

Confirmed by the CFD simulation results, a smaller volume of the cavity results in high pressure-drops in the geometry and accelerates the airflow rate. However, a geometry with a larger cavity volume does not experience a relatively high pressure-drop, a considerable increase of airflow rate or eddies and backflows.

Geometry 1	Larger cavity volume (G1-A)	Main geometry (G1)	Smaller cavity volume (G1-B)
Cavity volume (cm^3)	949	898	823
Normalized pressure drop ($\Delta P/P_{inlet}$)	0.58	0.81	0.98
Inlet velocity (m/s)	2	2	3.5
Average outlet velocity (m/s)	2.07	3.16	5.1

Table 18: High pressure-drops in the variation with smaller cavity volume, compared to the main geometry and the variation with a larger cavity volume . Source: Author.

While a geometry with large cavity volume does not induce a substantial change to the airflow pattern, the effect of a small cavity-volume can be intensified by the base texture of the geometry. For instance, in a geometry with small cavity-volume, if the base texture has a horizontal dominant direction, it experiences much fewer eddies. The pressure drop in such geometry is high due to the small volume of the cavity but still is lower than the pressure drop in a small cavity-volume in a geometry based on texture with a vertical direction. If the texture has a vertical direction, the pressure-drops are much higher, the flow is more turbulent and the occurrence of backflows and eddies is mostly placed in the areas with vertical channels.

Geometry 4	Horizontal direction	Vertical direction
Cavity volume (cm^3)	930	947
Average inlet pressure (Pa)	45.02	37.58
Average outlet pressure (Pa)	20.25	6.25
Normalized pressure drop ($\Delta P/P_{inlet}$)	0.55	0.83
Inlet velocity (m/s)	2	2
Average Outlet velocity (m/s)	5.31	2.63

Table 19: A geometry based on a texture with vertical direction experiences much higher pressure-drops and eddies compared to the one based on a texture with horizontal direction. Source: Author.

6. What is the potential contribution of additive manufacturing to this process and research?

Facilitated by additive manufacturing, the complexity of a design is now less limited compared to using conventional manufacturing processes. Additive manufacturing is the most promising and

efficient technique to produce complex geometries with cavities as using conventional technologies such as casting is impractical and costly. Also, the composition of the structure can be locally adjusted and based on the performance or aesthetics requirements, materials with different visual properties can be used, such as translucent or opaque materials. In this process, 4D printing can be used to obtain a responsive structure.

4D printing is printing 3D objects that can deform and reconfigure themselves over time. The reconfiguration is a response to the external stimuli, such as temperature change, light, electrical currents, pressure, etc, that is induced to the structure. Research suggests shape memory polymers as a good choice of material. Enabled by the inherent shape memory effect of the material, reversible changes of the structure can occur to optimize the performance of dynamic insulation. Using shape memory polymers is cost-effective and allows for rapid prototyping and desired post-processing. Polymers have low thermal conductivity and have excellent performance as insulators. However, shape memory polymers do not have high mechanical strength and stiffness and thus, cannot be used as part of a load-bearing structure.

Yet, a detailed selection of the materials and 4D printing of the designed geometries including the programming of the adaptive geometries remains a part of the future investigations of this research as they have not been explored in-depth in this thesis.

REFLECTION

Aspect 1: The relationship between research & design

This graduation thesis focuses on designing a complex microstructure for dynamic insulation that can contribute to airflow regulation and eventually provides better performance for the system. Broad research was done through a literature review that covered different aspects involved in the design, such as the conventional ventilation systems, the essential information about dynamic insulation, different materials, additive manufacturing processes and materials, optimization, etc. Despite being introduced in the 1970s, dynamic insulation is still a novel technology and the lack of precedent projects was clear. As a result, the papers and articles were the primary source of information which made it quite challenging in terms of the validity of the results. As an example, a paper with physical experiments had contradictory results compared to other papers, which later was pulled out of the sources as there were no other papers to support the idea.

In the early stages of the literature review, it was noticed that the material's potential can have a significant influence on the design and performance of the system and it could be a driving force in the design process. Therefore, extensive research was done on different materials that could either be used or their concept could be implemented such as traditional thermal insulators, functionally graded materials, latent heat storage materials, and texture-based meta-materials. Texture-based meta-materials created a whole new field to explore which at the end resulted in the main design concept for this thesis.

Considering the very small amount of work that has previously been done on this topic, there is a need for further research and focusing on details of the system and how it would be applied to practice.

Aspect 2: The relationship between your graduation (project) topic, the studio topic (if applicable), your master track (A,U, BT, LA, MBE), and your master program (MSc AUBS)

Sustainable Design Graduation Studio is the Building Technology studio that focuses on designing for sustainability. Concerning this, the chosen graduation topic aims to increase the efficiency of dynamic insulation. To do so, the optimal goal is to design a fluid microstructure inside the dynamic insulation that adapts itself according to the velocity of the airflow; thus, making the airflow rate independent of pressure difference. This approach ensures that dynamic insulation performs efficiently regardless of the environmental conditions. Improving the performance of dynamic insulation makes it a practical design option that could be implemented in the design of the building envelope; thus, resulting in having a natural ventilation supply/exhaust for the building. Thus, it can reduce the energy use of the building significantly. Although the constructability aspect of the microstructure is not fully explored in this thesis due to lack of time, it is expected that this system would be 4D printed.

Aspect 3: Elaboration on research method and approach chosen by the student in relation to the graduation studio methodical line of inquiry, reflecting thereby upon the scientific relevance of the work.

This graduation thesis followed the methodical approach of the graduation studio. Previous related thesis projects were also considered as references. The research methodology of this thesis has been structured into the following phases: Literature review, establishing design requirements, design through research, evaluation and conclusion.

To establish the design requirements, different parameters were defined as the preliminary design requirements based on the results of the literature study. These parameters were later adjusted and refined in the design-through-research phase. During design through research, the design process started by experimenting with the approaches that textures could be translated to create geometries. This part was quite time-consuming to figure out how to set the workflow, as related reference papers had done their work using processing platforms.

Design through research and evaluation are in an iterative loop. Therefore it was necessary to start the CFD simulations to understand how to take the design further. After P2, to decide which CFD software to use for validating the results, there were several discussions and meetings with the mentors and experts of CFD simulations from other departments of the faculty. During all the meetings, it was mentioned that the type of geometries in this thesis is rather complex and doing a CFD simulation would be very challenging. Also, due to the existing excessive complexity of the geometries and design, it was decided that the optimal goal, achieving a fluid-structure interaction, should be simplified and static geometries should be used for the CFD simulations.

At first, it was intended to use a general CFD software for an initial screening and then using detailed analysis. However, the general software that was available such as Phoenics did not provide proper results which could be due to the complexity of the geometry or the micro-scale of the geometry. Other tools such as Butterfly plugin in Grasshopper were also tested. However, during the simulation, it was observed that this tool was more aimed for outdoor/indoor airflow simulations and using it to simulate airflow inside a cavity would not produce accurate results.

After testing several CFD software, it was decided to use Ansys Fluent, which was earlier chosen as the final software for detailed analysis. Fluent is a solver in Ansys workbench and it's a powerful and accurate tool. However, it's a very complicated software and just learning the basics and how to work with it would take roughly two-three months. Since this amount of time was not available due to the limited timeline, Ansys Fluent had to be explored while working on the geometries to validate them. Moreover, earlier plans were made to get guidance on Fluent from specialized mentors at the Aerospace faculty. However, due to the spread of Covid-19 and the shutdown of the university, this was not possible anymore. This quite affected the process of using the software.

Aspect 4: Elaboration on the relationship between the graduation project and the wider social, professional and scientific framework, touching upon the transferability of the project results.

Scientific relevance:

The current lack of information and resources about dynamic insulation in the built environment is quite evident. While many papers and articles can be found about this subject, only two built projects exist that could be taken as precedents (although very little information about these projects was available). In this thesis, the aim has been to combine different topics including dynamic insulation, complex geometries, material design and constructability. Although the constructability aspect was not fully explored due to the selected approach in the methodology, it has the potential to be further investigated in terms of the construction process and material selection. While the microstructure of the material can have a rather high impact on its function and performance, the influence of air channels with complex geometries on the airflow rate and pattern is not yet investigated in the design of dynamic insulation. Implementing complex microstructures introduces various aspects to the design

of the system and allows for optimization and improving the performance of the system by changing the geometry of the microstructure, the selection of materials, etc. The optimal goal of this thesis (fluid-structure interaction) was beyond the scope of the master studies and therefore, the target had to be adjusted. Plans are made regarding continuing the research after graduation. Still, the link between the dynamic insulation, the mechanical ventilation system and user comfort has to be addressed. Initial calculations suggested good thermal comforts for the user; however, further analysis is needed. In further developments of the research, it is expected that a design toolkit could be created which is based on specific established guidelines.

Societal relevance:

Despite being introduced in the 1970s, the topic of dynamic insulation is still relatively new and there are vague aspects that need to be explored and investigated. As a result, this system is not commonly known in the building industry and the traditional insulation systems are still used in the design and construction process.

Due to the variable U value, dynamic insulation allows for thinner insulation layers, resulting in more lightweight construction. However, this benefit is not explored in the current constructions.

As 3D printing allows for combining multiple design variables, optimum complex geometry can be designed and manufactured according to the climate and context. However, there is a trade-off between the more lightweight, efficient construction and the production cost, which I think would be less problematic in the future once this system is more recognized in the building industry.

REFERENCES

Alongi, A., Angelotti, A., & Mazzarella, L. (2019). Measuring a Breathing Wall's effectiveness and dynamic behaviour. *Indoor and Built Environment, 0* (0), 1–10. doi: 10.1177/1420326X19836457

Arquis, E., & Langlais, C. (1986). What scope for 'dynamic insulation'?. *Batiment International, Building Research and Practice, 14* (2), 84-93. doi: 10.1080/01823328608726724

Ascione, F., Bianco, N., De Stasio, C., Mauro, G. M., & Vanoli, G. P. (2015). Dynamic insulation of the building envelope: Numerical modeling under transient conditions and coupling with nocturnal free cooling. *Applied Thermal Engineering , 84* , 1-14.

Ashby, M. F., & Medalist, R. M. (1983). The mechanical properties of cellular solids. *Metallurgical Transactions A , 14* (9), 1755-1769.

ASTM International. (2010). F2792-10 Standard Terminology for Additive Manufacturing Technologies . Retrieved from https://doi.org/10.1520/F2792-10

Baker, P. H. (2003). The thermal performance of a prototype dynamically insulated wall. *Building Services Engineering Research and Technology , 24* (1), 25-34.

Cao, X., Dai, X., & Liu, J. (2016). Building energy-consumption status worldwide and the state-of-the-art technologies for zero-energy buildings during the past decade. *Energy and buildings , 128* , 198-213.

Costa, A., Keane, M. M., Torrens, J. I., & Corry, E. (2013). Building operation and energy performance: Monitoring, analysis and optimisation toolkit. *Applied Energy , 101* , 310-316.

Craig, S., & Grinham, J. (2017). Breathing walls: The design of porous materials for heat exchange and decentralized ventilation. *Energy and buildings , 149* , 246-259.

de Gracia, A. (2019). Dynamic building envelope with PCM for cooling purposes - Proof of concept. *Applied energy , 235* , 1245-1253.

Dimoudi, A., Androutsopoulos, A., & Lykoudis, S. (2004). Experimental work on a linked, dynamic and ventilated, wall component. *Energy and Buildings , 36* (5), 443-453.

Durgin, F. H., & Proffitt, D. R. (1996). Visual learning in the perception of texture: Simple and contingent aftereffects of texture density. *Spatial vision, 9*(4), 423-474.

Estrado, E. (2019) *Optimisation of complex geometry buildings based on wind load analysis* [Master's thesis, Delft University of Technology]. Retrieved from https://repository.tudelft.nl/islandora/object/uuid%3Abea970ba-da91-40e5-b31d-53cf0cb15ec3?collection=education

European Union. (2010). Directive 2010/31/EU of the European Parliament and of the Council of 19 May 2010 on the energy performance of buildings (recast). Official Journal of the European Union, 53, 13–35. Retrieved from http://doi.org/doi:10.3000/17252555.L_2010.153.eng

Farrugia, E. (2018). *Thermal Morphology: A Geometrically Optimized Trombe Wall* [Master's thesis, Delft University of Technology]. Retrieved from https://repository.tudelft.nl/islandora/object/uuid%3A0ad5f3cc-a5e9-45c0-a37e-75e139713409?collection=education

Gan, G. (2000). Numerical evaluation of thermal comfort in rooms with dynamic insulation. *Building and Environment , 35* (5), 445-453.

Gibson, I., Rosen, D., & Stucker, B. (2015). *Additive Manufacturing Technologies: 3D Printing, Rapid Prototyping, and Direct Digital Manufacturing* . New York: Springer. doi: 10.1007/978-1-4939-2113-3

Guo, N., & Leu, M. C. (2013). Additive manufacturing: technology, applications and research needs. *Frontiers of Mechanical Engineering , 8* (3), 215-243.

Homem, J. T. L. A. (2016). *Dynamic insulation as a strategy for net-zero energy buildings* [Master's thesis, Eindhoven University of Technology]. Retrieved from http://www.janhensen.nl/team/past/master/Homem_2016.pdf

Hu, H. H. (2012). *Computational fluid dynamics*. In P. Kundu & I. Cohen & D. Dowling (Eds), Fluid mechanics (pp. 421-472). Waltham, MA: Academic Press.

Ibrahim, A.T. (2019). *3D Printing Clay Facade Walls: Integrating Ventilation systems into printing process* [Master's thesis, Delft University of Technology]. Retrieved from https://repository.tudelft.nl/islandora/object/uuid%3A82330bb4-85ff-47a8-a48f-06ea01c52154?collection=education

Imbabi, M. S. E. (2006). Modular breathing panels for energy efficient, healthy building construction. *Renewable Energy , 31* (5), 729-738.

Imbabi, M. S. E. (2012). A passive–active dynamic insulation system for all climates. *International journal of sustainable built environment , 1* (2), 247-258.

Jelle, B. P. (2011). Traditional, state-of-the-art and future thermal building insulation materials and solutions - Properties, requirements and possibilities. *Energy and Buildings , 43* (10), 2549-2563. doi: 10.1016/j.enbuild.2011.05.015

Jin, Q., Favoino, F., & Overend, M. (2015). The potential opaque adaptive façades for office buildings in a temperate climate. *Proceedings of building simulation 2015 conference* , 98-105.

Khathun, A. S. (2018). *Functionally graded materials - an overview* [slides]. Retrieved from https://www.slideshare.net/sabihakhathun/overview-of-functionally-graded-materials-97027240

LaFrance, M. (2013). Technology Roadmap: Energy efficient building envelopes. Paris: IEA. Retrieved from https://www.oneplanetnetwork.org/sites/default/files/technology_roadmap_energy_efficient_building_envelopes.pdf

Li, A., Challapalli, A., & Li, G. (2019). 4D printing of recyclable lightweight Architectures using high recovery stress shape memory polymer. *Scientific reports, 9*(1), 1-13.

Loh, G. H., Pei, E., Harrison, D., & Monzon, M. D. (2018). An overview of functionally graded additive manufacturing. *Additive Manufacturing, 23* , 34-44.

Mahamood, R. M., & Akinlabi, E. T. (2017). Types of functionally graded materials and their areas of application. In C. P. Bergmann (Ed.), *Functionally Graded Materials*. (pp. 9-21). Cham, Switzerland: Springer.

Melchels, F.P., Bertoldi, K., Gabbrielli, R., Velders, A.H., Feijen, J., & Grijpma, D.W. (2010). Mathematically defined tissue engineering scaffold architectures prepared by stereolithography. *Biomaterials, 31*(27), 6909-6916 .

Patel, S. V., Mignone, P. J., Tam, M. K. M., & Rosen, D. (2017). Reverse natures: Design synthesis of Texture-Based Metamaterials (TBMs). In *Proceedings of the 21 st International Conference on Engineering Design (ICED 17), 1 (8)*, 509-518.

Patel, S. V., & Mueller, C. T. (2015). 3dj: 3d Sampling Haptic and Optically Performative Textures Remixed from 3d Scans. In M. R. Thomsen, M. Tamke, C. Gengnagel, B. Faircloth, F. Scheurer (Eds),

Modeling Behavior. (pp. 527-541). Cham, Switzerland: Springer.

Patel, S. V., Tam, M. K., & Mueller, C. T. (2017). 3DJ: An analytical and generative design system for synthesizing high-performance textures from 3D scans. In J. Gero (Ed.), *Design Computing and Cognition'16* , 477-494. Cham, Switzerland: Springer. doi: https://doi.org/10.1007/978-3-319-44989-0_26

Patel, S. V., Tam, K. M. M., Pushparajan, S., & Mignone, P. J. (2017). 3D Sampling Textures for Creative Design and Manufacturing. Disciplines & Disruption - *Proceedings Catalog of the 37th Annual Conference of the Association for Computer Aided Design in Architecture, ACADIA 2017* , 464-473.

Shinohara, Y. (2013). Functionally Graded Materials. In S. Somiya (Ed.), *Handbook of advanced ceramics: materials, applications, processing, and properties*. (pp. 1179-1187). MA, USA: Academic press.

Taylor, B. J., & Imbabi, M. S. (1998). The application of dynamic insulation in buildings. *Renewable energy , 15* (1-4), 377-382. doi: 10.1016/S0960-1481(98)00190-6

Toledo, L., Cropper, P. C., & Wright, A. J. (2016). Unintended consequences of sustainable architecture: Evaluating overheating risks in new dwellings. PLEA 2016 Los Angeles - 32th International Conference on Passive and Low Energy Architecture. Cities, Buildings, People: Towards Regenerative Environments . Retrieved from https://www.researchgate.net/publication/305619149_Unintended_consequences_of_sustainable_archite cture_Evaluating_overheating_risks_in_new_dwellings

Van der Aa, A., Heiselberg, P. & Perino, M. (2011). IEA-ECBCS Annex 44: Designing with Responsive Building Elements [Booklet]. Retrieved from: https://www.ecbcs.org/Data/publications/EBC_Annex_44_RBE_Design_Guide.pdf

Versteeg, H. K., & Malalasekera, W. (2007). *An introduction to computational fluid dynamics: the finite volume method*. Harlow, England: Pearson Education.

Voss, K., Sartori, I., & Lollini, R. (2012). Nearly-zero, net zero and plus energy buildings – How definitions & regulations affect the solutions. *REHVA journal , 49* (6), 23-27.

Wehringer, F., Scherberich, M., Groezinger, J., Boermans, T., John, A. S. J., & Seehusen, J. (2014). Overview of Member States information on NZEBs Working version of the progress report - final report (BUIDE14975). Retrieved from https://ec.europa.eu/energy/sites/ener/files/documents/Updated%20progress%20report%20NZEB.pdf

Wit, de, M. H. (2009). Convective Heat and Moisture Transfer. In W.H. van der Spoel (Ed.), *Heat, air and moisture in building envelopes*. (pp. 63-87). Eindhoven: Technische Universiteit Eindhoven.

Yoon, S., & Hoyano, A. (1998). Passive ventilation system that incorporates a pitched roof constructed of breathing walls for use in a passive solar house. *Solar energy , 64* (4-6), 189-195.

Zhao, Y., Zhang, T. T., Wang, S., & Geng, Y. (2011). An active breathing wall to improve indoor environment. *Proceedings of Building Simulation*, 429-435.

Zhou, D. (2006). *Texture Analysis and Synthesis using a Generic Markov-Gibbs Image Model* (Phd thesis). Retrieved from https://www.cs.auckland.ac.nz/~georgy/research/texture/thesis-html/thesis.html

Websites

3D Hubs. (n.d.). *Additive Manufacturing Technologies: An Overview*. Retrieved December 6, 2019, from https://www.3dhubs.com/knowledge-base/additive-manufacturing-technologies-overview/

ANSYS. (n.d.). *ANSYS Fluent*. Retrieved from https://www.ansys.com/products/fluids/ansys-fluent

ANSYS. (n.d.). *ANSYS CFX*. Retrieved from https://www.ansys.com/products/fluids/ansys-cfx

Comfort and Low Energy ARchitecture. (n.d.). *Air Infiltration*. Retrieved from https://www.new-learn.info/packages/clear/interactive/matrix/d/hot_climate/air_infiltration.html

COMSOL. (n.d.). *COMSOL Multiphysics*. Retrieved from https://www.comsol.nl/comsol-multiphysics

COMSOL. (2017). *Fluid-Structure Interaction*. Retrieved from https://www.comsol.com/multiphysics/fluid-structure-interaction

Connor, N. (2019). *What is Friction Factor for Turbulent Flow – Colebrook Equation – Definition*. Retrieved from https://www.thermal-engineering.org/what-is-friction-factor-for-turbulent-flow-colebrook-equation-definition/

Gaia Research. (n.d.). *Dynamic Insulation*. Retrieved November 26, 2019, from http://www.gaiagroup.org/assets/pdf/publications/dynamic%20insulation%20web.pdf

Ladybug Tools. (n.d.). Retrieved from https://www.ladybug.tools/butterfly.html

Loughborough University. (n.d.). *About Additive Manufacturing*. Retrieved December 10, 2019, from https://www.lboro.ac.uk/research/amrg/about/the7categoriesofadditivemanufacturing/vatphotopolymerisation/

NASA Glenn Research Center. (n.d.). *Beginner's Guide to Aeronautics*. Retrieved from https://www.grc.nasa.gov/www/k-12/VirtualAero/BottleRocket/airplane/drag1.html

Neoperl. (n.d.). *Flow regulators*. Retrieved February 22, 2020, from https://www.neoperl.net/en/oem/products/flowregulators/introduction_new.html

PERM Inc. (n.d.). *Fundamentals of Fluid Flow in Porous Media*. Retrieved from https://perminc.com/resources/fundamentals-of-fluid-flow-in-porous-media/chapter-2-the-porous-medium/porosity/

Tractus3D. (n.d.). *Advantages of 3D printing*. Retrieved December 8, 2019, from https://tractus3d.com/what-is-3d-printing/advantages-of-3d-printing/

https://goodcalculators.com/friction-loss-calculator/

APPENDIX

A. Full and abbreviated titles of responsive building elements

AIF – TVF	Transparent Ventilated Façade
AIF – OVF	Opaque Ventilated Façade
AIF – PVT	Integrated Photovoltaic, Transparent façade
AIF – PVO	Integrated Photovoltaic, Opaque façade
AIF – SC	Integrated solar air/water Collector
AIF – TIM	With Transparent Insulation Materials
TMA – SA	Thermal Mass Activation – Surface Activation
TMA – CA	Thermal Mass Activation – Core Activation
DI	Dynamic Insulation
PCM	Phase Change Materials
TVR	Transparent Ventilated Roof
OVR	Opaque Ventilated Roof
PVTR	Integrated Photovoltaic, Transparent Roof
PVOR	Integrated Photovoltaic, Opaque Roof
SCR	Integrated Solar air/water Collector – Roof
TIMR	Transparent Insulated Materials - Roof

B. Sample textures used for geometries

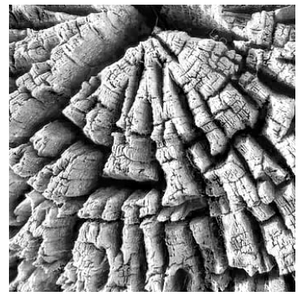

Texture 10

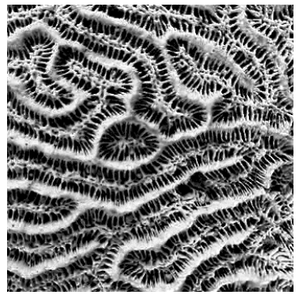

Texture 12

Texture 22

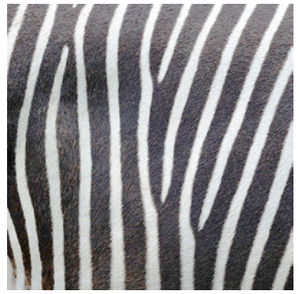

Texture 30

Texture 10 from https://steemit.com/nature/@lazariko12/is-wood-cutting-really-that-bad-for-nature
Texture 12 from http://gigl.scs.carleton.ca/node/1162
Texture 22 from http://www.cbdpools.com/ceramics-close-up/ceramic-gl-tx-007/
Texture 30 from https://www.gettyimages.no/detail/photo/close-up-view-of-zebra-stripes-royalty-free-image/170615172?adppopup=true

C. Sample textures

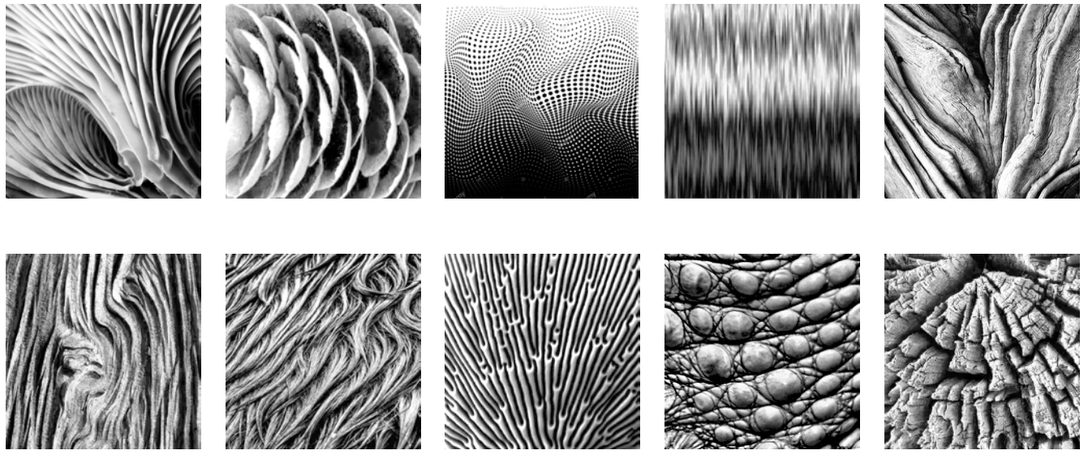

Texture 1 from https://i.pinimg.com/736x/cd/4a/cd/cd4acd03882b26e35245fe2c4cab0064.jpg
Texture 2 from https://www.pinterest.co.uk/pin/394416879845839240/
Texture 3 from https://www.shutterstock.com/image-vector/abstract-halftone-texture-motion-gradient-mesh-1064388377
Texture 4 from https://marketplace.secondlife.com/es-ES/p/Hair-texture-Black-White/10206314?lang=es-ES
Texture 5 from https://www.pinterest.com/pin/424534702370212385/
Texture 6 from https://www.pinterest.ca/pin/332070172505059723/
Texture 7 from https://www.adorama.com/alc/join-adorama-and-gurushots-for-the-worlds-greatest-photography-game
Texture 8 from https://www.pinterest.co.uk/pin/463659724127121520/
Texture 9 from https://www.pinterest.com/pin/633529872555782248/
Texture 10 from https://steemit.com/nature/@lazariko12/is-wood-cutting-really-that-bad-for-nature

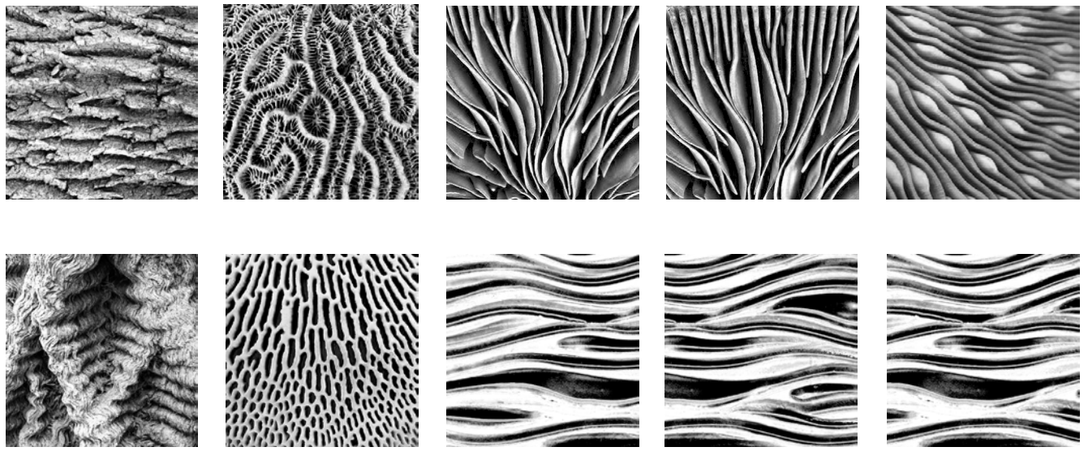

Texture 11 from https://www.goodfon.com/download/wood-tree-brown-dark-natural/3456x2304/
Texture 12 from http://gigl.scs.carleton.ca/node/1162
Texture 13, 14 from https://www.pinterest.com/pin/345229127671339761/
Texture 15 from https://www.pinterest.at/pin/512354895092725379/
Texture 16 from https://www.jharrisonphoto.com/Landscapes/Abstracts-in-Nature-photos/i-3nGCSTn
Texture 17 from https://www.pinterest.cl/pin/659847782892768183/
Texture 18, 19, 20 from http://www.cbdpools.com/ceramics-close-up/ceramic-gl-tx-007/

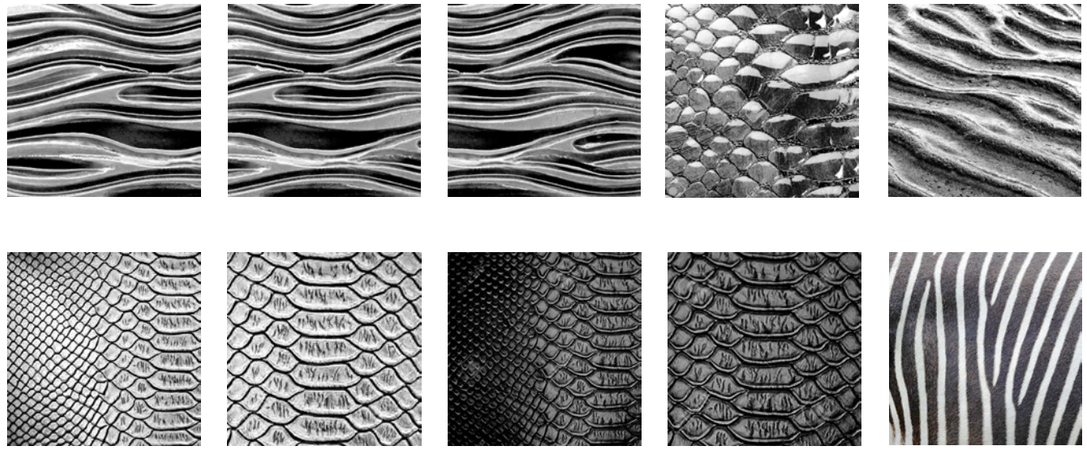

Texture 21, 22, 23 from http://www.cbdpools.com/ceramics-close-up/ceramic-gl-tx-007/
Texture 24 from https://www.shutterstock.com/image-photo/red-snake-skin-texture-47504905
Texture 25 from https://jooinn.com/sand-ridges-texture.html
Texture 26, 27, 28, 29 from https://www.shutterstock.com/image-photo/red-snake-skin-pattern-texture-background-300346820
Texture 30 from https://www.gettyimages.no/detail/photo/close-up-view-of-zebra-stripes-royalty-free-image/170615172?adppopup=true

D. Meshing failures & challenges

Meshing the geometry in Ansys Fluent was definitely the most challenging and time-consuming part of the entire thesis. Due to complexity of the geometries, it was not easy to just follow the tutorials as they mostly did not apply to these cases. The discussed examples in this section are just a small part of the whole process of trial and error and there were more settings that were tried which are not included in this part.

Initially, the whole domain of the geometries were modeled. However, the number of mesh elements was around 11M.

One of the options provided by Fluent is that if there is symmetry in the geometry, symmetry boundary condition or axis boundary condition can be applied to the geometry. This allows for modeling a smaller geometrical domain and thus, less mesh elements, computational demand and time for the software. This options was used to achieve less number of mesh elements. However, the mesh was too fine.

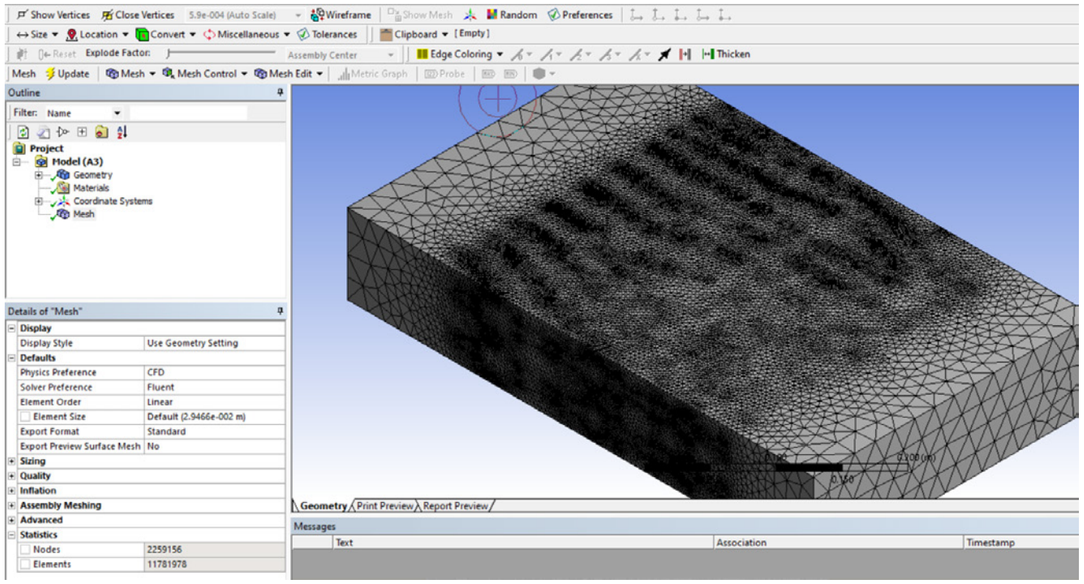

To simplify the mesh, capture proximity was set to off, which results in less number of mesh elements. Changing this setting by itself did not make a large difference.

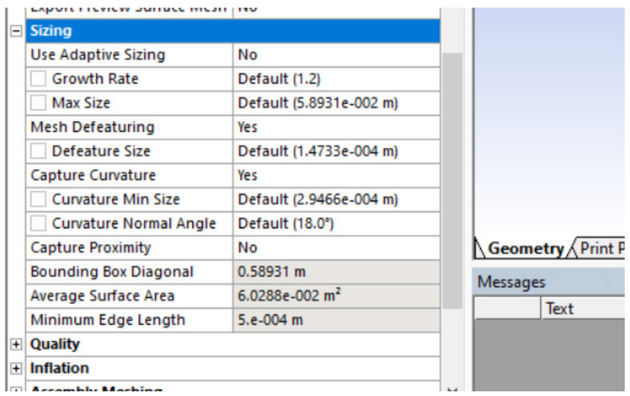

Different defeature sizes and capture curvature sizes were tested in combination with the previous setting. Yet, the change was still small.

As another try, the growth rate was also increased. This ensured that the cell sizes would increase without compromising on orthogonality and skewness. The inflation layers on specific cells were also implemented. Furthermore, few attempts were done using different types of grids.

After using the above settings, the growth rate, defeature size and curvature size were increased. It reduced the number of mesh elements from 11M to 1M. The decrease was significant, but it was still above the 512K limit.

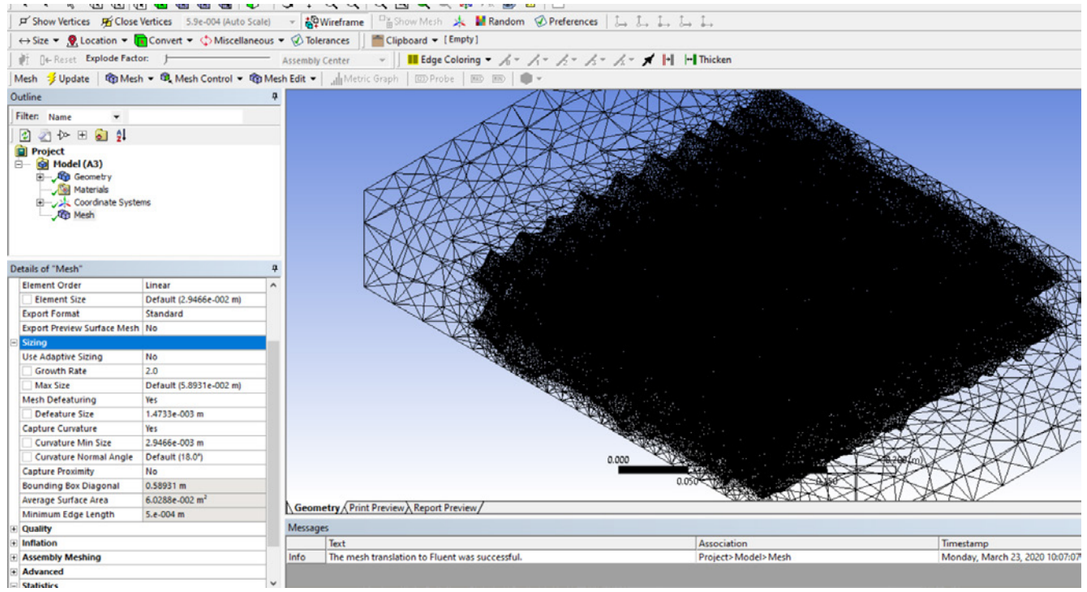

Another approach that was taken was reducing the thickness of the layers in the geometry, to have a lower number of mesh elements. This was not successful as the thickness became too thin for Fluent to mesh and it could not place more than one element on the faces. During this step, an error showed up which was about having an intersection in the geometry, which is displayed in the figure below. This problem was solved by adjusting the distance between the layers.

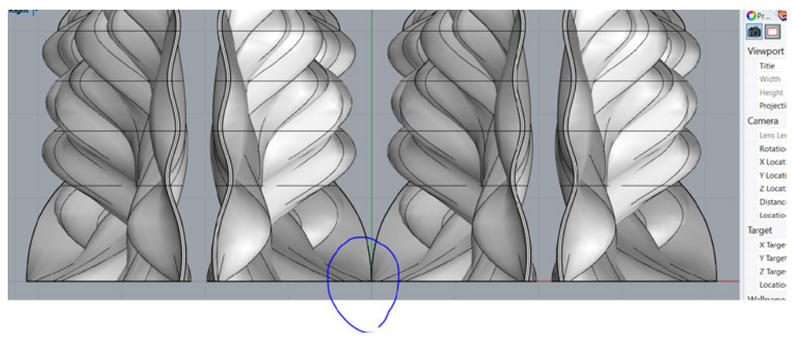

Still, the meshing was not successful with the tried setting. As this was a trial and error process, various settings in combination were tried together, which took more than a few weeks.

F. Calculations for geometry 2

inputs	**u (m/s)**	2	2	2	2	2	2	2	2	2	2	2	2	2	lower velocity scenario
	μ (Kg/m.s)	0.000018	0.000018	0.000018	0.000018	0.000018	0.000018	0.000018	0.000018	0.000018	0.000018	0.000018	0.000018	0.000018	20 degree celsius
	rho (kg/m3)	1.2	1.2	1.2	1.2	1.2	1.2	1.2	1.2	1.2	1.2	1.2	1.2	1.2	
	L (cm)	0.25	0.95	0.63	1.3	2.93	0.36	3.1	1.37	1.54	3.11	3.6	3.17	0.84	
	hydraulic diameter	0.5	1.9	1.26	2.6	5.86	0.72	6.2	2.74	3.08	6.22	7.2	6.34	1.68	3.561538462
Output	**Re**	666.6667	2533.333	1680	3466.666667	7813.333	960	8266.667	3653.333	4106.667	8293.333	9600	8453.333	2240	4748.717949
	Main geometry														
	absolute roughness (cm)	0.25													
	diameter (cm)	1.49			Ansys results										
	Relative roughness	0.167785			inlet pressure	26.7									
	Re	4748.718			outlet pressure	4.31									
	friction factor	0.1													
	length (m)	0.3													
	pressure drop	4.832215			pressure drop	22.39									
inputs	**u (m/s)**	3.5	3.5	3.5	3.5	3.5	3.5	3.5	3.5	3.5	3.5	3.5	3.5	3.5	higher velocity scenario
	μ (Kg/m.s)	0.000018	0.000018	0.000018	0.000018	0.000018	0.000018	0.000018	0.000018	0.000018	0.000018	0.000018	0.000018	0.000018	20 degree celsius
	rho (kg/m3)	1.2	1.2	1.2	1.2	1.2	1.2	1.2	1.2	1.2	1.2	1.2	1.2	1.2	
	L (cm)	0.25	0.95	0.63	1.3	2.93	0.36	3.1	1.37	1.54	3.11	3.6	3.17	0.84	
	hydraulic diameter	0.5	1.9	1.26	2.6	5.86	0.72	6.2	2.74	3.08	6.22	7.2	6.34	1.68	
Output	**Re**	1166.667	4433.333	2940	6066.666667	13673.33	1680	14466.67	6393.333	7186.667	14513.33	16800	14793.33	3920	

E. Calculations for geometry 1

inputs	**u (m/s)**	2	2	2	2	2	2	2	2	2	2	2	2	2	lower velocity scenario
	μ (Kg/m.s)	0.000018	0.000018	0.000018	0.000018	0.000018	0.000018	0.000018	0.000018	0.000018	0.000018	0.000018	0.000018	0.000018	20 degree celsius
	rho (kg/m3)	1.2	1.2	1.2	1.2	1.2	1.2	1.2	1.2	1.2	1.2	1.2	1.2	1.2	
	L (cm)	0.17	2.28	0.7	1.7	0.48	2.26	0.39	2.52	0.57	2.8	0.41	2.55	2.88	
	hydraulic diameter	0.34	4.56	1.4	3.4	0.96	4.52	0.78	5.04	1.14	5.6	0.82	5.1	5.76	3.032307692
Output	**Re**	453.3333	6080	1866.667	4533.333333	1280	6026.667	1040	6720	1520	7466.667	1093.333	6800	7680	4043.076923
	Main geometry														
	absolute roughness (cm)	0.28													
	diameter (cm)	1.47			Ansys results										
	Relative roughness	0.190476			inlet pressure	38.61									
	Re	4043.077			outlet pressure	7.08									
	friction factor	0.1													
	length (m)	0.3													
	pressure drop	4.897959			pressure drop	31.53									
inputs	**u (m/s)**	3.5	3.5	3.5	3.5	3.5	3.5	3.5	3.5						higher velocity scenario
	μ (Kg/m.s)	0.000018	0.000018	0.000018	0.000018	0.000018	0.000018	0.000018	0.000018						20 degree celsius
	rho (kg/m3)	1.2	1.2	1.2	1.2	1.2	1.2	1.2	1.2						
	L (cm)	0.75	3.18	1.88	0.45	1.65	2.87	4.61	0.3						
	hydraulic diameter	1.5	6.36	3.76	0.9	3.3	5.74	9.22	0.6						
Output	**Re**	3500	14840	8773.333	2100	7700	13393.33	21513.33	1400						

H. Calculations for geometry 4

inlet	u (m/s)	2	2	2	2	2	2	2	2	2	2	2	2	2	2	2	
	μ (Kg/m.s)	0.000018	0.000018	0.000018	0.000018	0.000018	0.000018	0.000018	0.000018	0.000018	0.000018	0.000018	0.000018	0.000018	0.000018	0.000018	
	rho (kg/m3)	1.2	1.2	1.2	1.2	1.2	1.2	1.2	1.2	1.2	1.2	1.2	1.2	1.2	1.2	1.2	
	L (cm)	3.99	1.85	3.23	0.82	2.98	0.65	3.72	1.5	0.86	3.54	1	3.5	1.1	3.83	1.39	
	hydraulic diameter	7.98	3.7	6.46	1.64	5.96	1.3	7.44	3	1.72	7.08	2	7	2.2	7.66	2.78	
Output	Re	10640	4933.333	8613.333	2186.666667	7946.667	1733.333333	9920	4000	2293.333	9440	2666.666667	9333.333	2933.333	10213.33	3706.667	
outlet	u (m/s)	2	2	2	2	2	2	2	2	2	2	2	2	2	2	2	
	μ (Kg/m.s)	0.000018	0.000018	0.000018	0.000018	0.000018	0.000018	0.000018	0.000018	0.000018	0.000018	0.000018	0.000018	0.000018	0.000018	0.000018	
	rho (kg/m3)	1.2	1.2	1.2	1.2	1.2	1.2	1.2	1.2	1.2	1.2	1.2	1.2	1.2	1.2	1.2	
	L (cm)	0.32	0.47	0.49	0.41	0.6	0.21	2.39	0.61	0.64	0.48	0.56	0.94	0.64	1.87	0.7	
	hydraulic diameter	0.64	0.94	0.98	0.82	1.2	0.42	4.78	1.22	1.28	0.96	1.12	1.88	1.28	3.74	1.4	
Output	Re	853.3333	1253.333	1306.667	1093.333333	1600	560	6373.333333	1626.667	1706.667	1280	1493.333333	2506.667	1706.667	4986.667	1866.667	

Main geometry	inlet						Main geometry	outlet						
absolute roughness (cm)	0.3						absolute roughness (cm)							
diameter (cm)	1.54			Ansys			diameter (cm)	1.45			Ansys			
Relative roughness	0.194805			inlet pressure	45.02		Relative roughness	0			inlet pressure	45.02		
Re	6037.333			outlet pressure	20.25		Re	1678.519			outlet pressure	20.25		
friction factor	0.1						friction factor	0.1						
length (m)	0.3						length (m)	0.3						
pressure drop	4.675325			pressure drop	24.77		pressure drop	4.965517			pressure drop	24.77		

G. Calculations for geometry 3

inlet	u (m/s)	2	2	2	2	2	2	2	2	2	2	2	2	2
	μ (Kg/m.s)	0.000018	0.000018	0.000018	0.000018	0.000018	0.000018	0.000018	0.000018	0.000018	0.000018	0.000018	0.000018	0.000018
	rho (kg/m3)	1.2	1.2	1.2	1.2	1.2	1.2	1.2	1.2	1.2	1.2	1.2	1.2	1.2
	L (cm)	0.46	2.82	1.26	1.83	3.1	0.51	1.08	2.54	0.63	2.19	1.39	3.14	1.07
	hydraulic diameter	0.92	5.64	2.52	3.66	6.2	1.02	2.16	5.08	1.26	4.38	2.78	6.28	2.14
Output	inlet Re	1226.667	7520	3360	4880	8266.667	1360	2880	6773.333	1680	5840	3706.666667	8373.333	2853.333
outlet	u (m/s)	2	2	2	2	2	2	2	2	2	2	2	2	2
	μ (Kg/m.s)	0.000018	0.000018	0.000018	0.000018	0.000018	0.000018	0.000018	0.000018	0.000018	0.000018	0.000018	0.000018	0.000018
	rho (kg/m3)	1.2	1.2	1.2	1.2	1.2	1.2	1.2	1.2	1.2	1.2	1.2	1.2	1.2
	L (cm)	0.46	1	0.45	0.68	3	1.17	3.22	0.84	0.61	2.76	0.45	1.5	1.17
	hydraulic diameter	0.92	2	0.9	1.36	6	2.34	6.44	1.68	1.22	5.52	0.9	3	2.34
Output	inlet Re	1226.667	2666.667	1200	1813.333333	8000	3120	8586.666667	2240	1626.667	7360	1200	4000	3120

Main geometry	inlet					Main geometry	outlet				
absolute roughness (cm)	0.31					absolute roughness (cm)	0.31				
diameter (cm)	1.45			Ansys		diameter (cm)	1.45			Ansys	
Relative roughness	0.213793			inlet pressure	13.49	Relative roughness	0.213793			inlet pressure	13.49
Re	4516.923			outlet pressure	3.58	Re	3937.778			outlet pressure	3.58
friction factor	0.1					friction factor	0.1				
length (m)	0.3					length (m)	0.3				
pressure drop	4.965517			pressure drop	9.91	pressure drop	4.965517			pressure drop	9.91

I. Geometry 3 with horizontal channels

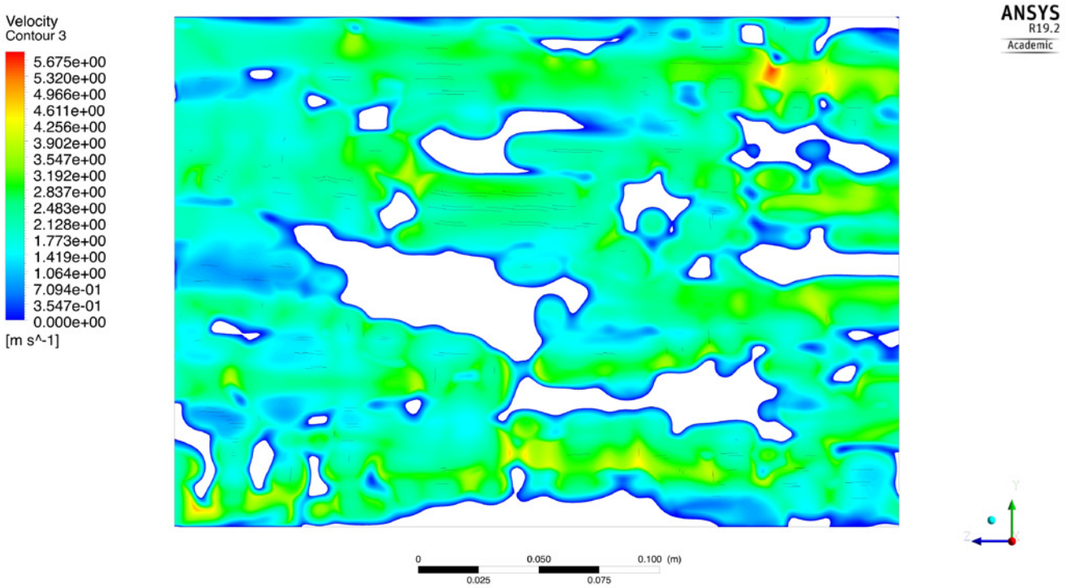

J. Geometry 3 with vertical channels

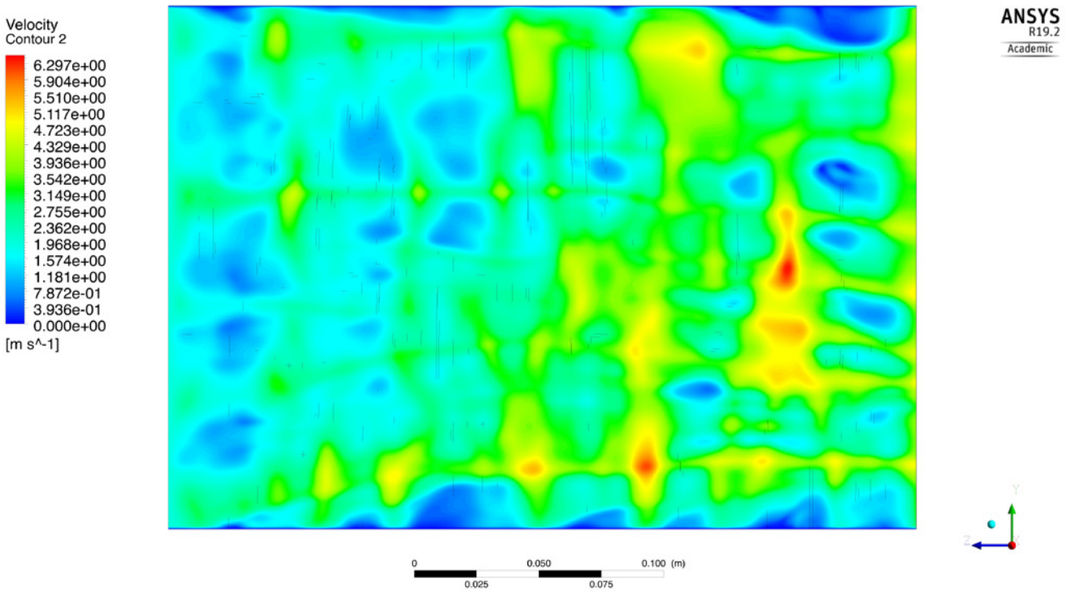

K. Geometry 4 with horizontal channels

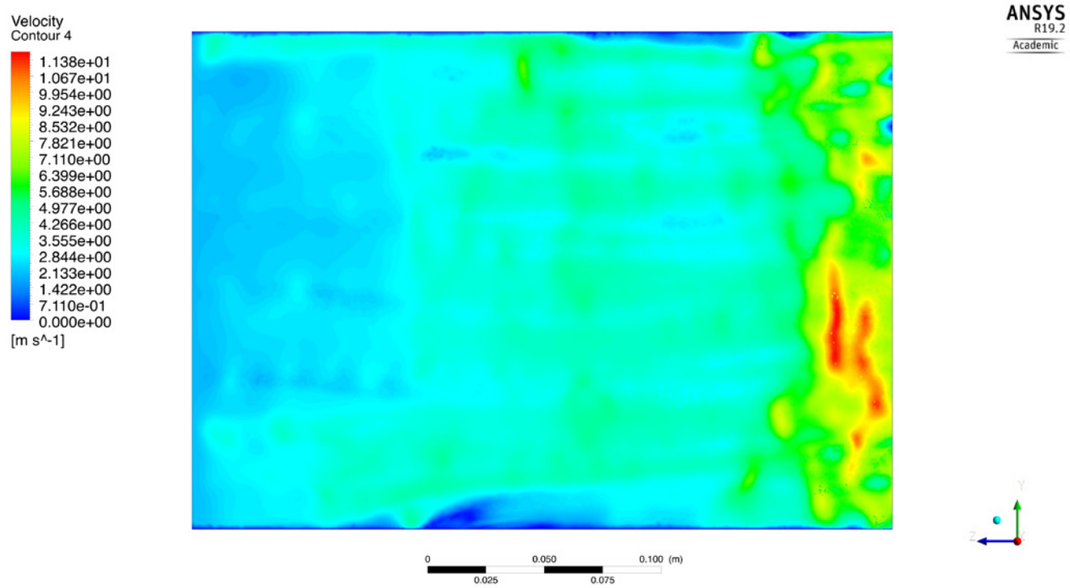

L. Geometry 4 with vertical channels

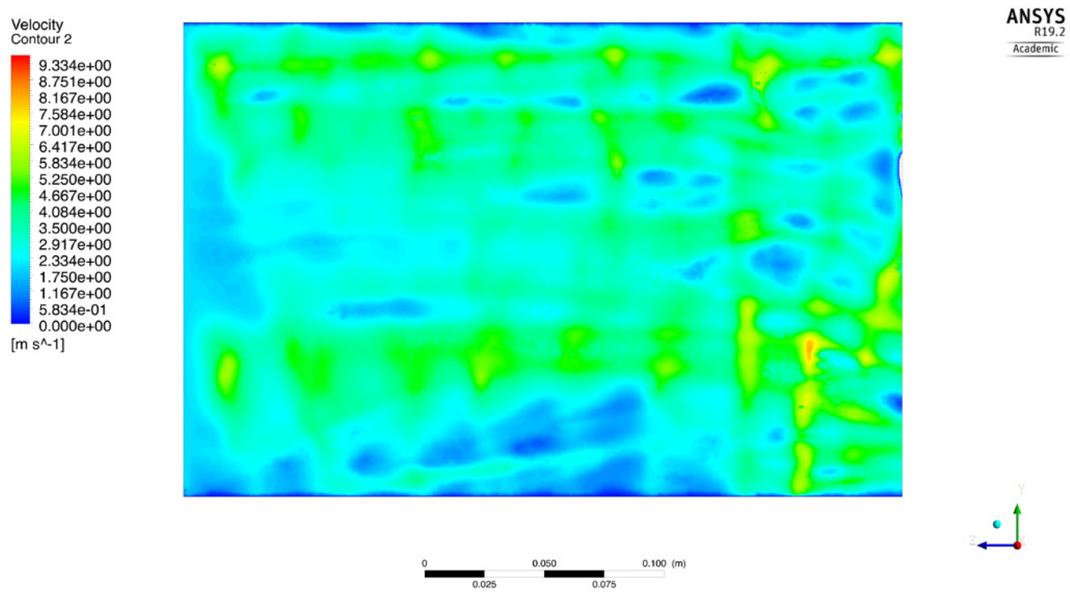

M. Geometry 4 with horizontal channels - smaller cavity volume

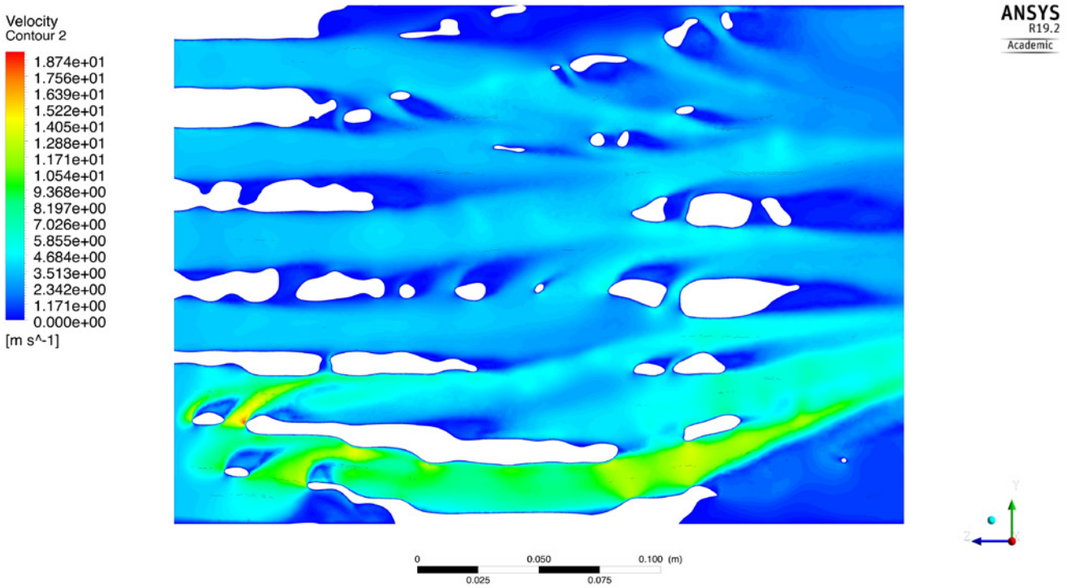

N. Geometry 4 with different inlet velocities

Inlet velocity (m/s)	Average outlet velocity (m/s)	Pressure drop (Pa)	Volume flow rate (m^3/h)
0.0625	0.15	0.13	1.045
0.125	0.32	0.36	2.10
0.25	0.64	1.01	4.21
0.50	1.3	2.84	8.56
1	2.63	8.09	17.32
2	5.31	24.77	34.98